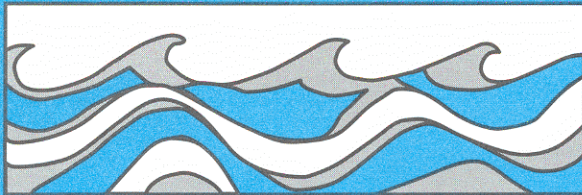


University of Washington
Department of Civil and Environmental Engineering



UPDATING A MACROSCALE HYDROLOGIC MODEL WITH SATELLITE SCATTEROMETER DATA

Ulysses Hillard



Water Resources Series
Technical Report No. 163
February 2001

Seattle, Washington
98195

Department of Civil Engineering
University of Washington
Seattle, Washington 98195

UPDATING A MACROSCALE HYDROLOGIC MODEL WITH SATELLITE
SCATTEROMETER DATA

by

Ulysses Hillard

Water Resources Series
Technical Report No. 163

February 2001

ABSTRACT

Microwave remote sensing from satellite platforms can provide all-weather information about conditions at the land surface that affect surface hydrologic fluxes. Microwave backscatter in particular responds to the liquid moisture content of snow. A drop in backscatter of about 4dB at Ku band (1.7-2.4 cm) has been observed at the onset of snow thaw. Microwave backscatter measured by sensors aboard the NSCAT (operational August 1996 to June 1997) and QuikSCAT (operational from July 1999) satellites was examined for its capability to improve predictions of a hydrological model. The Variable Infiltration Capacity model (VIC), a macroscale hydrological model, was configured to run at an 1/8th degree resolution over the upper Mississippi River basin during the winters of 1996/97 and 1999/2000. Backscatter measured by these sensors was compared with estimates of snow cover inferred from in situ climatic observations, and with VIC model predictions. The comparisons indicate a weak relationship between the observed and modeled snow surface variables (snow extent, and freeze-thaw status) and NSCAT and QuikSCAT backscatter. Tests were performed to indicate whether updating the model snow surface freeze/thaw state with backscatter would improve streamflow predictions. The results showed that the updating process had little effect on model accuracy.

TABLE OF CONTENTS

	Page
List of Figures	iii
List of Tables.....	v
Chapter 1: Introduction.....	1
1.1 Overview	1
1.2 Objectives.....	5
1.3 Approach	5
Chapter 2: Background	8
2.1 Overview	8
2.2 Snow Data	8
2.2.1 Snow Surveys	8
2.2.2 Automated Measurement of Snow Water Equivalent.....	9
2.2.3 Gamma Ray Surveys	10
2.2.4 Snow Depth	10
2.2.5 Visible Band Satellite Imagery.....	12
2.3 Snowmelt Thermodynamics.....	12
2.4 Microwave Sensors	13
2.4.1 Synthetic Aperture Radar	17
2.4.2 Scatterometers	19
2.5 Microwave Response to Freeze/Thaw State	25
2.5.1 Backscatter	25
2.5.2 Dielectric Properties of Snow.....	27
2.5.3 Volume Scattering.....	29
2.5.4 Surface Scattering.....	33
2.5.5 Canopy Vegetation Effects.....	34
2.6 Freeze/Thaw Change Detection	37
2.7 Study Area.....	39
2.8 The VIC Hydrological Model	39
2.9 Updating	43
2.10 Overview	45
2.11 Microwave Backscatter	45
2.11.1 Incidence Angle.....	46
2.11.2 Smoothing and Filling	49
2.11.3 Choice of Channel	53
2.11.4 QuikSCAT	57
2.11.5 Freeze/Thaw Change	58
2.12 Meteorological Change	58
2.12.1 Snow Depth	58

2.12.2 Maximum Daily Air Temperature.....	59
2.12.3 Snow Surface Temperature	60
2.13 Backscatter Comparisons	60
2.14 Updating	61
2.14.1 Preliminary Trail-Updating	62
2.14.2 Updating Freeze/Thaw State	63
2.15 Analysis of Results.....	64
2.15.1 Spatial Comparisons.....	64
2.15.2 Summary Statistics	64
2.15.3 Discharge.....	65
Chapter 3: Results.....	69
3.1 Overview	69
3.2 Snow Depth Updating	70
3.2.1 Snow Depth Spatial Predictions	70
3.2.2 Runoff Sensitivity.....	70
3.3 Backscatter Correlations	77
3.3.1 Observed Snow Depth.....	87
3.3.2 Observed Temperature	91
3.4 Backscatter Relationships: Specific Events	95
3.4.1 Midwinter Melt.....	95
3.4.2 Cold Snap	109
3.4.3 Late Season Snow Storm.....	113
3.5 Updating	124
3.5.1 Snow Depth Spatial Predicitons	124
3.5.2 Discharge.....	125
3.6 Overview	137
3.7 Snow Depth Updating	137
3.7.1 Snow Depth Spatial Predictions	137
3.7.2 Runoff.....	138
3.8 Visual Comparison of Specific Events.....	141
3.8.1 Overview	141
3.8.2 Signal-to-Noise Ratio	142
3.8.3 Time of Observation.....	142
3.8.4 Mismatch Between Model Predictions.....	149
3.8.5 Backscatter Response to Vegetation	150
3.9 Freeze/Thaw Updating	151
3.9.1 Snow Depth Spatial Prediction.....	151
3.9.2 Runoff.....	153
Chapter 4: Conclusions.....	157
4.1 Overview	157
4.2 Recommendations	159
List of References	161

LIST OF FIGURES

Number	Page
Figure 1-1. Mean discharge in the upper Mississippi River basin.....	1
Figure 1-2. Areal extent of snow - March and April, 1997.....	2
Figure 2-1. Locations of NCDC cooperative observer stations	11
Figure 2-2. Typical meteorological snowpack characteristics during active melt	15
Figure 2-3. Earth-observing sensor imaging swath with definitions	18
Figure 2-4. Schematic depicting NSCAT ground imaging pattern.....	21
Figure 2-5. NSCAT repeating swath pattern.....	23
Figure 2-6. QuikSCAT swath pattern.....	25
Figure 2-7. Illustration of volume scattering from Ulaby et al, 1982.	29
Figure 2-8. Time series of normalized backscatter cross section.....	31
Figure 2-9. Illustration of surface scattering from Ulaby et al, 1982.....	33
Figure 2-10. Land cover.	35
Figure 2-11. Incidence angle correction for NSCAT.....	47
Figure 2-12. Backscatter for a single pixel.....	51
Figure 2-13. Comparison of NSCAT beams.....	55
Figure 2-14. Study sub-basins.	67
Figure 3-1. St. Croix River – winter of 1996/97.	71
Figure 3-2. Mississippi River at Anoka, Minnesota - winter of 1996/97.....	75
Figure 3-3. Snow depth - winter of 1996/97.	79
Figure 3-4. Daily maximum air temperature - February to April, 1997.	81
Figure 3-5. Snow depth - 1999/2000.....	83
Figure 3-6. Daily maximum air temperature - February to March, 2000.	85
Figure 3-7. Backscatter response, snow depth and areal extent of snow -1996/97.....	89
Figure 3-8. Backscatter response, snow depth and areal extent of snow -1999/2000... 89	89
Figure 3-9. NSCAT backscatter and daily maximum air temperature - 1996/97.	93
Figure 3-10. QuikSCAT backscatter and daily maximum air temp. -1999/2000.	93
Figure 3-11. Daily maximum air temperature - February, 1997.....	97
Figure 3-12. Snow pack surface layer liquid water content - February 15-20, 1997.....	99
Figure 3-13. Snow pack surface layer temperature - February 15-20, 1997.....	101
Figure 3-14. Snow pack surface layer water content and σ^0 -February 16-20, 1997... 103	103
Figure 3-15. Snow pack surface layer temperature and σ^0 - February 16-20, 1997. ... 105	105
Figure 3-16. Focus on two days - February 16 and 17, 1997.....	107
Figure 3-17. Snow pack surface layer liquid water content - March 12-15, 1997.....	111
Figure 3-18. Snow pack surface layer temperature - March 12-15, 1997.....	111
Figure 3-19. Snow pack surface layer water content and σ^0 - March 12-15, 1997.....	115
Figure 3-20. Snow pack surface layer temperature and σ^0 - March 12-15, 1997.....	117
Figure 3-21. Snow pack surface layer water content and σ^0 - April 11-14, 1997.....	119
Figure 3-22. Snow pack surface layer temperature and σ^0 - April 11-14, 1997.	121
Figure 3-23. St. Croix River with microwave backscatter updating, 1996/97.....	127
Figure 3-24. MS River near Anoka, MN with backscatter updating 1996/97..	129
Figure 3-25. St. Croix River - 1999/2000.	133

Figure 3-26. Mississippi River near Anoka, Minnesota -1999/2000.	135
Figure 3-27. Snow depth updating - timeseries of model variables, 1996/97.....	139
Figure 3-28. Raw and smoothed σ^0 , February 16-20, 1999.....	143
Figure 3-29. Raw and smoothed σ^0 , March 12-15, 1997.....	145
Figure 3-30. Raw and smoothed σ^0 , April 11-15, 1997.....	147
Figure 3-31. Backscatter updating - timeseries of model variables, 96/97.....	153

LIST OF TABLES

Number	Page
Table 2-1. Freeze/thaw state change detection algorithms	38
Table 2-2. Rain/snow partitioning of precipitation	41
Table 2-3. Model freeze/thaw updating scheme.	63
Table 2-4. USGS gaging stations.	67
Table 3-1. Summary statistics: observed – predicted snow depth, winter 1996-97	124
Table 3-2. Summary statistics: observed – predicted snow depth, winter 99/00	124

ACKNOWLEDGEMENTS

Several individuals made contributions that made this research possible. Dr. Kyle McDonald of the Jet Propulsion Laboratory provided NSCAT data and was particularly helpful in assisting with the interpretation of those data. Dr. Son Nghiem, also of the Jet Propulsion Laboratory, provided the QuikSCAT data. Keith Cherkauer of the University of Washington provided the hydrology parameters and assisted with model implementation and interpretation of results.

Finally, the authors owe tremendous thanks to the members of the Surface Water Modeling Group at the University of Washington who provided assistance and support in the best spirit and tradition of university research.

This research was funded under grant NAG-6505 from the National Aeronautics and Space Administration, support from which is gratefully acknowledged by the authors.

Chapter 1: Introduction

1.1 Overview

In the north central United States, many of the largest floods are associated with snowmelt, often in conditions when the underlying soil is frozen. Figure 1-1 illustrates how this dependence on snowmelt is manifested in seasonal maximum flows for three tributaries of the upper Mississippi River basin. One recent snowmelt-dominated flood, the Red River of the North flood of 1997, caused an estimated 4 billion dollars in damages (IRRBTF, 1999). The Red River flood caused renewed interest in improving forecasting capabilities for snowmelt floods in the region.

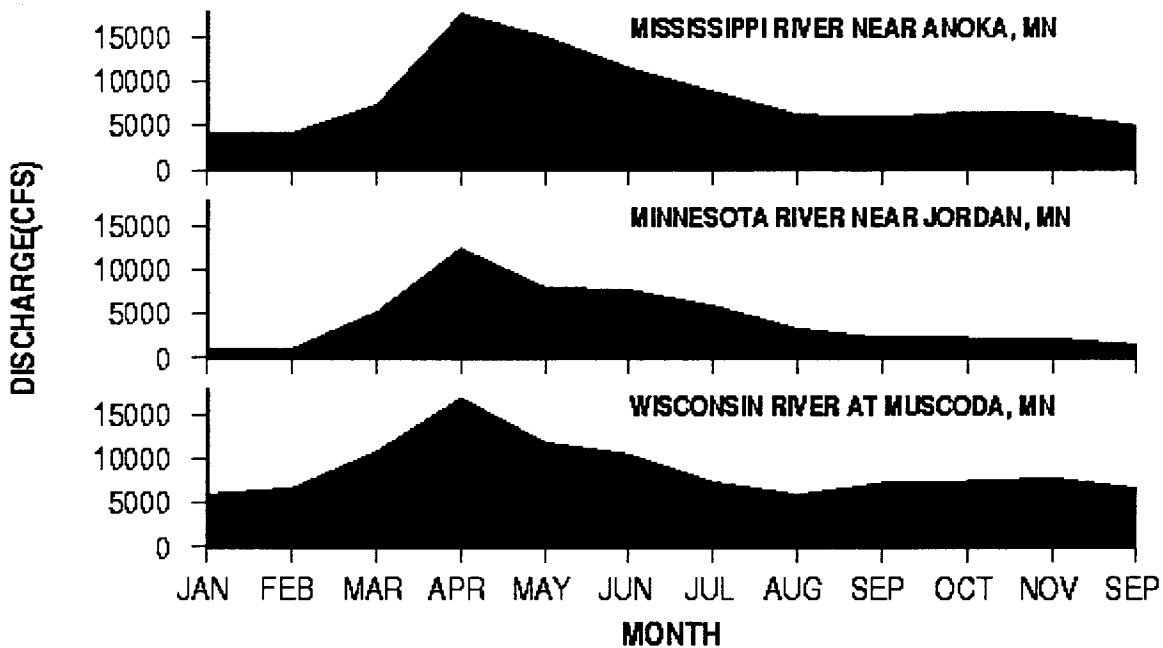


Figure 1-1. Mean discharge, by month, from three tributaries in the upper Mississippi River basin. All three basins have a period of record in excess of 40 years.

The quantity of water stored in the snowpack and other snow properties that determine the risk of snowmelt flooding are difficult to measure over large areas. The present procedure for estimating snow water equivalent across the north central U. S. is based on point surveys at a limited number of locations and airborne gamma remote sensing transects flown by the National Weather Service. (Josberger et al, 1998) Unfortunately, these methods give fairly local and infrequent estimates of a critical hydrologic variable over a region that includes several large river basins and as many as eight states. Satellite remote sensing offers a method for collecting spatially and temporally coherent data across such large areas. The National Weather Service currently plots snow areal extent

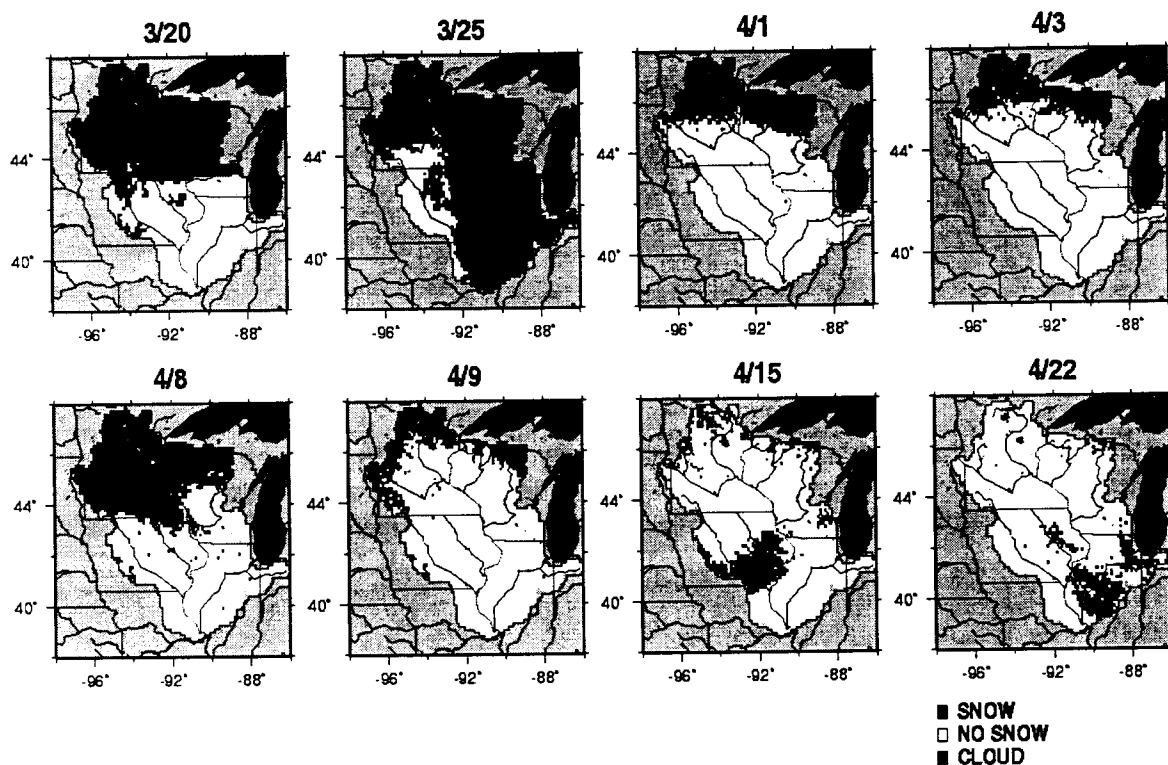


Figure 1-2. Areal extent of snow derived from visible band satellite data by NOHRSC for the upper Mississippi River basin for March and April, 1997

across the entire United States using visible band satellite imagery (Figure 1-2) but frequently cloud cover obscures these plots. (Carroll, et, 1999)

Clouds are effectively transparent to microwave radiation of wavelength longer than 2 cm and attenuation by even intense rain is small due to the small size and sparse distribution of rain particles relative to these wavelengths (Ulaby et al, 1981). Moreover, the response of water to microwave radiation is such that the frozen versus liquid state of water present upon or within a given area as open water, ice or within vegetation can be distinguished by microwave scattering properties (Stiles and Ulaby, 1980).

The microwave backscattering characteristics of a material depend on the physical geometry and roughness of the material. Some materials interact with incident radiation, reflecting and absorbing that radiation, while other materials are transparent to it. The degree to which a given material interacts with or is transparent to radiation of a given frequency is defined by its dielectric properties. Materials with high dielectric constants interact more with incident radiation than do materials with low dielectric constants. Liquid water has a dielectric constant significantly higher than does ice. As a result, microwave remote sensing has the potential to extract whether snow on the ground is frozen or thawed. (Ulaby et al, 1981)

Microwave scatterometers flown on satellites measure backscatter in swaths on the order of 1000 km in width and their orbits take them over the same location as often as twice a day depending

on the location of the target area. Because of this ability to measure surface characteristics over large areas relatively often, and because of the all weather capability of microwave sensors, microwave scatterometers may be a valuable source of hydrologic data.

This study evaluates the potential of microwave scatterometers for improving hydrologic predictions. Hydrologic models are used for regional water resources management, for flood control, for retrospective analysis and for planning purposes. Hydrologic models can predict snow accumulation, melt, flooding, and other hydrologic phenomena, but are inevitably limited by data availability and accuracy. If more accurate observations of key hydrologic state variables, such as soil moisture and snow water storage could be observed more frequently and over larger areas, these data could be used for model updating, which arguably would result in more accurate forecasts. The pursuit of methods for improving hydrologic predictions has led to an interest in microwave and other remote sensors. The capabilities of microwave sensors have reached the point that methods for incorporating this potential new source of data into hydrologic modeling is now needed. Furthermore, guidance is needed on how future directions in modeling and in remote sensing research for hydrologic analysis should progress, in light of the capabilities of such sensors.

1.2 Objectives

The purpose of this research is to evaluate the hydrologic utility of backscatter measurements produced by satellite microwave scatterometers. This objective is motivated by an interest in measurements by microwave scatterometers as a new source of hydrologic data for improving the predictive capabilities of macroscale hydrologic models. This interest arises from research that has demonstrated a correlation between microwave backscatter measurements and the freeze/thaw state of the land surface (Rignot et al, 1994; Wismann and Boehnke, 1996; Way et al, 1997; McDonald et al, 1999; Kimball et al, 2000). This thesis has the following specific objectives:

- Evaluate the potential for improving predictions of land surface hydrological state variables by updating model snow state variables;
- Examine the relationship between backscatter measurements produced by two scatterometers, NSCAT and QuikSCAT, and observed and model-predicted land surface meteorological conditions;
- Evaluate improvements to predictions by a land surface hydrological model updated specifically with microwave backscatter measurements.

1.3 Approach

The hydrologic utility of microwave backscatter is assessed in this study by evaluating the improvement in predictions of snow variables produced by a hydrologic model when microwave backscatter is used to update model state variables. Specifically, snow freeze/thaw state as

predicted by the Variable Infiltration Capacity (VIC) model (Liang et al., 1994; Nijssen et al., 1997; Cherkauer and Lettenmaier, 1999) is updated using microwave backscatter observations from two satellite platforms. The potential for updating freeze/thaw state in the VIC model has not previously been evaluated. The thermodynamics of melting snow are well represented by existing snow models, but no model exists which explicitly calculates a state variable that corresponds to snow freeze/thaw as measured by microwave backscatter.

The overall approach is as follows:

- 1) Implement the VIC model for the upper Mississippi River basin, at a space-time resolution that is similar to that of the satellite scatterometer products.
- 2) Evaluate products from two scatterometers, NSCAT and QuikSCAT (see Section 2.4.2 for descriptions), over the same area during the winters of 1996-1997 and 1999-2000.
- 3) Develop algorithms for extrapolating snow pack parameters from scatterometer products.
- 4) Determine whether updating with data extrapolated from the satellite products improves model predictions.

This thesis is organized into six chapters. Chapter 2 describes the physics that underlie the estimation of snow properties using microwave scatterometer data. Chapter 3 describes the approach followed to evaluate microwave backscatter for updating snow predictions produced by the VIC macroscale hydrology model. Chapter 4 summarizes test applications of the updating method using scatterometer products derived from NSCAT and QuikSCAT and presents the

results of these tests. Chapter 5 explains and interprets the results of the study. Chapter 6 presents conclusions from the study and recommends future research directions.

Chapter 2: Background

2.1 Overview

In the northern Great Plains of the United States and in other regions where snowfall is significant, the timing of snowmelt can be the single most important factor affecting spring runoff peaks. Knowledge of the state of the snowpack is therefore a key component for predicting the timing and magnitude of snowmelt runoff. This thesis evaluates the potential of microwave scatterometry as a new source of data for estimation of snowpack properties over large areas. This chapter describes existing methods for measuring snow properties and then describes the conceptual basis for their estimation from microwave scatterometry.

2.2 Snow data

2.2.1 Snow surveys

Hydrologically, the water equivalent of snow is most directly related to runoff processes. Snow water equivalent is traditionally measured by snow surveys which use a coring tube, a hollow aluminum tube thrust into the snowpack and removed with a snow core, to extract a sample of the snow pack (USDA, AIB 536). The contents of the tube are weighed to determine the water equivalent of the snowpack. Several such samples are averaged to provide a representative value. This method is labor intensive and time consuming, and cannot account for spatial variations over areas larger than the area sampled (typically a few tens of meters in spatial extent). Such surveys are often taken only a few times per year at specified locations

("stations"), and for this reason the spatial density of observation stations is much lower than for snow depth.

2.2.2 Automated measurement of snow water equivalent

Snow water equivalent can also be measured automatically by weighing lysimeters and snow pillows. A weighing lysimeter is typically a wide platform sitting on top of an automatic weighing device. The water equivalent of the snow is determined from its weight. Snow pillows are large bags filled with fluid at a known pressure. The water equivalent of the snow is inferred from the pressure increase within the bag as the overlying snow accumulates. Measurements produced by these devices are taken automatically and are either recorded by a data logger on-site or transmitted to a central data collection station.

Both weighing lysimeters and snow pillows suffer from design problems such as ice bridging. The primary problem with such devices, though, is that they are too expensive to manufacture and operate for the purposes of gauging snow amount with even modest spatial density (e.g., approaching that of the snow depth network shown in Figure 2-1) across an area as vast as the upper Mississippi River basin. Furthermore, access in remote areas is inevitably a problem, so that while such automated devices are less labor intensive than manual snow surveys, they do entail considerable labor costs.

2.2.3 Gamma ray surveys

Beginning in 1978, the National Operational Hydrologic Remote Sensing Center (NOHRSC), an office of the U.S. National Weather Service, has inferred snow water equivalent from an aircraft-mounted instrument that measures the attenuation of gamma rays emitted from the ground surface. The measured attenuation varies with moisture content of the snowpack, allowing water content to be inferred from comparison with background measurements (snow free) observations taken prior to the snow accumulation season (Peck et al, 1980). As a result, the method measures the total difference in moisture between the two measurement times, rather than directly inferring the water equivalent of the snow on the ground. Therefore, it effectively measures changes in water storage in the combined snowpack and soil column, rather than just the snowpack. Also, gamma-ray attenuation measurements cannot be made accurately from earth orbit, and are therefore limited to aircraft applications. For this reason, the data provided are for transects, typically several tens of kilometers in length. Although the transect information is an improvement over point measurements, it does not fully characterize the spatial extent and variability of snow water equivalent.

2.2.4 Snow depth

The National Climatic Data Center (NCDC) archives historical snow depth records from over 900 cooperative observer stations in the upper Mississippi River basin. Snow depth measurements are taken using a measuring stick, and measurements usually are averaged over multiple locations within a small (tens of meters in spatial extent) area to account for

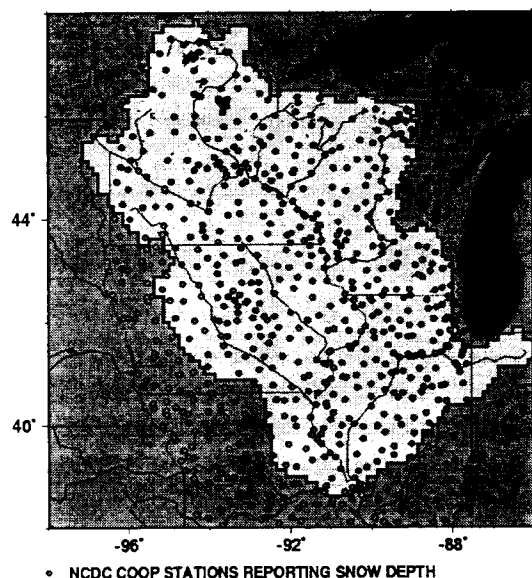


Figure 2-1. Locations of NDCD cooperative observer stations reporting snow depth in and around the upper Mississippi River basin during the winters of 1996/97 and 1999/2000.

different types of cover and drifting. Measurements are taken at irregular intervals when there is snow on the ground. In some cases, the observing interval may be daily, while at other times it can be a week or longer. Following error checking, the data are archived by the National Climatic Data Center.

Snow depth is somewhat problematic for hydrologic purposes as snow properties that are associated with snowpack microphysical processes (e.g., water equivalent, temperature, grain size) are not related directly to depth. Snow depth can vary due to selective densification, for instance, and due to crystal metamorphosis within the pack. However, as shown in Section 3.3.1, the snow depth observations can form the basis for mapping of snow cover extent.

2.2.5 Visible band satellite imagery

NOHRSC generates maps of snow extent from visible band satellite data. The maps are produced by classifying satellite imagery from AVHRR (Advanced Very High Resolution Radiometer) and GOES (Geostationary Operational Environmental Satellite) sensors on a pixel by pixel basis as snow-covered, snow-free or cloud-obscured. The resulting maps have a resolution of about 1 km. The classification method relies on differences between brightnesses in different bands sensed by the GOES and AVHRR visible sensors but also includes some subjectivity (Carroll et al, 1999). Images are composited over several days in order to maximize the number of cloud-free pixels. The resulting maps can be quite accurate in the Great Plains because the terrain is relatively flat and wintertime vegetation is sparse compared to other regions of the United States.

However, even with compositing, cloud cover is a severe limitation.

2.3 Snowmelt thermodynamics

The remote sensing methods described in this thesis utilize information about the physical state of snow as it melts that are based on the thermodynamics of snowmelt. A brief background is provided in this section. As an isothermal snowpack begins to melt due to a net flux of energy to the snowpack surface, the surface moisture content increases. This increase is usually evidenced first as a diurnal cycle whereby the moisture content increases during the daylight hours and then refreezes at night (Figure 2-2). Later in the season, as air temperatures begin to exceed 0 C at

night as well as during the day, water remains entrained in the pack during the night as well. Unless the pack experiences a re-freezing event, the snow pack continues to contain liquid water throughout the melt period.

2.4 Microwave sensors

Active microwave sensors, also known as radar (RADio Detection Array), differ from other sensors that use electromagnetic radiation because they both transmit and receive the signal that they measure. Most other types of sensors measure passive signals, either radiance from the sun reflected by a target, or the inherent emitted radiance of the target itself. In the case of earth observing sensors, the targets are regions on the surface of the earth.

Sensors which measure radiance in the visible and near infra-red regions of the electromagnetic spectrum, with wavelengths measured in nanometers and microns, such as AVHRR or LandSat, can produce images of the Earth's surface at relatively fine resolution. Their spatial resolution capabilities are defined by the following equation for instantaneous field of view (IFOV),

$$\text{IFOV} = 2 \operatorname{atan}(0.5wf^{\prime}) \quad (2-1)$$

where w is the width of sensing elements within a sensor and f is the sensor's focal length (Schowengerdt, 1997). The LandSat Thematic Mapper, for instance, has a resolution of 30m and AVHRR has a resolution of 1km. At microwave frequencies, however, sensor spatial resolution is defined by the wavelength of the sensor. The evolution of equations in this and the following section are adapted from Ulaby et al (1982).

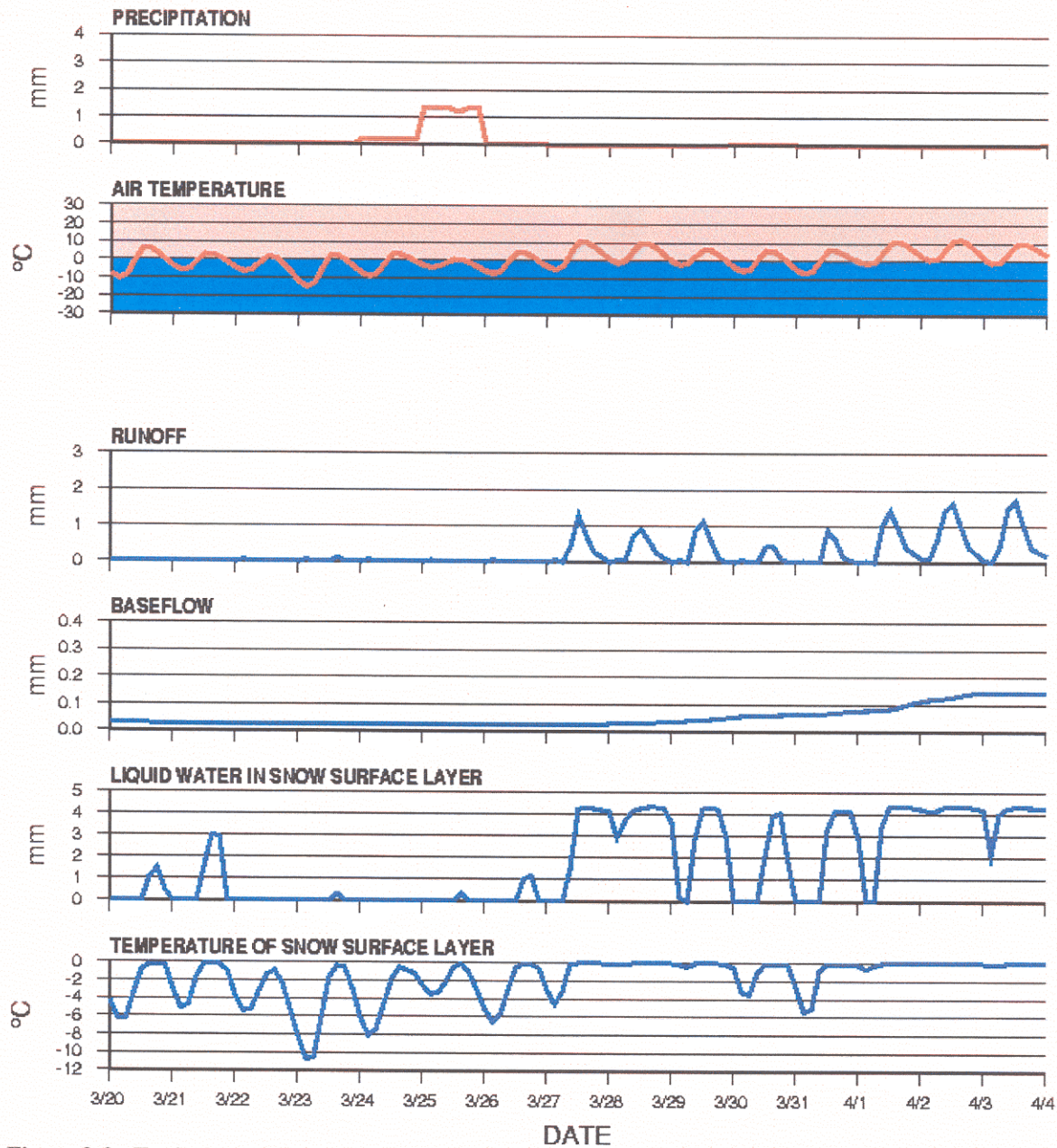


Figure 2-2. Typical meteorological snowpack characteristics for a hypothetical snowpack during a period of active melt. Model output variables (blue) are produced by the Variable Infiltration Capacity (VIC) model (see Section 2.8 for details).

For microwave instruments, the equation for IFOV is

$$\text{IFOV} = \beta h l^{-1}, \quad (2-2)$$

where β is sensor beam width, h is sensor range to target, and l is the length and width of a square aperture or the diameter of a circular aperture and sensor beam width, $\beta = k\lambda$, where k is a constant for given antenna configuration and λ is sensor wavelength, (Ulaby et al, 1981). For microwave scatterometers, (see Section 2.3.2.2) most analysis is done with pixels of about 25 km resolution.

1.1.1 Synthetic Aperture Radar

Imaging radars achieve a better spatial resolution than given by equation 2-2 by sending out discrete pulses and using the movement of the sensor to create an image of an area along a swath. Along-track resolution is given by

$$r_a = \beta_h R = \beta_h h / \cos \theta \quad (2-3)$$

where r_a is the azimuthal (along-track) range, β_h is the sensor beamwidth, R is the range to the target, h is the sensor altitude and θ is the angle of incidence of the beam upon the target (see Figure 2-3).

Synthetic Aperture Radar (SAR) achieves much finer spatial resolution than would otherwise be possible for microwave instruments by emulating aperture sizes

much larger than the physical antenna. Through use of signal processing techniques, the viewing aperture is expanded to a synthetic aperture, that can be hundreds of kilometers in length. The along-track resolution for a SAR sensor is

$$r_a = \beta_{hs} R = \frac{\lambda R}{2L} a_{hs} \quad (2-4)$$

where r_a is the along-track resolution; β_{hs} is the along-track beam width of the synthetic aperture; R is the range to the target; λ is the sensor wavelength; L is the length of the synthetic aperture and a_{hs} is the aperture illumination taper factor, which is usually on the order of one.

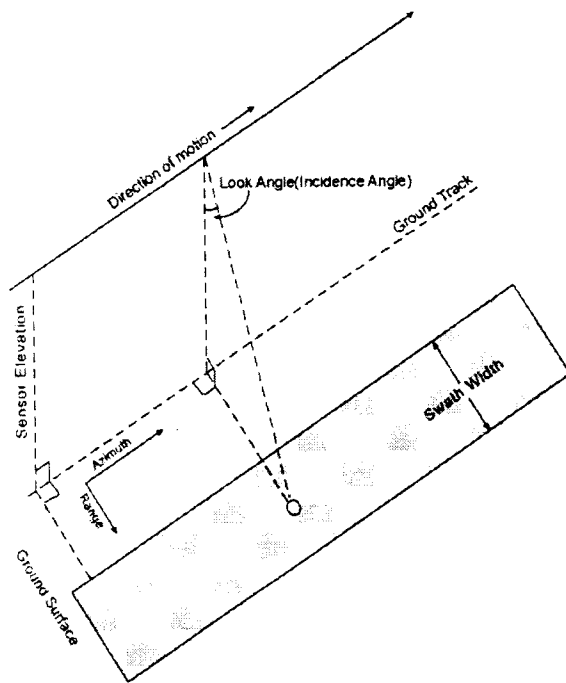


Figure 2-3. Earth-observing sensor imaging swath with definitions, adapted from Dubin and Lettenmaier, (1999)

By a series of substitutions, Equation 2-5 can be simplified to show that

$$r_a \cong \frac{l}{2} \quad (2-5)$$

meaning the resolution theoretically possible with a SAR instrument is on the order of $1/2l$ where l is the length of the instrument's receiving antenna. In this way, SAR can achieve spatial resolutions similar to that of visible band instruments. SAR instruments have been flown in space on board SeaSat, the ERS series of satellites, RADARSAT and ENVISAT, as well as the SIR-C/XSAR payloads aboard the space shuttle (Lillesand and Kiefer, 1994).

The drawback to SAR instruments is that they, like high resolution visible band imaging sensors such as SPOT or LandsAT, have narrow swaths and relatively long repeat intervals (typically tens of days) compared to lower resolution instruments. The infrequent repeat interval afforded by the SAR instruments is insufficient for hydrological model updating, particularly during highly dynamic periods like flood events. While SAR products were originally considered for use in this research, their infrequent repeat intervals lead instead to a focus on scatterometer products, which have much more frequent overpasses, albeit at much coarser spatial resolution.

2.4.2 Scatterometers

Scatterometers are radar devices that transmit and receive signals across a wide swath (1800 km in the case of QuikSCAT) that are aggregated to produce a coarse resolution backscatter grid with individual pixels typically on the order of 25 km on a side. Ulaby et al (1981) describe a

scatterometer as a radar device that has been specifically calibrated to measure the backscatter characteristics of a target, such as the magnitude and polarity of a signal scattered back to the sensor. This definition distinguishes a scatterometer from early radar devices that measured only the time for a transmitted signal to travel to and return from a target. However, it does not distinguish between instruments such as the scatterometers used in this project (see Sections 2.3.2.1 and 2.3.2.2) and SAR and side-looking aperture radar instruments. This definition has evolved somewhat now that scatterometers are among the pantheon of earth observing sensors. Designating a device as a “scatterometer” now distinguishes a radar device that does not record target images from imaging radars (personal communication, Kyle McDonald, Jet Propulsion Laboratory). Note that even this definition can seem loose, because modern analysis of scatterometer data typically involves processing the data in such a way that images can be extracted from the data, albeit at much coarser spatial resolutions than can be achieved by SARs. This post-processing is significantly different, though, from imaging radars which are designed specifically to associate a particular recorded brightness with a particular pixel on the ground.

2.4.2.1 NSCAT

A K_u band scatterometer, NSCAT (NASA Scatterometer), was flown on the Japanese ADEOS I satellite (also called Midori by the Japanese Space Administration) and began reporting calibrated data beginning September 15th, 1996. Unfortunately, ADEOS I suffered a permanent power failure on June 15, 1997 which resulted in termination of NSCAT operations on that date.

NSCAT had six antennae and measured backscatter with four beams. The beams extended out from the spacecraft at different azimuth angles and at different polarizations and extended to both sides of the platform. The beams thus created a dual set of sensed tracks along the ground with a 200 km wide track directly beneath the satellite which was not imaged (see Figure 2-4). Of the four beams, one extended forward to both sides, two

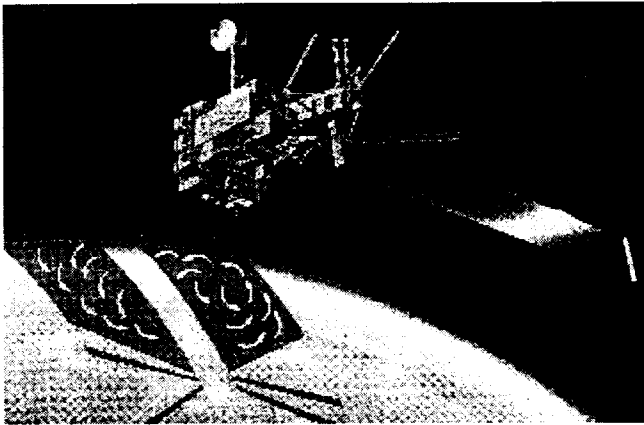


Figure 2-4. Schematic depicting NSCAT ground imaging pattern. Note that a track directly beneath the sensor is not imaged.

extended laterally to both sides and one extended aft to both sides. Of the two laterally oriented beams one was horizontally polarized and one was vertically polarized. These two beams were parallel polarized meaning they transmitted signals at the same polarization as was observed.

The primary application of K_u -band scatterometer data is to extract ocean surface wind magnitude and direction. Wind over the ocean surface creates capillary waves oriented perpendicular to the wind's direction and with an amplitude corresponding to the speed of the

wind. K_u -band scatterometers measure the amplitude of these waves and different polarization beams allow measurement of the wave direction. Some studies (Frolking, et al 1999; Way, et al 1998; McDonald, et al 1999) have suggested that it might also be possible to extract from scatterometer data snow surface freeze/thaw state. This suggestion, along with the need for improved methods of updating snowmelt runoff predictions, motivated the research described in this thesis.

The design of scatterometer sensors is such that the incidence angle for a given pixel varies depending on how far the pixel is from the sensor in the direction perpendicular to the direction of travel of the satellite. This variation in incidence angle requires that calculations of backscatter include a procedure to normalize the incidence angle for each pixel to a stipulated standard incidence angle.

NSCAT was flown in a sun-synchronous polar orbit with overpasses of the upper Mississippi study area at around 10 AM local time in the descending orbit and 10 PM in the ascending orbit. Some of the swaths in this set of flyovers included much of the study area and some included none of it (Figure 2-5). This day-to-day patchiness of data in the study area is an important consideration in the choice of both the signal processing and change detection approaches described in Sections 3.2.2 and 3.2.4.

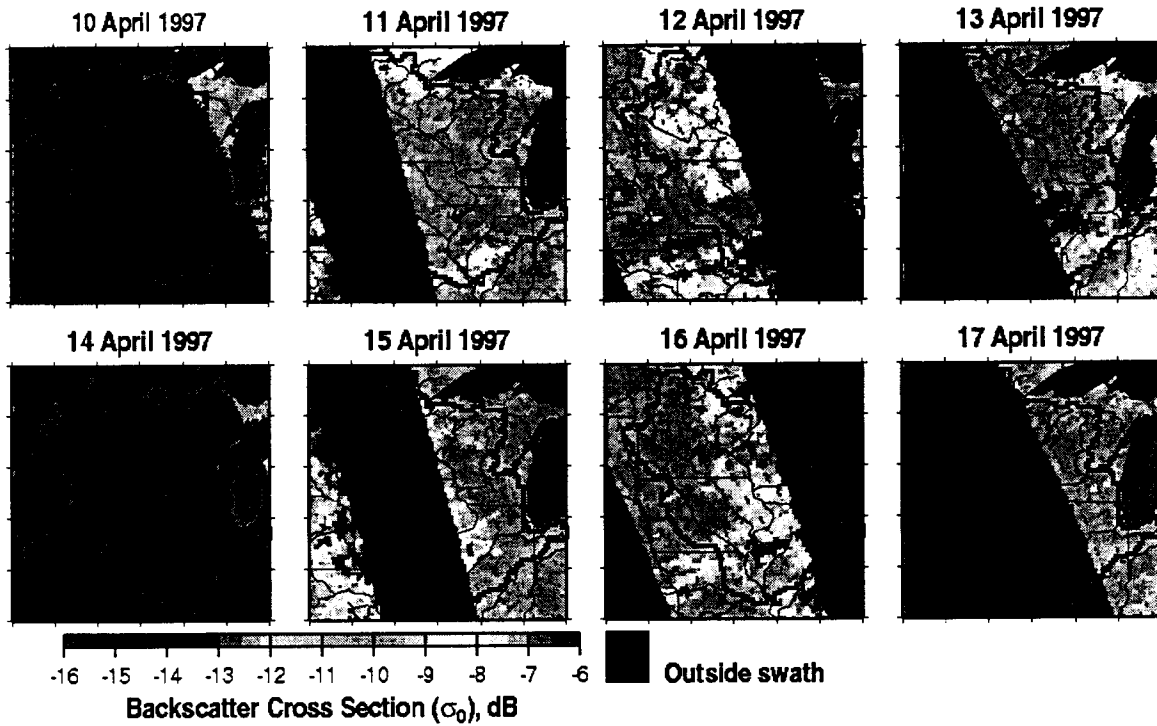


Figure 2-5. NSCAT repeating swath pattern.

2.4.2.2 QuikSCAT

NSCAT was considered a major success because of its ability to provide information about ocean winds that had not previously been available. Subsequent to loss of the instrument, NASA quickly began work on a replacement mission. The resulting sensor, SeaWinds, flies on a satellite platform called QuikSCAT. QuikSCAT was launched on June 19, 1999 and went into full operation later the same summer. The design of the sensor differs from NSCAT in that all pixels are seen from the same incidence angle, which removes the need to correct for incidence

angle. With this design, however, the backscatter recorded for different pixels is observed at different azimuth angles and this factor may require normalization as does variation in incidence angle for NSCAT. Where relief is significant, such as in mountainous regions, the affect of azimuth angle is a concern. The upper Mississippi River basin is relatively flat region, however, and so variations in azimuth angle associated with QuikSCAT backscatter measurement required no correction for the analysis described in this thesis (personal communication, Son Nghiem, Jet Propulsion Laboratory).

QuikSCAT views swaths along the ground in a regular repeating four day pattern as compared to the imaging pattern of NSCAT, which was not regular (Figure 2-6). QuikSCAT also differs from NSCAT in that the backscatter from each flyover is

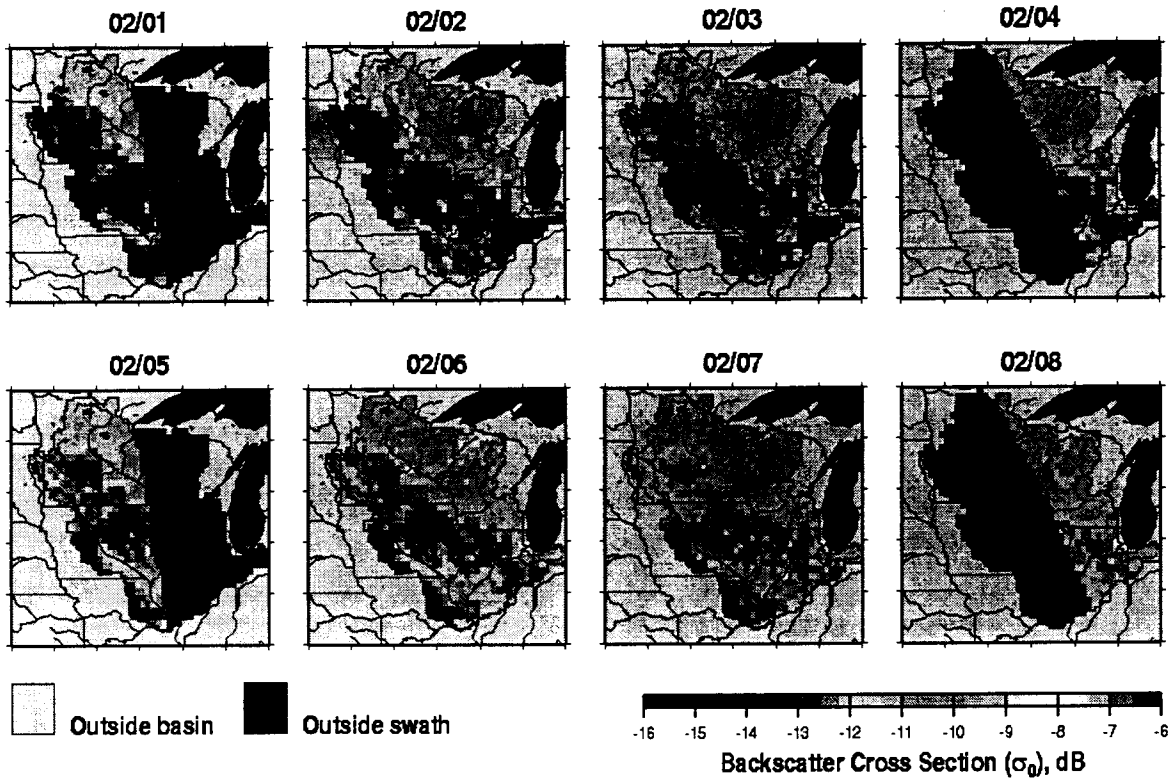


Figure 2-6. QuikSCAT swath pattern.

recorded in two channels rather than four. One of these channels corresponds to a horizontally polarized beam and the other to a vertically polarized beam.

2.5 Microwave response to freeze/thaw state

2.5.1 Backscatter

As noted in Section 2.4.2, scatterometers measure the scattering properties of targets at microwave frequencies. The power of an electromagnetic pulse scattered back to a sensor from a target after being transmitted at the target is given by the monostatic radar equation:

$$P_r = \frac{P_t A^2 \sigma}{4\pi\lambda^2 R^4} \quad (2-6)$$

where P_t is the power transmitted by the sensor at the target, A is the effective area of the antenna, σ is the scattering cross-section of the target, λ is the wavelength of the transmitted signal and R is the range from the sensor to the target. The equation is called monostatic because it refers to the case when the transmitter and receiver are at the same location. σ is defined as

$$\sigma = A_{rs}(1 - f_a)G_{ts}, \quad (2-7)$$

where A_{rs} is the effective area of the scatterer, f_a is the fraction of the signal power absorbed by the target, and G_{ts} is the gain of the scatterer in the direction of the sensor.

This defines the scattering properties for a single target. Any real world target is composed of a great number of individual targets, thus the scattering characteristics of targets are most often described in terms of the average value of the individual scattering cross-sections per each of their unit areas:

$$\sigma^0 = \frac{\sum_{i=1}^N \frac{\sigma_i}{\Delta A_i}}{N} \quad (2-8)$$

In this equation, σ^0 is called the *differential scattering coefficient* or, more commonly, simply the *scattering coefficient* and, with this term defined, the average power received by a transmitter can be defined by the area-extensive form of the radar equation:

$$\bar{P}_r = \frac{\lambda^2}{(4\pi)^3} \int_{\text{area illuminated}} \frac{P_t G^2 \sigma^0 dA}{R^4} \quad (2-9)$$

The properties which affect σ^0 for different targets are geometry, roughness and dielectric characteristics.

2.5.2 Dielectric properties of snow

Microwave backscatter is sensitive to the freeze/thaw state of water. This sensitivity is due to the different dielectric properties of ice and water. A material's dielectric properties are defined by two terms, one real and one imaginary, which together make up the *relative permittivity* of the material, ϵ (Ulaby et al, 1986). It is defined as the ratio $\epsilon_{\text{material}}/\epsilon_0$, where ϵ_0 is the *permittivity of free space*, i.e., a vacuum, and $\epsilon_{\text{material}}$ is the permittivity of the material in question. Physically, relative permittivity is the ratio of the capacitance of a capacitor with the material in question between its plates to a capacitor with a vacuum between its plates. Some sources prefer the symbol ϵ/ϵ_0 to designate relative permittivity (personal communication, Kyle McDonald,, Jet Propulsion Laboratory) while the texts by Ulaby, et al and others prefer simply ϵ . ϵ is complex and has a real part, ϵ' , and an imaginary part, ϵ'' such that $\epsilon = \epsilon' + \epsilon''$. Ulaby et al (1986) designate ϵ' to be the *dielectric constant* and Gray and Male (1981) designate both ϵ and ϵ' to be the dielectric constant. All sources call ϵ'' the *dielectric loss factor*. In general, materials with high dielectric constants interact with and are less transparent to electromagnetic radiation than materials that have low dielectric constants.

Both ϵ' and ϵ'' vary with the wetness of snow. At microwave frequencies in the K_u band, ϵ for liquid water is significantly higher than for ice. As a result, ice is nearly transparent to microwave radiation at the frequency employed by NSCAT and liquid water is not. Rather than passing directly through with little interaction as it does with ice, microwave radiation interacts with liquid water. The relationship between a material's response to incident radiation and the dielectric properties of the material are complicated and the reader is referred to the three volumes by Ulaby (Ulaby et al, 1981; 1982; and 1986), where the topic is described in exhaustive detail. Generally, though, when radiation is incident upon snow, some of the radiation is reflected and some is absorbed. How much is reflected and how much is absorbed depends on physical conditions which include the amount of liquid water present in the snow as well as other physical properties such as the characteristics of the crystals making up the snow. Cummings (1952) made some of the first investigations of the dielectric properties of snow at microwave frequencies and other investigators (Hallikainen et al, 1986; Linlor 1980; Linlor et al 1981; Ulaby and Stiles 1980) have expanded on that work to the point that the response of microwave backscatter to parameters such as temperature, density, particle size and wetness are reasonably well characterized.

The observable difference between backscatter in frozen and thawed snow varies depending on the frequency of the signal and the roughness and dielectric properties of the snowpack.

Roughness of the surface is important because, in general, the facets of a rough surface reflect more of a microwave signal when the signal wavelength is similar to the length of the object's

cross-section as it faces the sensor. NSCAT, for instance, operated with a wavelength of about 2.15 cm and was therefore sensitive to objects whose cross section was about 2.15 cm when seen from the instrument's observation angle.

2.5.3 Volume scattering

Radiation incident on dry snow is scattered back in nearly all directions at an intensity which decreases only slightly with increasing incidence angle. This occurs because the radiation penetrates into the snow pack and scatters back from multiple objects (like ice particles) at various depths within the pack (Figure 2-7). Scattering from dry snow by

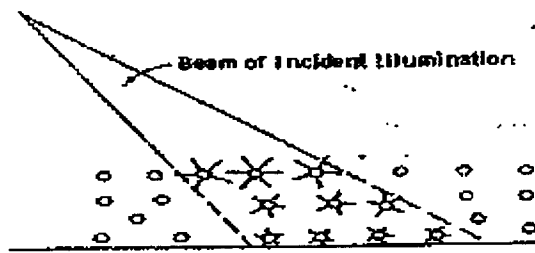


Figure 2-7. Illustration of volume scattering from Ulaby et al, 1982.

side-looking satellite sensors is therefore stronger than scattering from bare soil. This can be seen in Figure 2-8 which shows a timeline of NSCAT backscatter from a location at 94.3125°W by 47.8125°N in northwest Minnesota as the snow accumulated and then melted. This scattering mechanism for dry snow is called volume scattering (Ulaby et al, 1982).

NSCAT operated at a wavelength of 2.15 cm which is known as K_u -band. In general, K_u -band backscatter at a steep incidence angle is stronger from a surface with a significant amount of dry snow (snow which is completely frozen and thus contains very little entrained liquid moisture) than from a snow-free surface. This stronger signal is due to volume scattering. Microwave radiation interacting with Earth will not penetrate as far into the surface as it will into dry snow. As a result, the radiation scattered from a soil surface will be scattered most strongly in a direction corresponding to the angle of a beam of light reflected by the surface if the surface were a mirror (the *specular reflection angle*), and not very strongly at other angles.

For satellite-mounted radar devices such as the NSCAT and QuickSCAT scatterometers the transmitter and sensor are in the same location. Radiation scattered back to such a sensor near the specular reflection angle is only seen by the sensor if it is nadir-pointing, i.e., oriented straight down. If the sensor looks at the surface off-nadir, objects which scatter mostly in a direction close to the specular reflection angle will appear darker than objects which scatter signal back to the sensor.

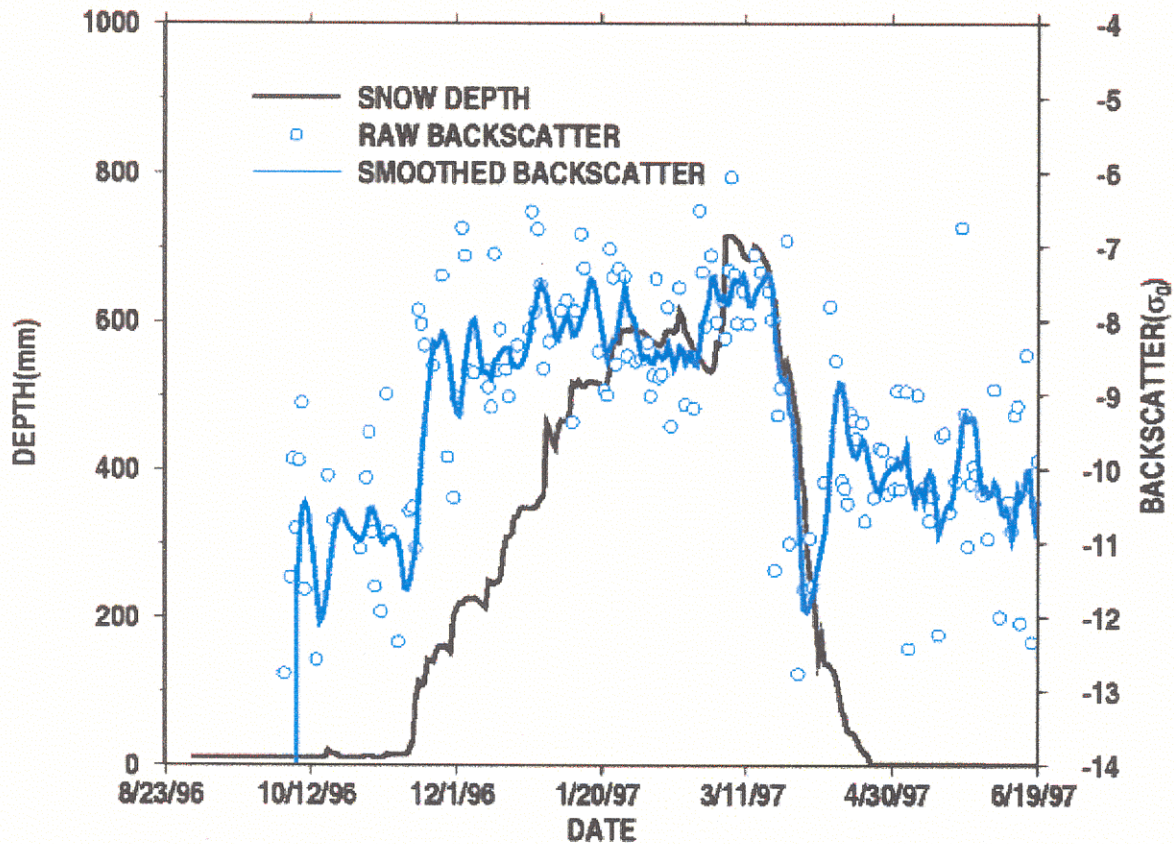


Figure 2-8. Timeseries of normalized backscatter cross section (σ^0) in dB and snow depth in mm for a pixel located at 94.3125°W by 47.8125°N in northwest Minnesota for the period from October 1996 to June 1997. The arrival of snow on the ground in late November correlates with an upward shift in σ^0 from -11dB to about -8dB. This first shift is due to a transition from volume scattering by bare soil to volume scattering by dry snow. The second shift occurs with a dramatic drop from -8dB to -12dB on about March 19th and then a return to about -10.5dB a few days later. The second drop is due to the appearance of liquid water in the snow near the surface as the snow begins to melt away. The drop is caused by the change from volume scattering to surface scattering.

2.5.4 Surface scattering

Surface scattering occurs when the properties of a surface cause interaction of the incident radiation with the surface. When K_u -band radiation is incident upon a snow pack with liquid water entrained in the surface layer, most of the radiation is either absorbed by the liquid moisture or reflected. Snow is usually rough enough that radiation does not reflect specularly but the radiation that does reflect rather than being absorbed generally reflects more strongly near the specular reflection angle unless the surface is very rough (see Figure 2-9). As a result, a region where radiation interacts by surface scattering will reflect less of the transmitted signal back to a side-looking instrument than a region where volume scattering is the dominant mode of interaction with incident radiation. In other words, snow with entrained liquid water scatters back less K_u -band radiation than dry snow because the transition from dry to wet snow creates a shift in scattering mechanism from volume to surface scattering.

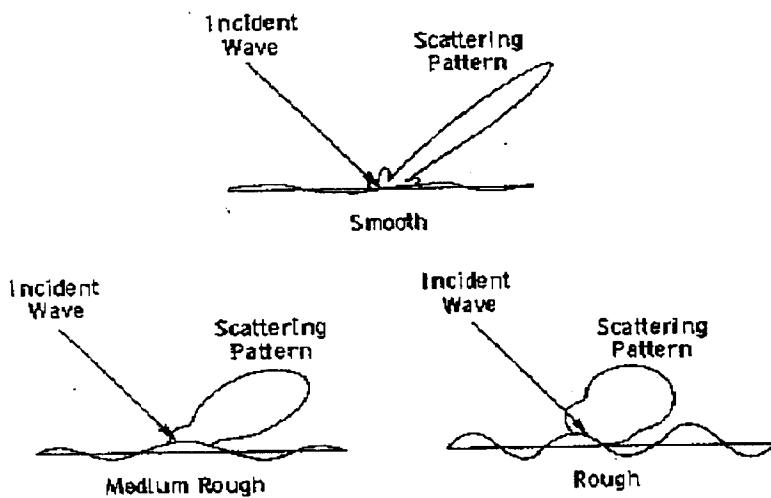


Figure 2-9. Illustration of surface scattering from Ulaby et al, 1982.

This shift in signal is particularly noticeable as a snowpack melts. When a snowpack begins to melt, liquid moisture appears at the surface and is entrained around the ice particles making up the snow. This liquid moisture interacts with incident radiation whereas the surface of a dry snow pack would be transparent. This causes a shift from volume to surface scattering which results in the telltale drop in K_u -band backscatter when a snow pack begins to ripen prior to melting.

2.5.5 Canopy vegetation effects.

In areas with dense foliage, the freeze/thaw state of the leaves and branches in the vegetation above the ground surface contribute to the backscatter response by volume scattering while frozen and by surface scattering when thawed. Way et al (1994) examined this interaction in detail at several wavelengths and with different vegetation species. In areas where canopy vegetation is sparse and snow is on the ground, however, the observed backscatter represents the state of the snow rather than the vegetation. Tilled farmland and prairie dominate the north central U.S. except in northwest Wisconsin, where mixed cover and deciduous broadleaf forests dominate (Figure 2-10). During the winter, the terrain other than in northwest Wisconsin is largely free of vegetation dense enough or of sufficient stalk or stem thickness or height to interfere with the signal from the ground surface as seen by microwave backscatter. Backscatter over the region was therefore assumed to be dominated by the characteristics of snow, where present, and soil, otherwise.

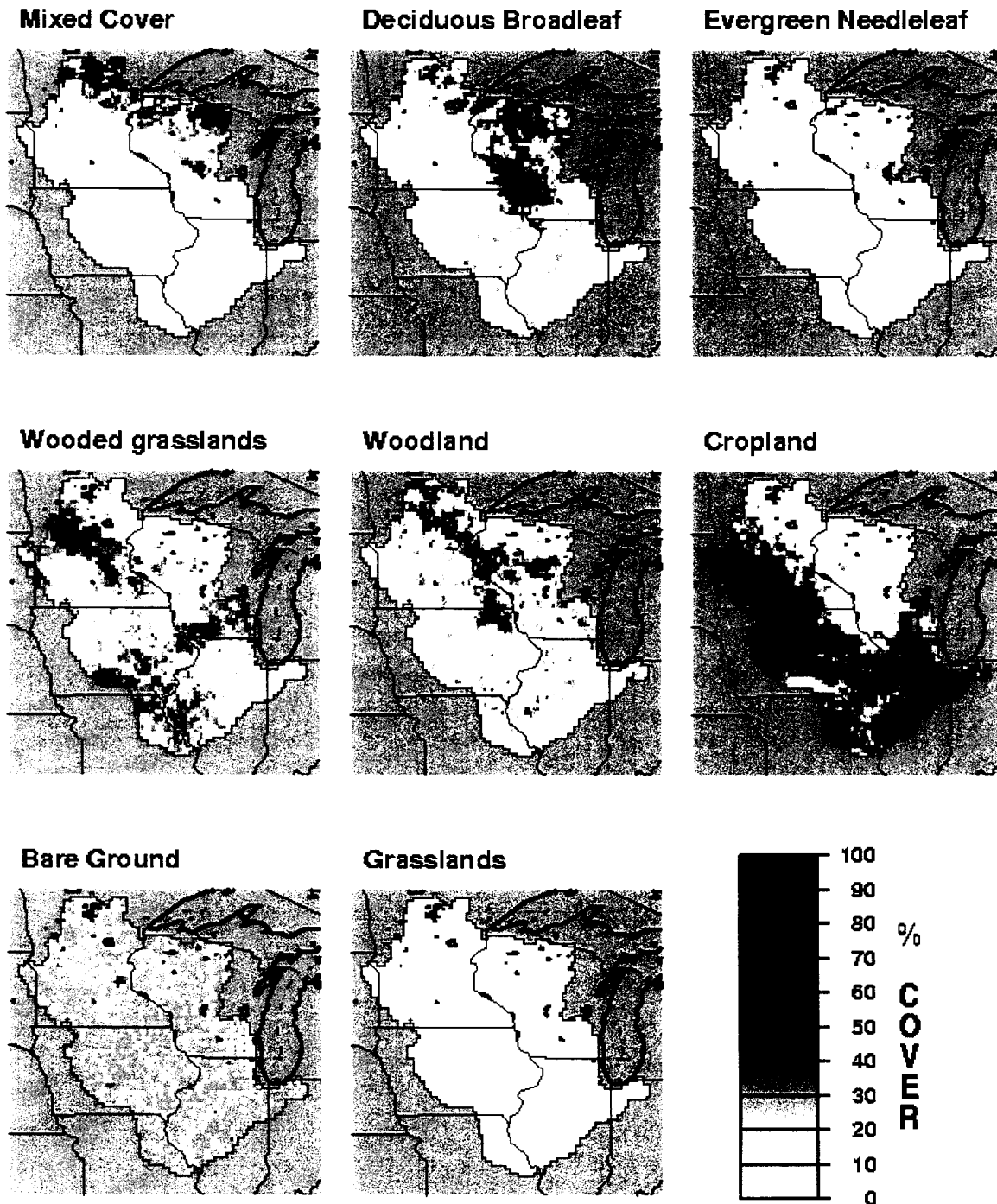


Figure 2-10. Coverage fraction for 8 land cover categories (Hansen et al, in press). Color represents coverage percent for each grid cell. Each grid cell is an $1/8^{\text{th}}$ degree on a side.

2.6 Freeze/thaw change detection

Previous research has investigated the relationship between freeze/thaw state of snow and other materials and microwave backscatter. Table 2-1 summarizes the findings of these previous investigations. Some of these authors describe the observed relationships in a way that could be inverted as a freeze/thaw change detection algorithm. In general, the studies listed in Table 2-1 found that transitions from a frozen to an unfrozen state, and vice versa, correspond to a shift in backscatter response. This is consistent with the explanation of this relationship in Section 2.4.2. The magnitude and direction, positive or negative, of the backscatter shifts varies with the surface properties of the target region and the wavelength of the sensor. Among the previous investigations, only three (McDonald et al (1999), Frolking et al (1999) and Kimball et al (2000)), used K_u-band backscatter. McDonald et al (1999), note a 3-5 dB drop in backscatter associated with the onset of thawing conditions in five stations in the BOREAS study area in northern Saskatchewan. Frolking et al (1999) proposed detecting the onset of thawing conditions in the same locations by looking for the first sustained drop of 2dB or more in a five day retrospective moving average of backscatter measurements. Kimball et al (2000) expanded the scope of the first two papers and predicted freeze/thaw conditions across Alaska by using a threshold backscatter level. The threshold level was calculated as the average of a mean summer and a mean winter value. This method has the advantage that it calculates a different threshold for each pixel based on the time series for that pixel.

Table 2-1. Freeze/thaw state change detection algorithms based on microwave backscatter.

Source	Instrument	Medium and Location	Change detection algorithm
McDonald, et al, 1999	NSCAT	Landscape, Saskatchewan	Observed 3 to 5 dB decrease with springtime thaw
Kimball, et al, 2000	NSCAT	Soil and canopy, Alaska	Threshold at mean of mean June 19-26 backscatter and mean Jan 1-10 backscatter - corresponds well with canopy thaw but occurs after snowmelt onset: backscatter < threshold indicates frozen & backscatter >= threshold indicates thawed
Frolking, et al, 1999	NSCAT	Snow and soil, BOREAS	Anomalous first differences of smoothed signal
Wismann and Boehnke, 1996	ERS-1 Scatterometer	Snow, Greenland	Observed 10db decrease in 3 day mean upon thaw
Way, et al, 1994	AirSAR polarimetric L-band SAR	Canopy and soil, Alaska	Tree species specific ranges for frozen and thawed conditions
Way, et al, 1997	ERS-1 C band polarimetric SAR	Vegetation, BOREAS	Observed 3dB decrease in backscatter upon vegetation freezing
Rignot and Way, 1994	ERS-1 C-band SAR	Snow, vegetation, canopy in Alaska	Backscatter coefficient decrease of 3dB from DOY 224 level corresponds with freeze
Boehnke and Wismann, 1996	ERS-1 Scatterometer	Soils, Siberia	Threshold at mean of mean summer backscatter and mean winter backscatter: two consecutive days when backscatter exceeds threshold indicates thaw - this is a very coarse method
Rignot, et al, 1994	ERS-1 SAR	Taiga forest, Alaska	3dB decrease in backscatter observed when soil and vegetation freeze.
Baghdadi, et al, 2000	RADARSAT	Wet snow, Canada	Expected mean wet snow backscatter would be 3dB less than mean dry snow backscatter - results better for smaller surface roughness and smaller incidence angles (suggests using RADARSAT beam S1 and not beam S7)
Koskinen, et al, 1997	ERS-1 SAR	Snow melt	Wet snow backscatter is 3dB less than dry snow backscatter
Pulliaainen, et al, 1998	ERS-1 Scatterometer	Soil, boreal forests in Europe	Sophisticated inversion algorithm narrow applicability

2.7 Study area

The upper Mississippi River basin was chosen as the study area for this project because the hydrology of the basin is strongly affected by snowfall and frozen soil processes, and because a macroscale hydrology model had already been implemented for the basin (Cherkauer and Lettenmaier, 1999). The upper Mississippi River basin is one of the Large Scale Areas (LSAs) in the GEWEX Continental-Scale International Project (GCIP) (Coughlan and Avissar, 1996). The upper Mississippi River basin was also attractive because of the high spatial density of climatological stations there.

2.8 The VIC hydrological model

The VIC (Variable Infiltration Capacity) hydrological model is a macroscale land surface hydrology model that balances water and energy in each grid cell. Liang, et al (1994) present the defining equations model's water and energy fluxes. Each grid cell within VIC can contain several land cover categories including a bare soil category. In basins where orographic effects play a role, each cell is also divided into elevation bands, though this option was not exercised for the upper Mississippi River basin because the region is quite flat. The model balances water and energy for each land cover category and then aggregates output variables by the area fraction associated with each category. Partitioning between subsurface runoff and baseflow follows the Arno formulation given in Francini and Pacciani (1991). Runoff and baseflow from each grid cell are then routed together through an explicitly defined routing network to an outlet point (Lohman et al, 1998). VIC represents soil process with a user defined number of soil layers

(Cherkauer and Lettenmaier, 1999) but all recent implementations of the VIC model including the one described here employ three soil layers.

VIC simulates snow accumulation and melt with a two layer scheme described by Cherkauer and Lettenmaier (1999), which uses an energy balance approach similar to the point snow melt model developed by Anderson (1976). The snowpack accumulation and ablation model is described here because it is central to the adaptations made to the VIC model to allow updating of snow state variables. For more details the reader is referred to Storck (2000). Most of the description included here is taken from Storck (2000).

Energy in the snow model is balanced following the general formula,

$$\rho_w c_s \frac{dWT_s}{dt} = Q_r + Q_s + Q_e + Q_p + Q_m \quad (2-10)$$

where ρ_w is the density of water, c_s is the specific heat of ice, W is the water equivalent of the snowpack surface layer, T_s is the temperature of the surface layer, Q_r is the net radiation flux, Q_s is the sensible heat flux, Q_e is the latent heat flux, Q_p is the energy flux given to the snow via rain or snow, and Q_m is the energy flux given due to liquid water refreezing or taken during melt.

Energy fluxes into the pack are defined as positive. If the flux terms are expressed in W/m^2 then W is given in meters. The application of this balance over the discrete amount of time defined by a model time step (Δt) uses a forward-looking finite difference scheme, as follows.

$$W^{t+\Delta t}T_s^{t+\Delta t} - W^tT_s^t = \frac{\Delta t}{\rho_w c_s} (Q_r + Q_s + Q_e + Q_p + Q_m) \quad (2-11)$$

All the energy terms except Q_m , the term for energy lost due to snow melting or gained due to liquid water freezing, are taken as terms in a balance at the surface layer of the snow pack, which is defined by a user-specified maximum thickness in snow water equivalent. The values for the flux terms are for the current time step. A second layer of the model exists below the surface layer when the snow on the ground is greater than the surface layer maximum thickness. Otherwise only the surface layer is present. The second layer is referred to as the lower layer in the remainder of this section, although Storck (2000) refers to it as the pack layer.

The model starts each time step with temperature and depth of the snow pack at the end of the previous time step (initial conditions at the start of the model run). New precipitation as rain or snow and values for net downward radiation, sensible heat and latent heat fluxes during the time step constitute the forcings to the snow model. Precipitation is partitioned as either rain or snow using the scheme suggested by the US Army Corps of Engineers (1956):

Table 2-2. Rain/snow partitioning of precipitation

Air Temperature, T_a	Resulting partitioning of precipitation (P), as snow (P_s) or rain (P_r)
$T_a \leq T_{min}$	$P_s = P; P_r = 0$
$T_{min} < T_a < T_{max}$	$P_s = \frac{T_{max} - T_a}{T_{max} - T_{min}} P; P_r = P - P_s$
$T_a \geq T_{max}$	$P_s = 0; P_r = P$

The model adds new precipitation to the pack as moisture and as accompanying energy content and distributes the mass and energy of the pack plus the new precipitation into the surface and lower layers. Water can be present in the pack as snow, that is, as particles of ice, or as liquid water entrained in the pack. The change in the amount of water present as ice and as water includes precipitation and exchange between the two phases. The exchange is derived from the amount of net energy, Q_{net} available after solving for energy exchange in the surface layer.

The process for determining Q_{net} is more elaborate than a simple summation of energy terms. The model calculates Q_{net} by initially assuming that the final surface layer temperature at the end of the balance will be 0 degrees. The calculation also determines available energy for refreezing or melting. If the result of the calculation is that Q_{net} is equal to zero, the initial assumption was correct. The model then melts the appropriate amount of snow from the surface layer and adds that melted water to the water entrained in the surface layer or freezes the appropriate amount of liquid water. If the liquid water after melting is more than can be held by the snow matrix, the remainder drips down to the lower layer, if enough snow is in the pack to include a lower layer, or to the ground, otherwise.

If the value for Q_{net} is less than zero, the initial assumption was incorrect and the model iteratively solves the snow pack energy balance with successively more negative surface layer temperatures until a surface layer temperature is found that balances the energy within the

surface layer within a specified tolerance. The model then calculates Q_{net} again using the new value for surface layer temperature. In such a case, the surface layer was necessarily colder than freezing and, if liquid water was present in the pack, some or all of that liquid water will freeze and the net energy will be energy lost by the pack in freezing the water. If all the water in the pack is frozen and Q_{net} is not exhausted, the remaining Q_{net} decreases the temperature of the lower layer, if present.

Once the model has solved the surface layer energy balance, the total masses of liquid water, ice and cold content for the pack are distributed again to the surface layer and lower layers. The last step in the process is to calculate a new temperature for both layers upon exiting the snow melt routine, based on the masses and cold contents calculated for the layers.

2.9 Updating

The central focus of this thesis is to evaluate the potential for updating model predictions of snowpack processes using freeze/thaw state predicted from microwave scatterometry. Updating is one method of data assimilation which is an already well-explored area of research (Houser et al, 1998; McLaughlin 1995). Assimilating data such as surface moisture and temperature estimations from remote sensing devices into land surface models is a particularly active area of research. Updating refers to changing the values of one or more state parameters within a model to reflect observations. The observations used for updating may not be at the same space-time resolution as the model, and may be subject to error. The state variables of a model are variables

such as snow depth and soil moisture that are usually set prior to the first model time step as initial conditions and are then calculated based on the model formulation and forcing data. In this context, one way of thinking about updating is as a way of re-initializing the model during run time (McLaughlin, 1995).

Approach

2.10 Overview

As described in Chapters 1 and 2, the goal of this thesis is to evaluate the hydrologic utility of microwave scatterometer for updating of a macroscale hydrologic model. The two main elements of the approach are to develop a scheme for updating snow parameters within a macroscale hydrologic model (VIC) and to develop a method for converting microwave backscatter observations into estimates of hydrologic state variables or related conditions in a form usable by the model. Scatterometer data available for development and testing of the procedure were provided by NSCAT for the winter of 1996/1997 and by QuikSCAT for the winter of 1999/2000. Model predictions were compared with both surface-based observations of snow depth over the upper Mississippi River basin, and with visible satellite imagery of snow extent over the same area. The remainder of this chapter describes the methods used in the preparation and analysis of both the scatterometer data and surface observations.

2.11 Microwave backscatter

A drop in K_u -band backscatter has been shown to be correlated with the ripening of snow which occurs prior to and during snow melt (Stiles and Ulaby, 1980; Koskinen et al, 1997). Based on this relationship, snow freeze/thaw state has been extracted from microwave scatterometer data (Frolking, et al, 1999; Kimball, et al, 2000; Way, et al, 1997). All of these earlier investigations have, however, been for latitudes higher than that of the Upper Mississippi River basin, in places where winters are generally colder and mid-season thawing and refreezing occurs less

frequently. Therefore, as a first step an exploratory analysis was conducted of the raw backscatter to evaluate spatial and temporal patterns. The methods used in this preliminary analysis are described in this chapter.

2.11.1 Incidence angle correction to NSCAT data

The NSCAT backscatter data were contained in the Merged Geophysical Data (MGD) product released by the Jet Propulsion Laboratory. Each set of the MGD product represented a complete revolution around the Earth. Within each revolution, the data were arrayed along the track of the orbit in rows containing 80 pixels in each row making up the track. Each row extended out on both sides of the sensor from the border of the un-imaged area beneath the sensor out to the edge of the sensor swath (see Figure 3-1). Each pixel represents the backscatter coefficient (σ_0) value from an area roughly 25 km on a side. As discussed in Section 2.5, the strength of backscatter varies with incidence angle, which, in-turn, varies with distance off-nadir. To account for this distortion, a routine was employed by the Jet Propulsion Laboratory which used the relationship between incidence angle and backscatter to normalize backscatter to an incidence angle of 40 degrees. As part of this process, the data were also resampled to a regular $1/10^{\text{th}}$

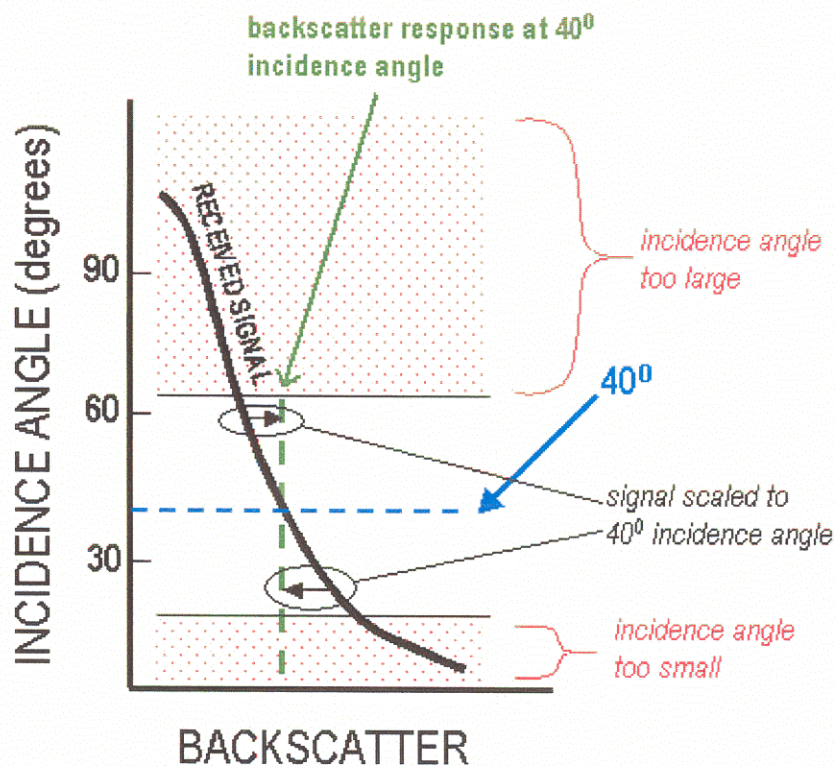


Figure 2-11. Incidence angle correction for NSCAT backscatter. For each row of pixels along the ground track of the satellite's orbit, a best fit relationship between incidence angle and backscatter coefficient was used to scale all backscatter so that all backscatter values could be compared as if the incidence angle was 40° .

degree grid. Subsequently, the 1/10th degree images were resampled to the 1/8th degree grid used in the VIC model via a nearest neighbor algorithm.

2.11.2 Smoothing and filling backscatter time series

2.11.2.1 NSCAT

After incidence angle correction, the time series of backscatter measured by NSCAT showed some trends in time, but contained too much scatter to allow extraction of a signal related to surface conditions (see comparison of raw and smoothed time series in Figure 2-7). Also, portions of the study area were unsampled on some days (see Figure 2-4). The data therefore required smoothing in time and filling in space.

When images of an entire area were part of an analysis previous researchers (e.g., McDonald et al (1999) and Kimball et al (2000)) created complete images of certain study areas by building mosaics out of several overpasses' worth of data. The mosaic routine they employed assembles all the values reported for a given pixel within a specified time prior to the target date and uses the first observed value for that pixel. This method was useful for creating images and animations from the data.

In the upper Mississippi River basin, however, the amount of swath overlap from flyover to flyover was significantly less than in higher latitude studies (e.g., McDonald, et al (1999);

Kimball, et al (2000); Frohling, et al (1999)) because both the NSCAT and QuikSCAT platforms are polar orbiting and progressively less swath overlap occurs away from the poles. This effect was responsible for the gaps in coverage mentioned earlier. Therefore, while some of the previous applications were able to composite entire study areas within as little time as 24 hours, in the upper Mississippi basin, two days' worth of flyovers are necessary and, even so, some parts of the basin remain unfilled. For this reason, the mosaic method was rejected as a method of spatial filling and it was determined to be most practical to fill the data in space while smoothing the data in time using a 5 day retrospective moving average.

For smoothing in time at individual locations, Frohling et al (1999) and Kimball et al (2000) employed a retrospective moving average at locations in the northern latitudes. A retrospective moving average is the average of the values for the given day and a specified number of previous days. The frequency of flyovers by NSCAT in those areas was sufficient that one backscatter value per day was available generally and only for a few days out of several months' worth of data was it necessary to use less than five days' worth of data to produce the moving averages. NSCAT imaged pixels in the upper Mississippi River basin significantly less often than once a day, though. As a result, generally only two or three backscatter values were available in any given retrospective five day window. Therefore, the moving average scheme used in the previous studies was modified to calculate an average for each day using as many observations as were available within a window consisting of the prior four days plus the current day (Figure 3-2). In this way, a smoothed time series was developed for each pixel in the study area.

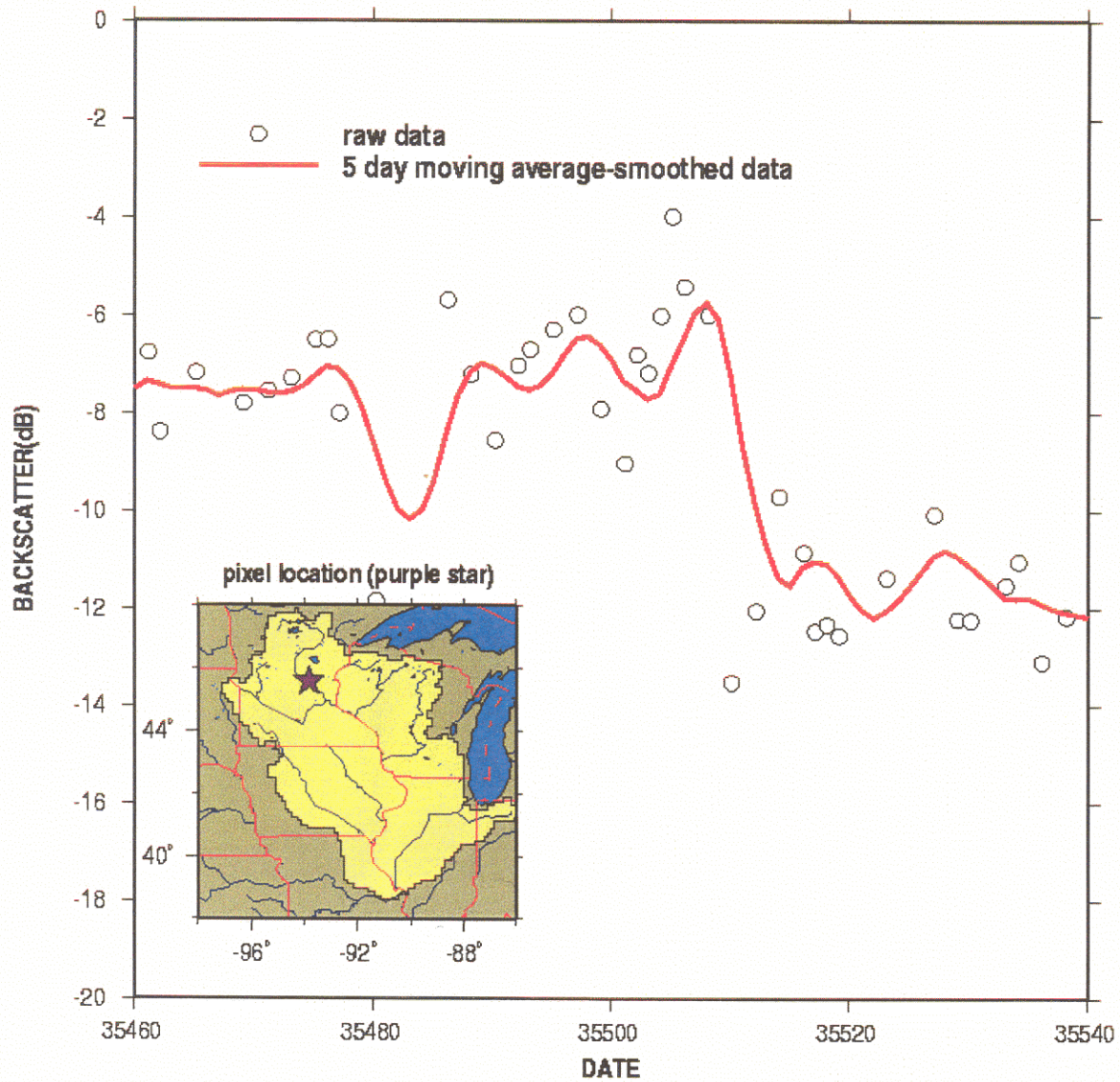


Figure 2-12. Backscatter for a single pixel centered at 93.85°W, 45.55°N smoothed with a 5 day retrospective moving average. The black circles are the raw data. The red line is the 5 day retrospective moving average.

The NSCAT data were then processed as eight subsets, defined by one of four beams (fore, aft, midship horizontally polarized and midship vertically polarized) and by whether the data were recorded on ascending or descending orbital passes as described in Section 2.3.2.1. The selection of the specific data sets used for analysis is described in Section 3.2.3.

2.11.2.2 QuikSCAT

QuikSCAT backscatter measurements were processed in a manner similar to that used for NSCAT. The Jet Propulsion Laboratory processed the data to a regular grid with cell dimensions of one-quarter degree. This grid was then disaggregated to the VIC 1/8th degree resolution using a nearest neighbor approach. Subsequently, each pixel's time series was smoothed using the same five day retrospective moving average algorithm as was used for the NSCAT data.

2.11.3 Choice of channel

2.11.3.1 NSCAT

The signals from the four NSCAT beams (see Section 2.4.2.1) were initially examined separately to determine if any particular beam or combination of beams was of particular interest (Figure 3-3). Although the signal strength of the different beams varied relative to one another at times, these variations did not appear to coincide with any shift in freeze/thaw state, which indicated that no single beam or set of beams had a more

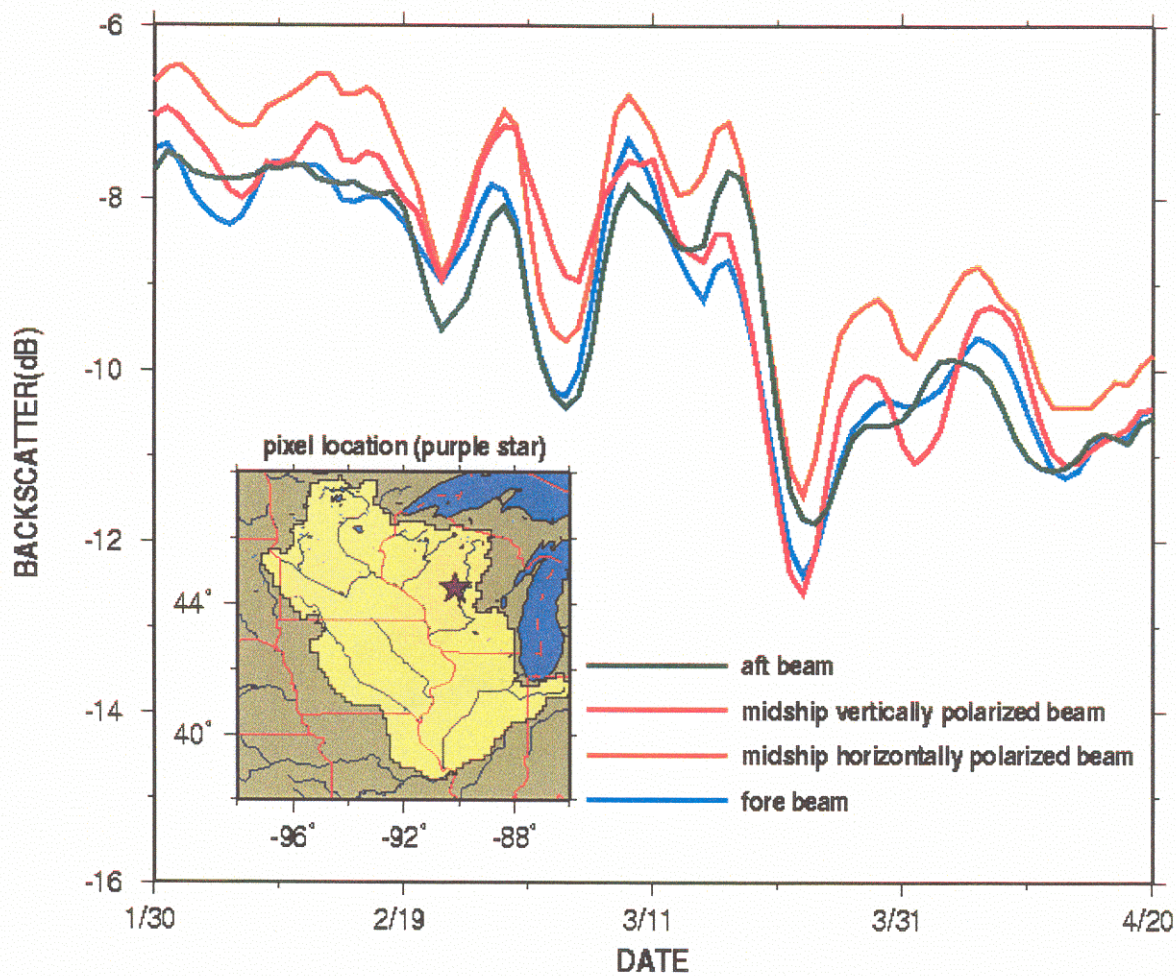


Figure 2-13. Comparison of timelines of NSCAT backscatter from all four beams, smoothed with a 5 day retrospective moving average for a single pixel centered at 90.15°W and 44.45°N.

significant response to surface conditions than the others. For this reason, all analyses were performed on only one of the beams, the forward oriented (fore) beam, rather than examining the response of all of the beams.

Images of the study area were taken on either an ascending or a descending orbit. NSCAT imaged the area at roughly 10 AM local time on descending orbits and 10 PM local time on ascending orbits. The thermodynamic state of snow is often differs between the morning and the evening, especially as a pack ripens and begins to melt. Therefore, the NSCAT backscatter images were further subdivided into ascending and descending orbits using the time stamp on the data. The choice of only the fore beam measurements therefore limited analysis to two data sets: the fore beam data measured on ascending orbits and the fore beam data measured on descending orbits. As with the NSCAT data, the QuikSCAT data from ascending and descending orbits was processed and examined separately.

2.11.4 QuikSCAT

QuikSCAT measures backscatter in two channels, one horizontally and the other vertically polarized. Consistent with previous findings (Stiles and Ulaby, 1980), an examination of the two channels similar to that performed on the NSCAT data showed little difference in the response to surface conditions. Therefore, further analysis was performed solely on the horizontally polarized channel.

2.11.5 Freeze/thaw change detection

Previous research has described algorithms for inferring freeze/thaw state of snow (as well as soil and vegetation) from microwave backscatter, as described in Section 2.4.4. and Table 2-1. The method described in Kimball et al (2000) was chosen as a starting point because it calculates a threshold which automatically adjusts to the range of backscatter and the magnitude of seasonal variation in backscatter of each pixel separately. Kimball et al (2000) used measurements from the period June 19-26, 1997 to calculate the mean summer backscatter value for 1997 and measurements from the period January 1-10, 1997 to calculate the mean winter backscatter value.

Following this methodology, freeze/thaw state was predicted for the upper Mississippi River basin from NSCAT backscatter for the winter of 1996 using the same periods for determining mean summer and winter backscatter values as were used by Kimball et al (2000). The product is a time series for each model grid cell with a binary flag that indicates the freeze/thaw state of the land surface in that pixel on each time step in the series. This time series was evaluated as a way of updating snow surface freeze/thaw state as described in Section 3.5.3.

2.12 Meteorological data

2.12.1 Snow depth

Measurements of snow depth at cooperative observer stations are made at irregular intervals and archived by the National Climatic Data Center (NCDC) as described in Section 2.2.4. These data are reported as frequently as daily but often have gaps of a week or more. In order to use these data for model updating, the records at each station were filled between reporting dates to create continuous time series of snow depth. Dates without observations were filled with the most recent reported record. The data were then re-sampled to the 1/8th degree grid used in the VIC model using the SYMAP algorithm (Dougenik and Sheehan, 1979).

The result of this procedure was a set of snow depth images over the study area for every day during the winters of 1996-97 and 1999-2000. Although the temporal persistence of the constructed images is greater than that of the (point) observations, due to the procedure used to fill missing data, the images are nonetheless useful as a basis for comparison of long-term properties of snowpack evolution, e.g., recession of the snow line northward in the spring, and/or major snow accumulation events.

2.12.2 Maximum Daily Air Temperature

Maximum daily air temperature data were extracted from NCDC archives. Images for each day in the study period were created using the SYMAP algorithm in the same way snow depth images were created with the exception that no filling between dates was necessary.

2.12.3 Snow surface temperature and liquid water content

Output from the VIC model was used to provide proxy data for snow surface temperature and liquid water content. These variables are more directly comparable to snow surface freeze/thaw state than is snow depth but direct observations are not available. The VIC model calculates snow properties using a two layer physically based algorithm (Cherkauer and Lettenmaier, 1999) that is driven by maximum and minimum daily air temperature, precipitation and wind.

2.13 Backscatter comparisons with meteorological conditions

After smoothing and filling the time series for each pixel, daily images were constructed and plots of the following surface meteorological variables were prepared for comparison:

- Daily snow depth
- Maximum daily air temperature
- Snow surface layer moisture content, 3 hour frequency
- Snow surface layer temperature, 3 hour frequency

Relationships between these variables and microwave backscatter were examined over the two winters studied (1996/97 and 1999-2000) and for three specific events in the winter of 1996/97:

an early winter thaw, a cold snap and a late season snow storm. The events were selected by examination of plots of daily maximum air temperature for the

winter of 1996/97. The analysis of specific events is intended to help understand the relationship between the meteorological conditions that accompany various backscatter signatures. The results of these comparisons are described in Sections 4.3 and 4.4.

2.14 Updating

The VIC model was modified so that snow state variables could be updated within the model. Specifically snow depth, snow pack liquid water content and snow surface temperature were updated. The direct insertion method was used, which assumes that model predictions are subject to error while observations are error-free. The updating algorithm assumes no *a priori* knowledge of error covariances associated with the model or the updating observations, as is required by schemes based on the Kalman filter (McLaughlin, 1995). At each model update time, the updating routine thus replaces the model-predicted state variable with the corresponding observation. The method was applied in a preliminary trial using the constructed gridded fields of snow depth observations (see Section 3.3, Meteorological Data), and was subsequently used to update model-predicted liquid water content of the snowpack and snow surface temperature with microwave backscatter. The remainder of this section describes both the scheme used for the preliminary trial as well as the updating using microwave backscatter.

2.14.1 Preliminary trial-updating snow depth

Before proceeding to an updating scheme based on microwave backscatter, the potential for improving model predictions by updating in general was evaluated. As a test case, gridded fields of historical snow depth as archived by NCDC were used to update the VIC model at irregular intervals.

Comparing model output with a data set that has been used to update the model, of course, shows nothing about the updated model's capabilities. In addition, persistence is a problem, because predictions are "contaminated" following an update for several time steps. Therefore, the model was updated only 18 times during the winter season so that there was an average of 5 days between model updating times during the winter. Model performance was evaluated using comparisons with snow depth observations for dates other than those on which the model updating occurred.

For the updating trial with historical snow depth data the model was updated roughly every five days. Snow water equivalent was then calculated by multiplying the snow depth after updating by the most recently model-calculated density. When updating added snow to a grid cell that was free of snow prior to updating, the density value used was either that calculated the last time snow was present in the cell, or if snow was never previously present in the cell, the value used by the model for new snow. If the total snow water equivalent for the cell after updating was greater than the maximum allowed snow water equivalent for the surface layer in the snow

model, the excess water equivalent was assigned to the lower or "pack" layer in the snow model. The moisture content was then calculated for the two layers separately by multiplying the new snow water equivalents for the respective layers by the moisture fraction for each layer prior to updating. The model predictions of snow were then compared with historical predictions on the basis of summary statistics of the difference between observations and model predictions with and without updating.

2.14.2 Updating freeze/thaw state

Following the evaluation of the updating scheme, a method was developed to allow updating based on microwave backscatter measurements. The model was adapted to update snow freeze/thaw state based on the freeze/thaw binary signal derived from microwave backscatter measurements. The variables modified within the model to reflect shifts in freeze/thaw state were snow surface layer moisture content and snow surface layer temperature, as indicated in Table 3-1.

Table 2-3. Model freeze/thaw updating scheme.

FREEZE/THAW BINARY FLAG	SNOW SURFACE LAYER VARIABLES	
	LIQUID WATER CONTENT	TEMPERATURE
FROZEN	→ 0.0	NO CHANGE
LIQUID	→ <i>MAX_LIQUID_WATER_CAPACITY</i>	→ 0.0° C

MAX_LIQUID_WATER_CAPACITY = 5% of snow layer depth measured as snow water equivalent

This scheme was used to update the model for winter of 1996/97 based on NSCAT backscatter measurements and the winter of 1999/2000 based on QuikSCAT backscatter measurements. By contrast with the scarce number of events used for updating in the case of snow depth, the model

was updated over 270 times during the winter of 1996/97. Updating freeze/thaw state in the manner described in Table 3.1 has much less effect on the conditions within the model than updating snow depth, however. The model was therefore configured to undergo updating frequently in order maximize the effect of the updating scheme to the degree that the effects would be detectable.

2.15 Analysis of results

2.15.1 Spatial comparisons

The predictions of snowmelt made by the updated model were compared with observed snow depth both spatially and as space-time averages. For evaluation of spatial predictive accuracy, images of predicted snow depth across the basin were compared with plots of the snow depth observations prepared as described in Section 3.3.1. The differences between predicted and observed snow depth for each model grid cell were also plotted for several representative days. The qualitative criteria for evaluation of the accuracy of predictions were the extent of snow, the timing of snow melt in different areas within the study area and the magnitudes of the snow depth where the snow is deepest. All of these characteristics can strongly affect snow melt volume and timing.

2.15.2 Summary statistics

Summary statistics were calculated to evaluate overall predictive accuracy with and without updating for both the winter of 1996/1997 and the winter of 1999/2000. Root mean square error (RMSE) and normalized root mean square error were calculated across all days and all cells.

The mean fractional error (MFE) for all cells for each day was also calculated and the mean of the MFE values for each day was reported as a single statistic for each set. Mean fractional error for each day was calculated as follows.

$$MFE = \frac{\sum_{i=1}^N \frac{|x_i - \hat{x}_i|}{x_i}}{N} \quad (3-1)$$

where x_i = observed value for cell i ;

\hat{x}_i = predicted value for cell i ;

N = total number of cells in study area for the day in question with sufficient snow to be included in summary statistics.

For all summary statistics, only grid cells where both predicted and observed snow depth were equal to or deeper than a given threshold snow depth of 80 mm were included.

2.15.3 Discharge

Runoff and baseflow predicted for both study periods by the model with and without updating were routed to specified stream gauge locations using the routing scheme described by Lohman, et al (1998b). The resulting routed hydrographs are discussed in Section 4.5.2. Predicted hydrographs were compared with observations at two US Geological Survey gages (see figure 3-4). These gages were chosen because snow on the ground during the winter extends over most of the basins which drain to these gages.

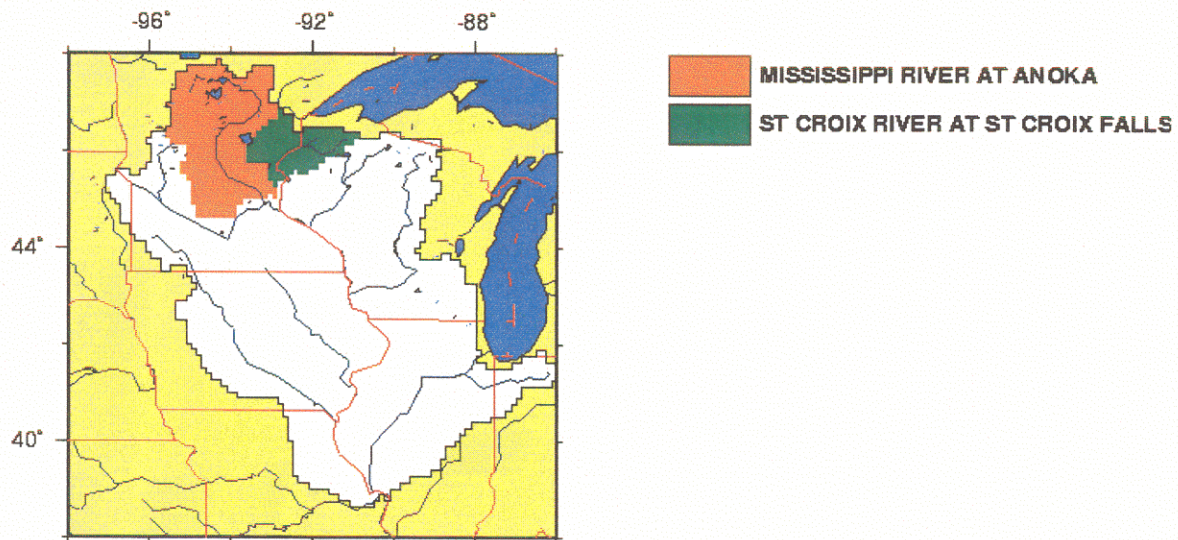


Figure 2-14. Sub-basins within the study area for which discharge predictions were compared with gage discharge.

Table 2-4. Basins for which model-predicted discharge were compared with gage discharge.

NUMBER	NAME	DRAINAGE AREA	LOCATION	
05288500	MISSISSIPPI R NR ANOKA, MN	19,100 miles ²	45°07'36"N	93°17'48"W
05340500	ST CROIX R AT ST CROIX FALLS, WI	6,240 miles ²	45°24'25"N	92°38'49"W

Chapter 3: Results

3.1 Overview

As described in previous chapters, this thesis seeks to evaluate the utility of hydrologic predictions based on microwave scatterometer measurements. The approach to this task was to investigate relationships between microwave backscatter observations and surface variables and then to develop and test a scheme for updating snow variables within the VIC macroscale hydrological model. The results of these investigations are presented in this chapter.

Model output and backscatter coefficient (σ^0) were analyzed in three stages.

- Predictions from the first updating trial, where the model was updated with snow depth observation, were examined qualitatively.
- σ^0 was compared qualitatively with snow depth observations derived from historical cooperative observer data, as described in Chapter 3 and with snow surface moisture content and snow surface temperature predicted by the VIC model. This analysis focused first on seasonal trends and then on particular events during the winter of 1996/1997. As explained in Section 2.5, a sustained drop in σ^0 was expected to coincide with the transition from frozen to thawed state.
- Predictions from the model updated based on σ^0 were compared quantitatively with observed snow depth and with gage discharge for selected river catchments within the study area.

3.2 Snow depth updating

3.2.1 Snow depth spatial predictions

The VIC model was run with snow depth updated intermittently using the method described in Section 3.3.1 for the winter of 1996/97. Without snow depth updating, the model had a consistent bias such that snow cover predicted in the study area extended several hundred kilometers further south than the extent of snow indicated by both snow depth observations and visible band satellite imagery. Updating snow depth in the model eliminated most of this bias. In addition, qualitative comparison of predicted snow depth with observations and with estimated snow areal extent from visible band imagery prepared by NOHRSC indicated that updating with snow depth may improve the model to the point that model predictions represent snow on the ground better than the gridded snow depth data set created by interpolating and filling historical station observations.

3.2.2 Runoff Sensitivity

Figure 4-1 demonstrates that the model overall simulates the shape of the gage discharge for the St. Croix River well for the winter of 1996/1997 until mid-May. However, the model tends to simulate events in the fall that are not observed, generally under-predicts

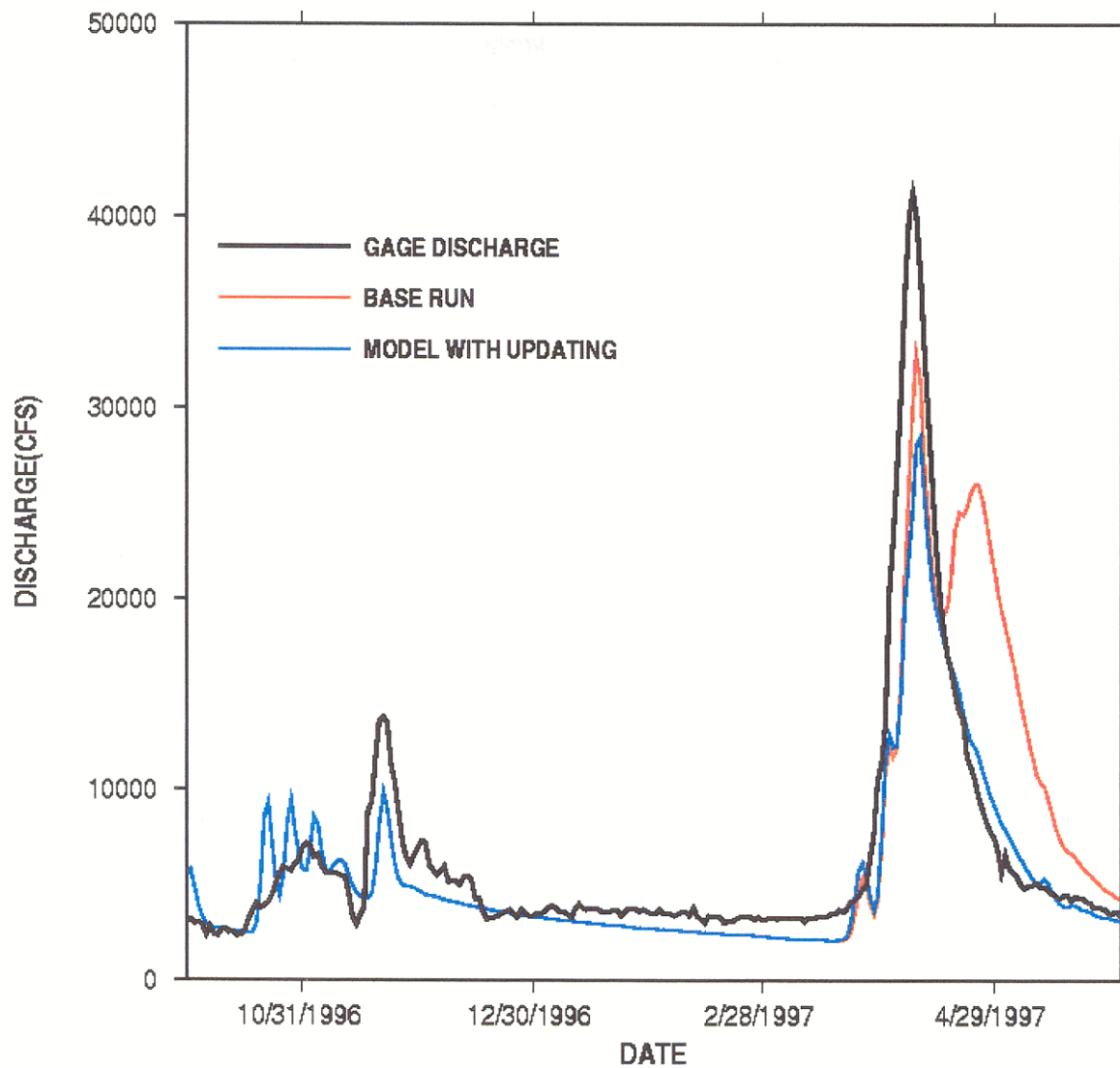


Figure 3-1. Hydrograph of observed and simulated discharge for the gage on the St. Croix River at St. Croix Falls, Wisconsin for the winter of 1996/97. Base run has no updating. Updated model uses direct insertion of gridded snow depth from historical observations approximately every five days.

peak flows and baseflow and, most significantly, the model predicts a second significant flood peak in mid-May that does not appear at all in the observations.

Snow depth updating reduced the magnitude of the early April flood predicted by VIC but also eliminated the second unobserved mid April peak predicted by the model without updating.

Although the underprediction of the early April flood was exacerbated, the shape of the resulting hydrograph fit the observed hydrograph better than the model predictions without updating.

Without updating, the model overpredicted the spring runoff peaks for the Mississippi River near Anoka, Minnesota (Figure 4-2). Also, the same storms in the early part of the season and the same unobserved mid-April peak are apparent.

As with the St Croix River predictions, updating snow depth reduced the volume of the predicted discharge for the early April flood, and almost eliminated the unobserved peak in mid-May, as well. Overall, updating improved the shape of the hydrograph both in shape and volume. The height of the early April peak predicted by the model with updating closely matches the peak observed discharge, although its timing is somewhat delayed relative to the observations.

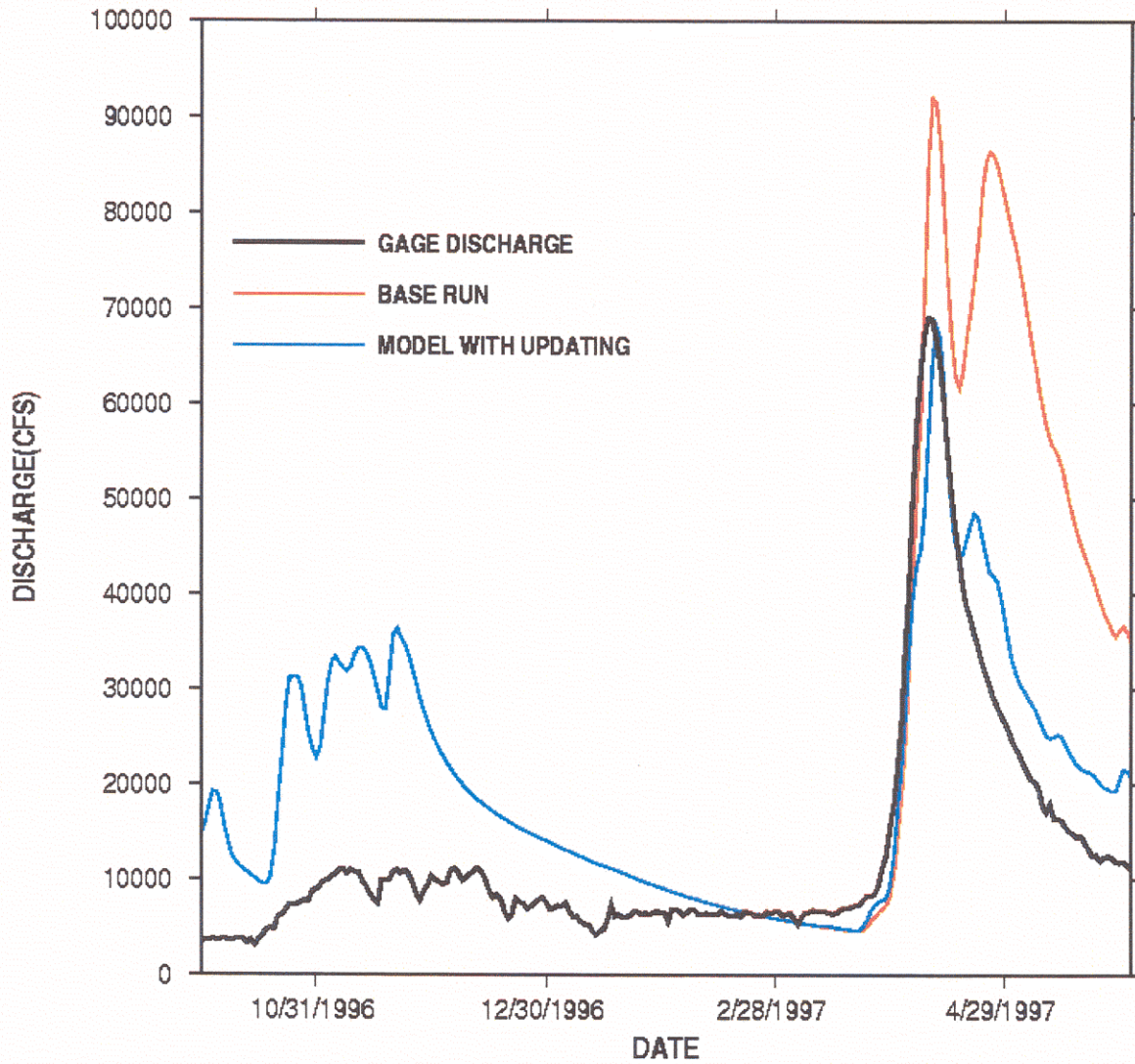


Figure 3-2. Hydrograph of observed and simulated discharge for the gage on the Mississippi River at Anoka, Minnesota for the winter of 1996/97. Simulated discharge is from the unadjusted model and the model with snow depth updated based on historical observations.

3.3 Backscatter Correlation - Seasonal Trends

Winter 1996/1997 was characterized by a deep snow pack in the northern part of the upper Mississippi River basin that lasted into early April (Figure 4-3). Catastrophic flooding occurred in the Red River of the North which borders the upper Mississippi River basin on the east. No such extreme flooding occurred in the upper Mississippi River basin, but the snow pack lasted into April and spring discharge was above average. The region experienced consistently below freezing temperatures as far south as Missouri from February 6th through February 15th when temperatures climbed above freezing during the day (Figure 4-4). Thereafter, temperatures remained generally above freezing during the daylight hours with freezing temperatures progressing southward and then receding back three more times before the end of the season.

During the winter of 1999/2000, by contrast, snow depths were relatively shallow and melt occurred early. The snow on the ground extended across the entire basin by the last week of January but was no more than 10 cm deep in most places and the snow pack was already retreating by early February (Figure 4-5). However, following this early melt, below freezing temperatures persisted over the northern part of the basin through most of February even while temperatures were above freezing as far north as Iowa (Figure 4-6).

As a result, snow continued to accumulate in the extreme northern part of the basin until about February 22nd, when the pack began melting throughout the basin. By late February, it was entirely gone.

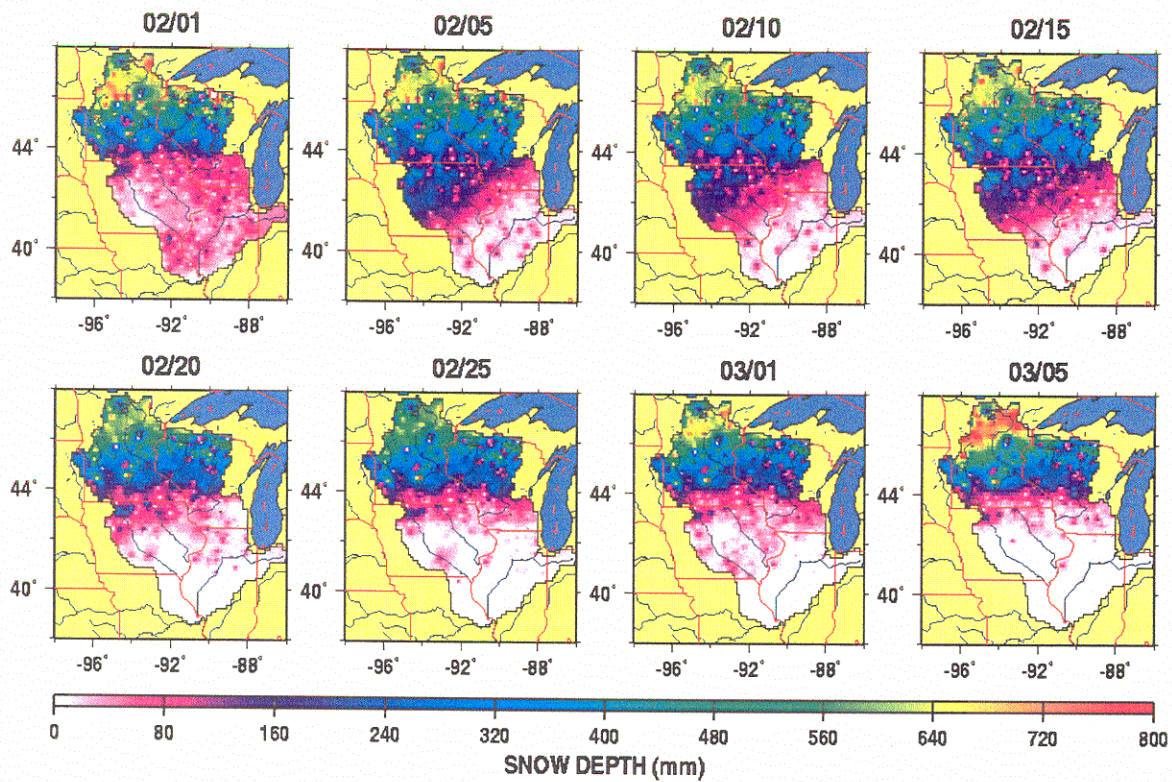


Figure 3-3. Snow depth in the upper Mississippi River basin during the winter of 1996/97. Snow depth measurements were made at over 900 cooperative observer stations and archived by the National Climatic Data Center. The data have been interpolated spatially and filled temporally as described in Section 3.3.1.

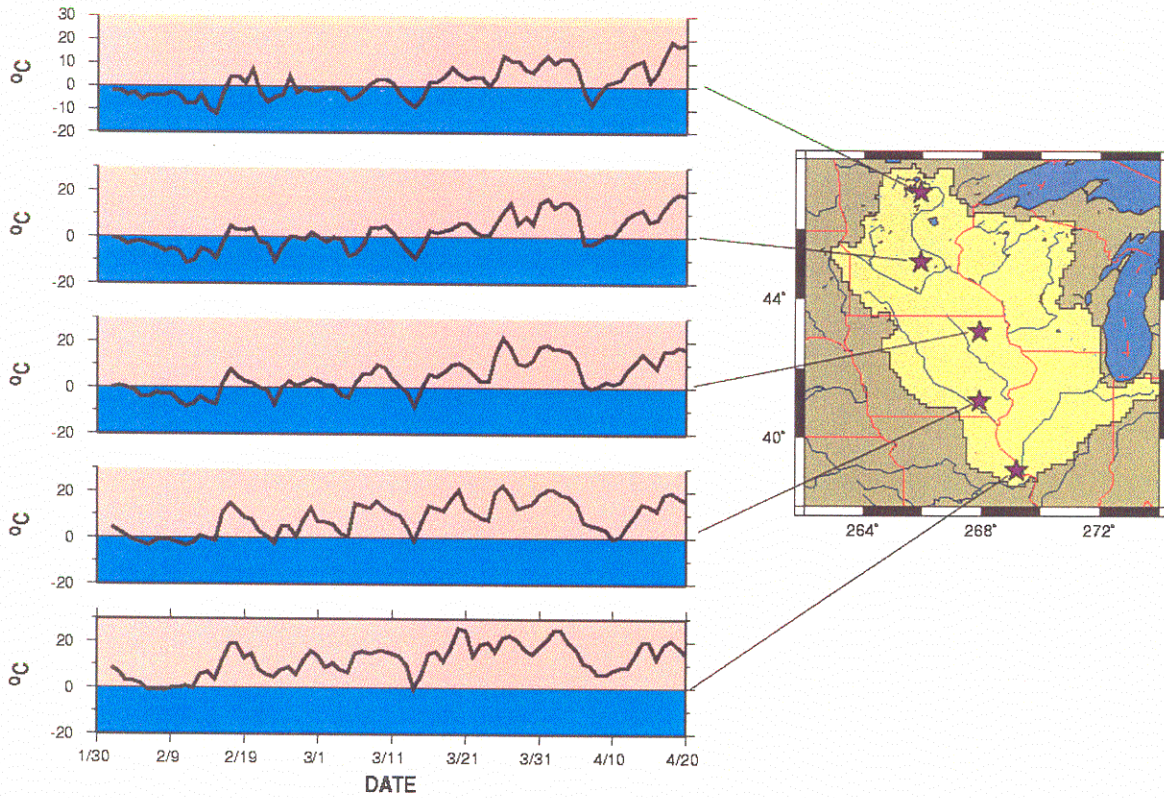


Figure 3-4. Daily maximum air temperature from February to April, 1997 for five grid cells from north to south through the upper Mississippi River basin.

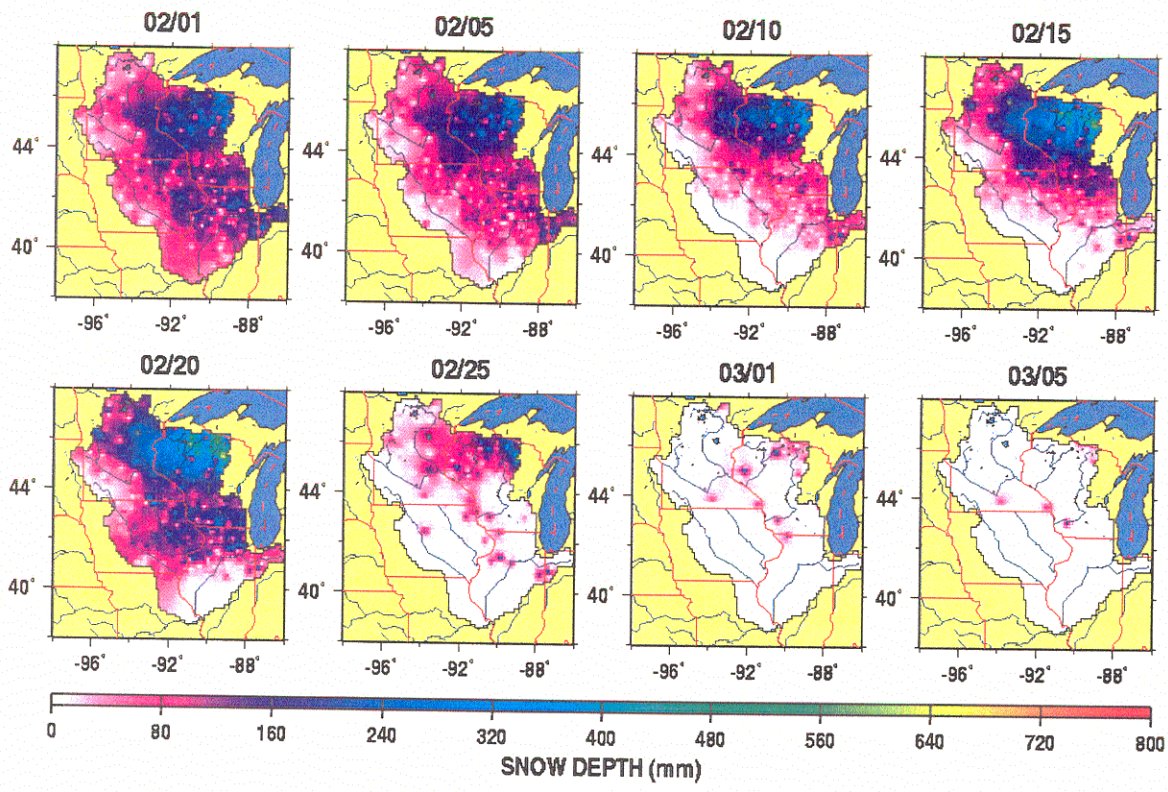


Figure 3-5. Snow depth in the upper Mississippi River basin for the winter of 1999/2000. Snow depth measurements were made at over 900 cooperative observer stations and archived by the National Climatic Data Center. The data have been interpolated spatially and filled temporally as described in Section 3.3.1.

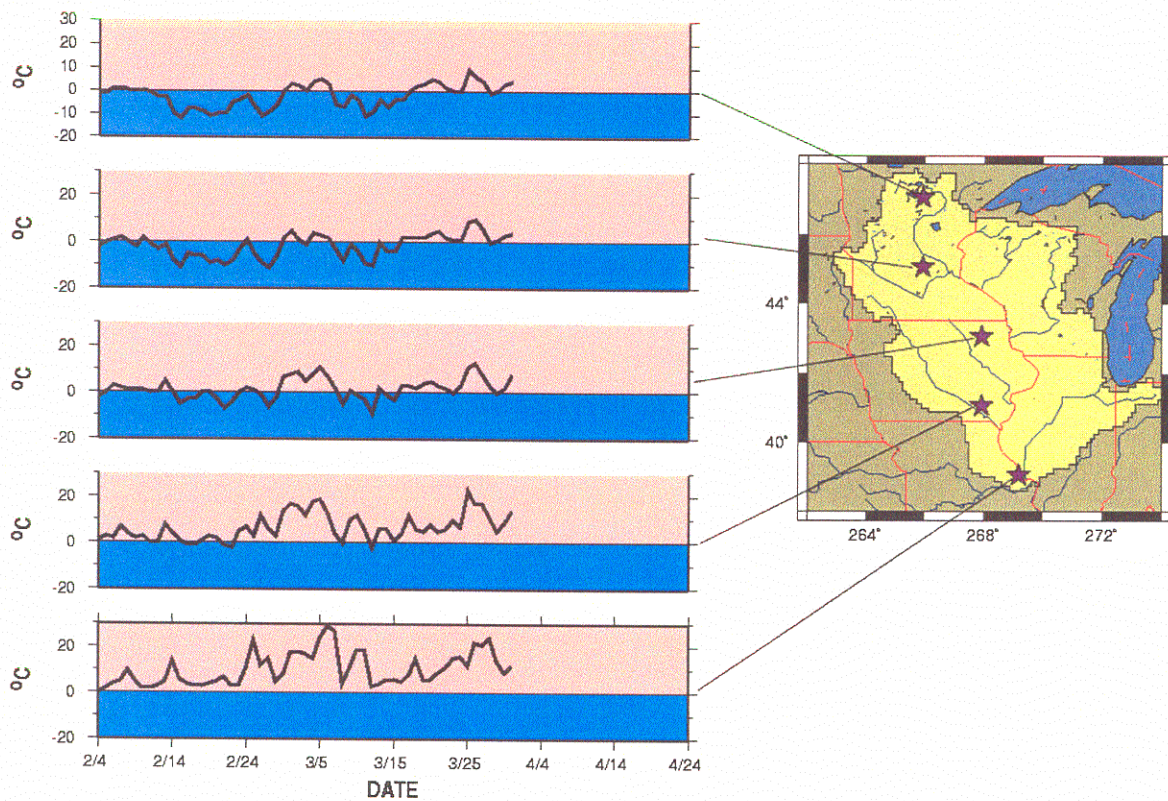


Figure 3-6. Daily maximum air temperature from February to March, 2000 for a north-south transect through the upper Mississippi River basin. Only data up to 3/31/2000 were used in the analysis.

3.3.1 Observed Snow Depth

3.3.1.1 NSCAT (1996/1997)

As shown in Figure 4-7, normalized backscatter cross-section (σ^0) was stronger in the north than in the south over the period when snow was present. The region where backscatter response was stronger in the north did not extend as far south as the southern extent of the snow cover as indicated by the historical snow depth records, however.

3.3.1.2 QuikSCAT (1999/2000)

As for the winter of 1996/1997, the spatial pattern of σ^0 agreed generally with the spatial pattern of snow depth, which was deeper in the northern end of the basin. However, σ^0 as measured by QuikSCAT had a different apparent range of values than σ^0 measured by NSCAT. The background level for the study area as measured by NSCAT was around 11dB while for QuikSCAT it was around 16dB. σ^0 measured by QuikSCAT indicated a trend towards stronger values particularly in the northeast corner of the basin, which is consistent with the snow depth observations, which indicate the deepest snow in Wisconsin. From about February 14th on, however, the plots of σ^0 do not match well with the distribution of snow (Figure 4-8).

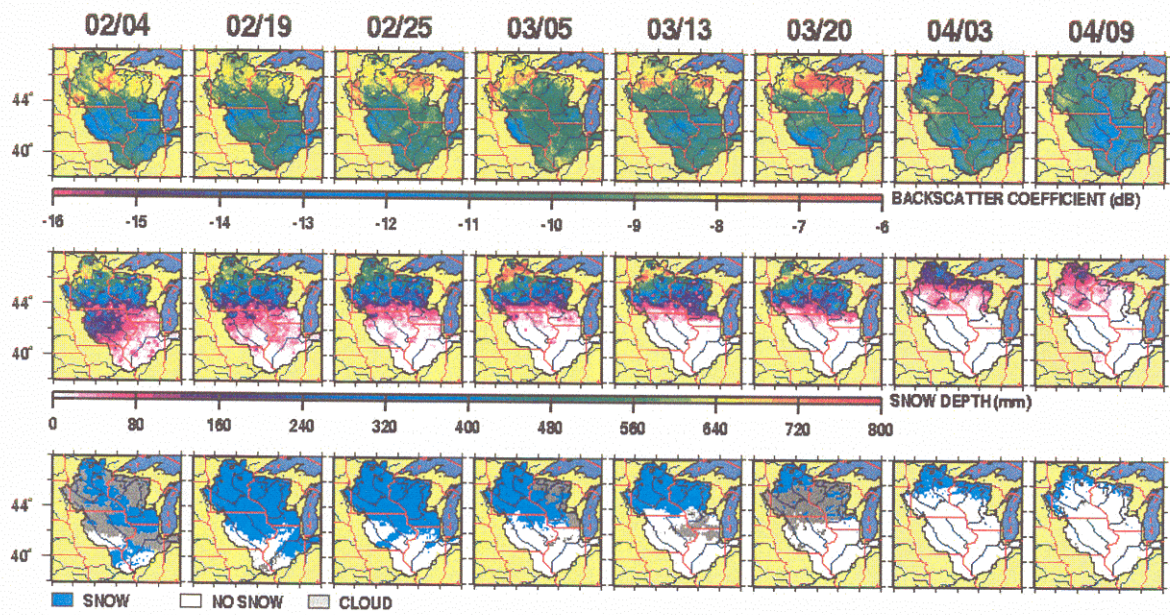


Figure 3-7. NSCAT backscatter (top row), snow depth (middle row) and area extent of snow estimated from visible band satellite imagery (bottom row) for 8 days in the winter 1996/97

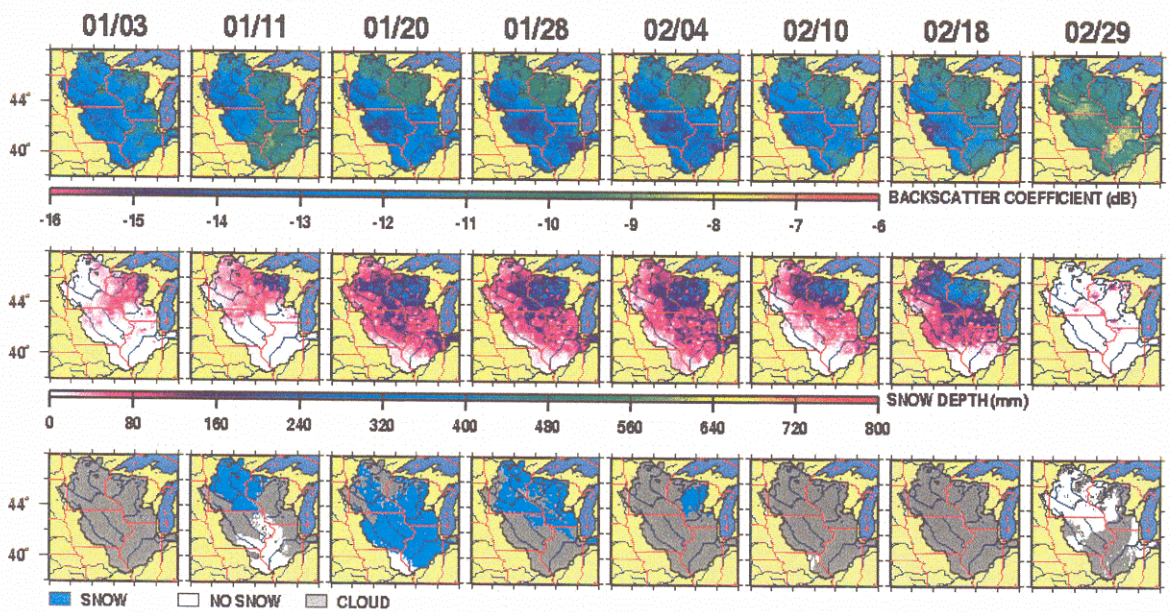


Figure 3-8. QuikSCAT backscatter (top row), snow depth (middle row) and area extent of snow estimated from visible band satellite imagery (bottom row) for 8 days in winter 1999/2000

3.3.2 Observed Temperature

3.3.2.1 Overview

Kimball et al, (2000) observed correlations between freeze/thaw state predicted by re-gridded daily maximum air temperature observations and by microwave backscatter measurements. Following this direction of analysis, daily maximum air temperature for the study area were plotted for February, March and April of 1997 and for January and February of 2000 for comparison with NSCAT and QuikSCAT σ^0 measurements from the same respective periods.

3.3.2.2 NSCAT

Plots of maximum daily air temperatures agree no more than generally over the season with patterns of σ^0 . The shape of advancing and receding freezing temperatures, in particular, do not correspond with the patterns in σ^0 measured by NSCAT (Figure 4-9).

3.3.2.3 QuikSCAT

σ^0 measured by QuikSCAT during the winter of 1999/2000 and daily maximum air temperature are related in the same manner as NSCAT measurements (Figure 4-10). It is difficult to say by visual comparison alone whether the agreement is any closer or more consistent than was the

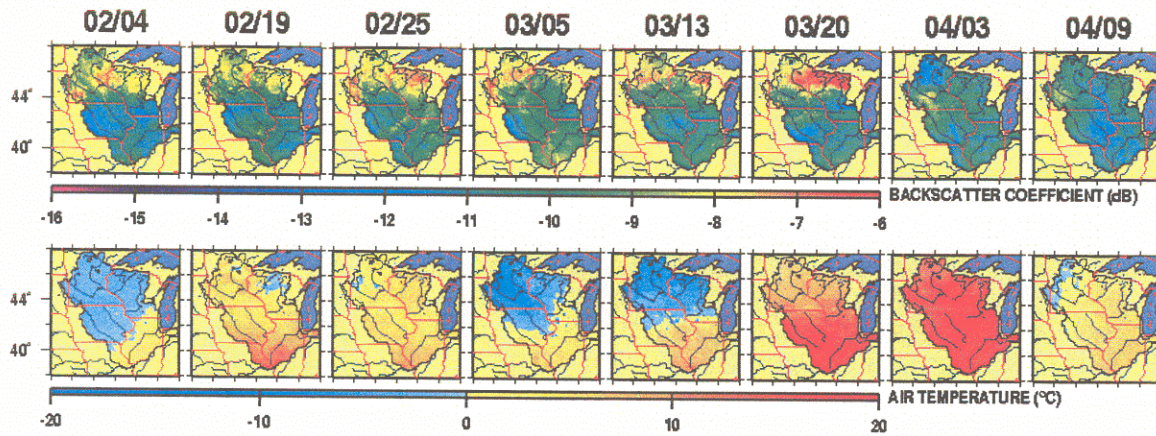


Figure 3-9. NSCAT backscatter (top row) and daily maximum air temperature (bottom row) for 8 days in the winter of 1996/97.

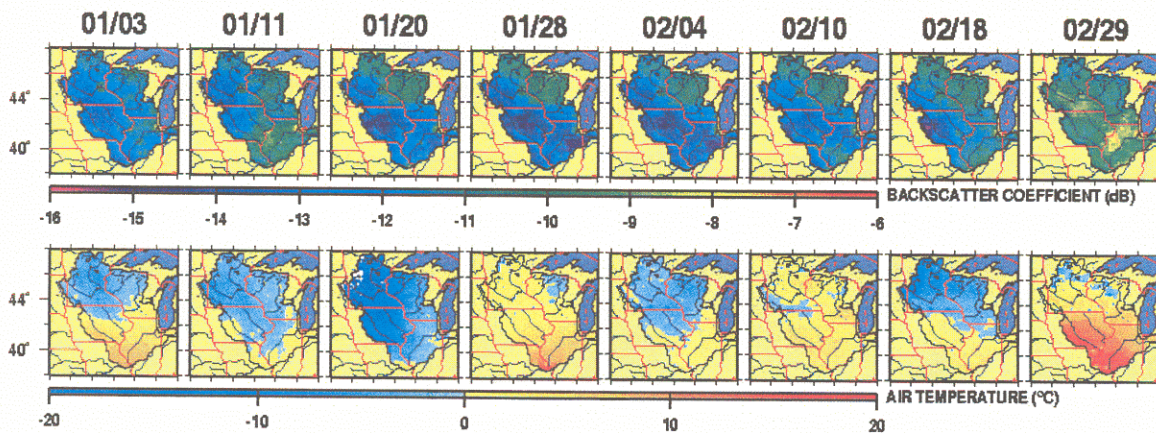


Figure 3-10. QuikSCAT backscatter (top row) and daily maximum air temperature (bottom row) for 8 days in the winter of 1999/2000.

case for NSCAT data, partially due to the thinner and shorter duration snow pack during the winter of 1999/2000.

3.4 Backscatter Relationships: Specific events

3.4.1 Midwinter melt: February 15 – February 21, 1997

Between February 16 and February 20, daily maximum air temperatures exceeded zero degrees (Figure 4-11) through most of the study area though runoff did not increase noticeably during this warm-spell. Diurnal plots of snow surface temperature and liquid water content indicated that melting conditions extended throughout the area, especially during the daylight hours between 12 noon and 6PM on February 18 and 19 (see Figures 4-12 and 4-13). The diurnal plots also indicate that liquid water which appeared during daylight hours froze again at night. Almost no liquid water was present in the pack on any of the days between 12 midnight and 3AM.

NSCAT flew over the region at roughly 10 AM on its descending orbit and again at 10 PM on its ascending orbit. The VIC model ran at 3 hour intervals beginning at local midnight, thus the most nearly coinciding timesteps were at 9 AM and at 9 PM (2100 hours). Figures 4-14 and 4-15 plot liquid water in the snow surface layer and snow surface temperature for those times juxtaposed with images of σ^0 for the corresponding orbital passes. These figures indicate that regions of low σ^0 appeared in the upper Mississippi River basin during the melt period,

consistent with expectations. These regions did not correspond, however, with the locations of regions of liquid water in the snow as predicted by the VIC model, except for in the ascending orbit images from February 19. On those days, a region where σ^0 was low appeared centered on the border between Minnesota and Iowa. This region overlapped a region where liquid water was present in the snow pack though the region of increased backscatter extended further west than the region of liquid water in the snow surface layer. The region was also notably absent in descending orbital pass images. Regions of low σ^0 also appeared on February

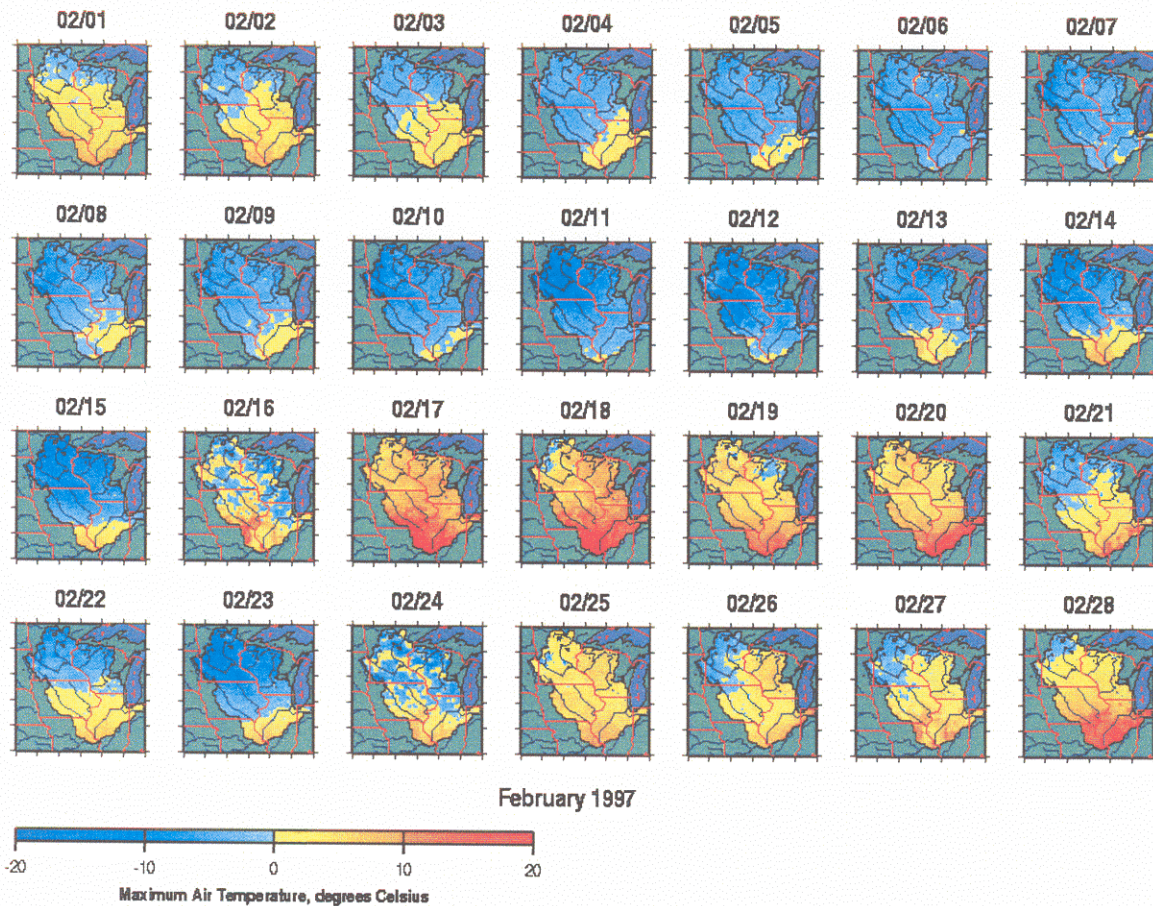


Figure 3-11. Daily maximum air temperatures for the upper Mississippi River basin for February, 1997. Daytime freezing temperatures extended across the basin and receded twice during February, interrupted by an early season thaw from the 16th to the 20th.

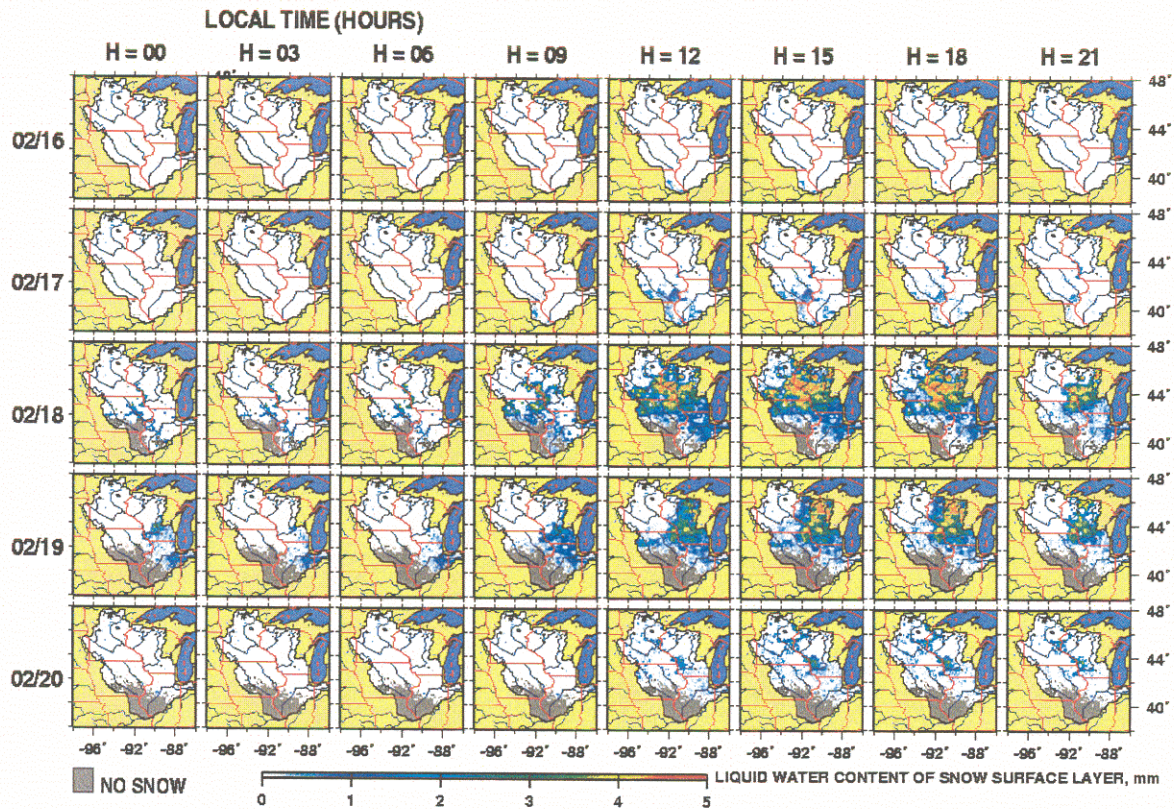


Figure 3-12. Diurnal variation in liquid water in the surface layer of the snow pack predicted by the VIC model for February 15 to February 20, 1997.

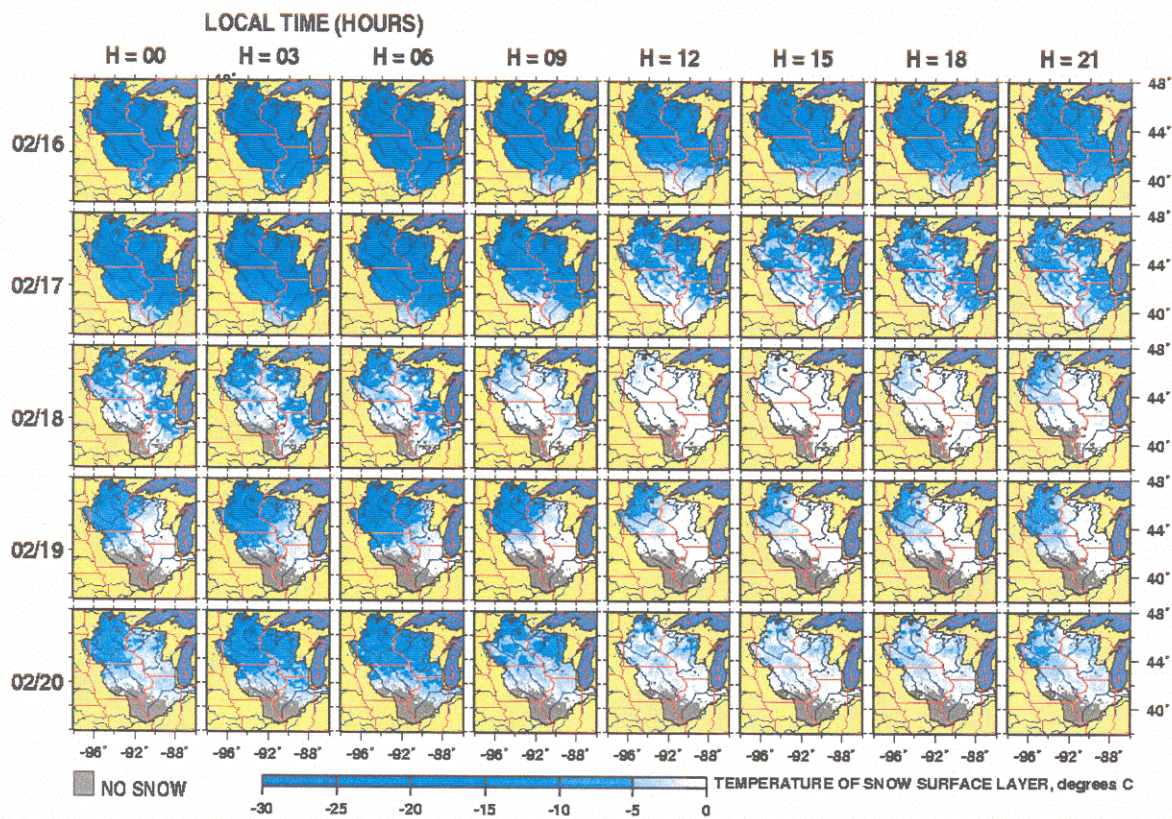


Figure 3-13. Diurnal variation in the temperature of the surface layer of the snow pack predicted by the VIC model for February 15 to February 20, 1997.

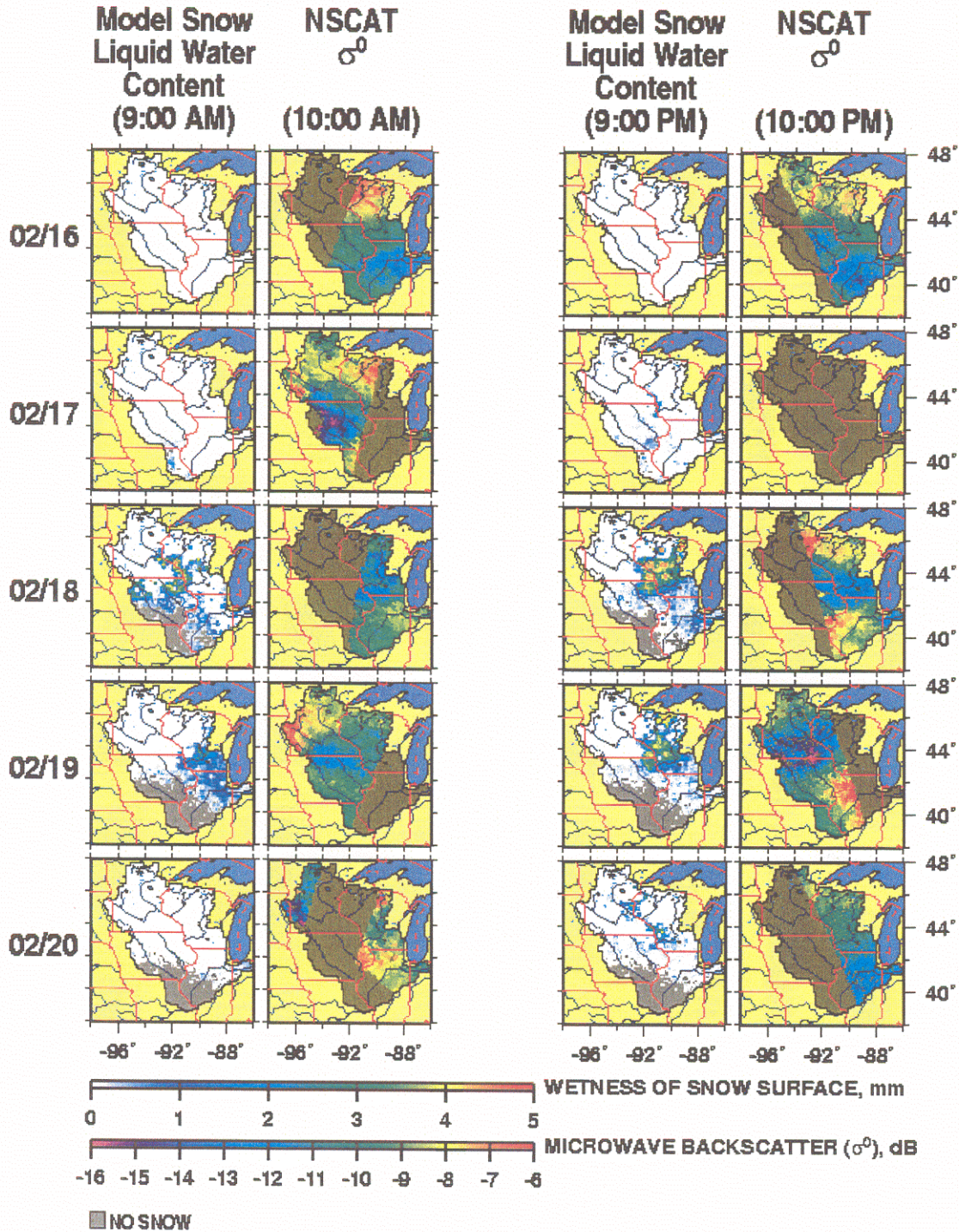


Figure 3-14. Snow pack surface layer liquid water content predicted by VIC and σ^0 for the early season melt conditions which existed between February 16 and February 20, 1997.

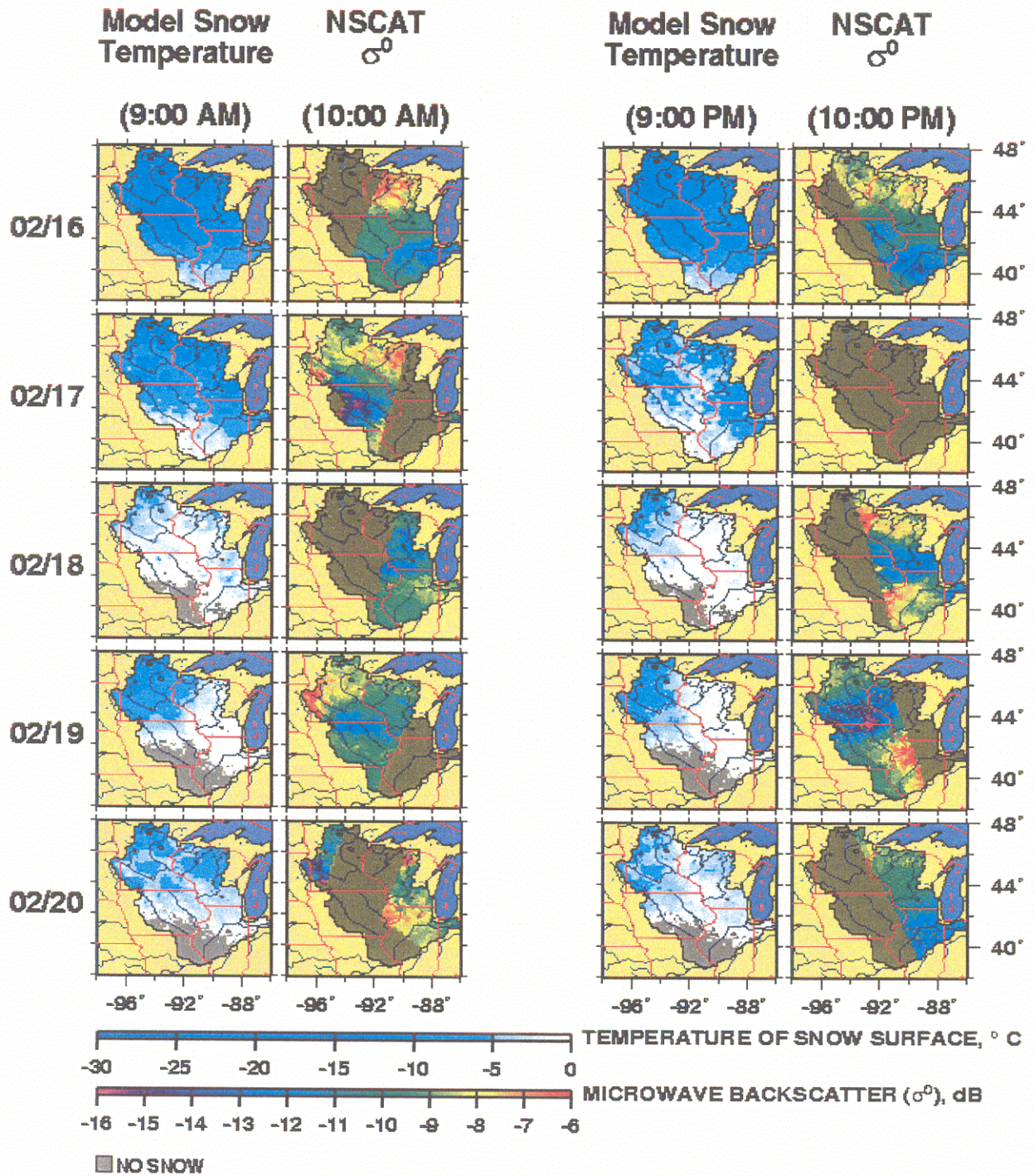


Figure 3-15. Snow pack surface layer temperature predicted by VIC and σ^0 for the early season melt conditions which existed between February 16 and February 20, 1997.

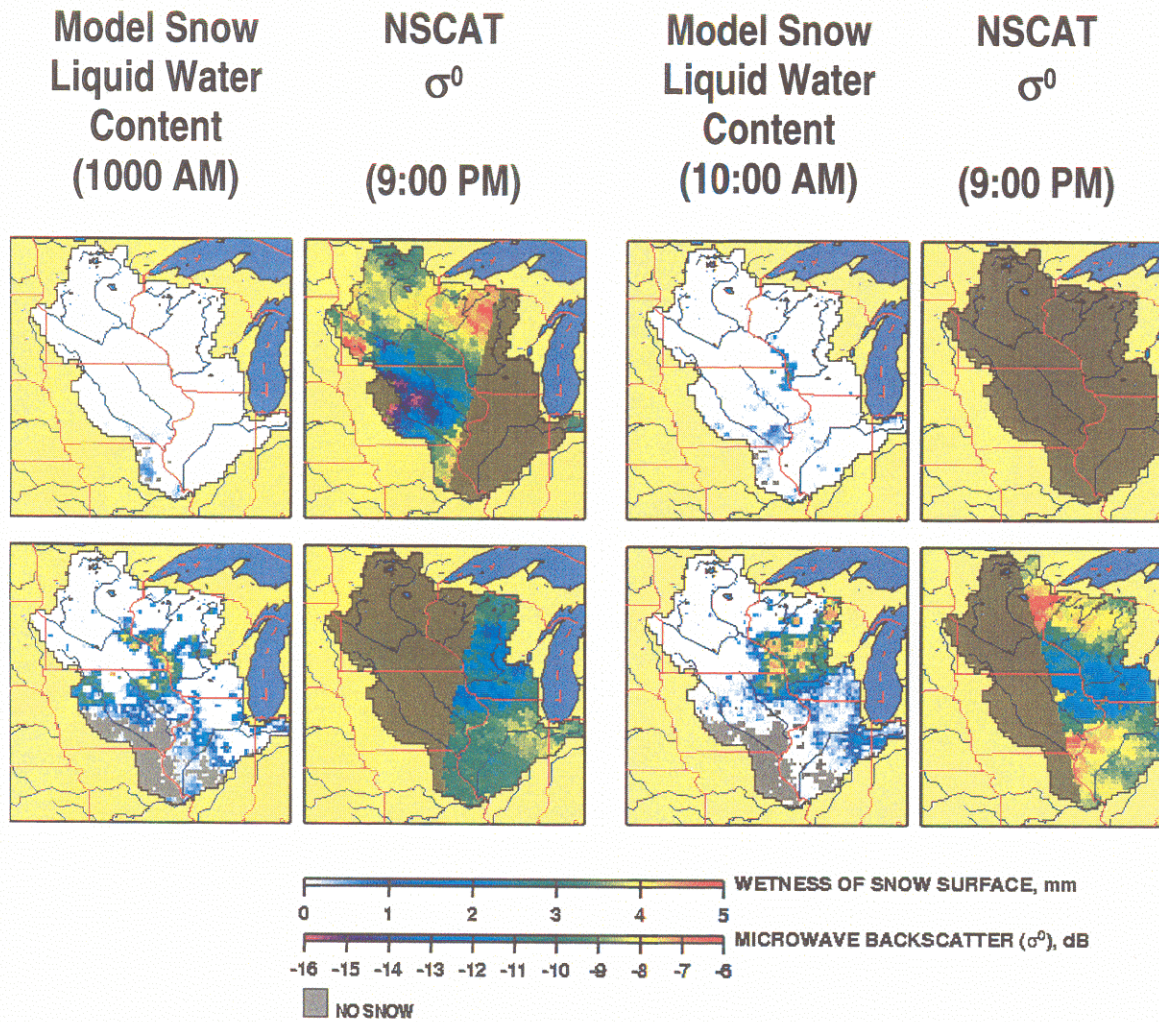


Figure 3-16. Focus on two days - February 16 and 17, 1997. The top and bottom rows correspond to February 16th and 17th, respectively.

16 and 17, but the VIC model predicted almost no surface water in the pack on those days at the times nearest to satellite overpasses. The location of the low σ^0 region on the 17th does correspond with a region of liquid water in the snow pack but that region is only present for images from 12 PM to 3 PM. Figure 4-16 shows two of these days in greater detail, illustrating where relationships existed in spatial patterns and where they did not.

3.4.2 Cold snap: March 12 – March 15, 1997

Daily maximum temperature observations indicate a cold snap occurred in the region beginning March 12, which peaked in temperatures at or below freezing across most of the entire region on March 14. The cold snap dissipated on March 15 and the daily maximum temperature across the region returned to above zero by March 16. In the surface variables calculated by VIC, the cold snap is manifested clearly in both snow surface temperature and liquid water content (Figures 4-17 and 4-18).

On March 12, snow surface temperature was at zero degrees during the day and was colder in the northern extreme of the basin at night. As the cold snap progressed, daytime temperatures dropped below zero, except where snow cover was very thin, and the snowpack surface temperature dropped as low as -20°C . Liquid water was present in the surface layer of the pack during the daylight hours in the southeastern portion of the basin where snow was on the ground on March 12, as would be expected in early season melt conditions when snow melt occurs during the day with re-freezing at night. The liquid water all but vanished between March 12 and

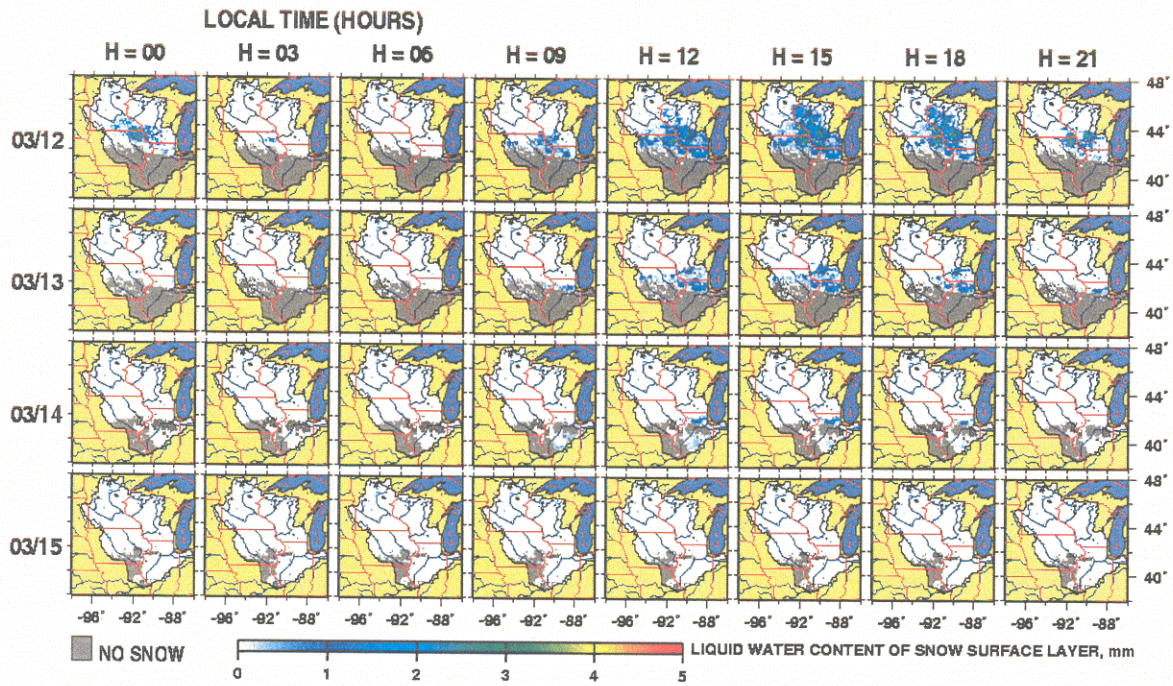


Figure 3-17. Diurnal variation in the snow pack surface layer liquid water content predicted by the VIC model for March 12 to March 15, 1997.

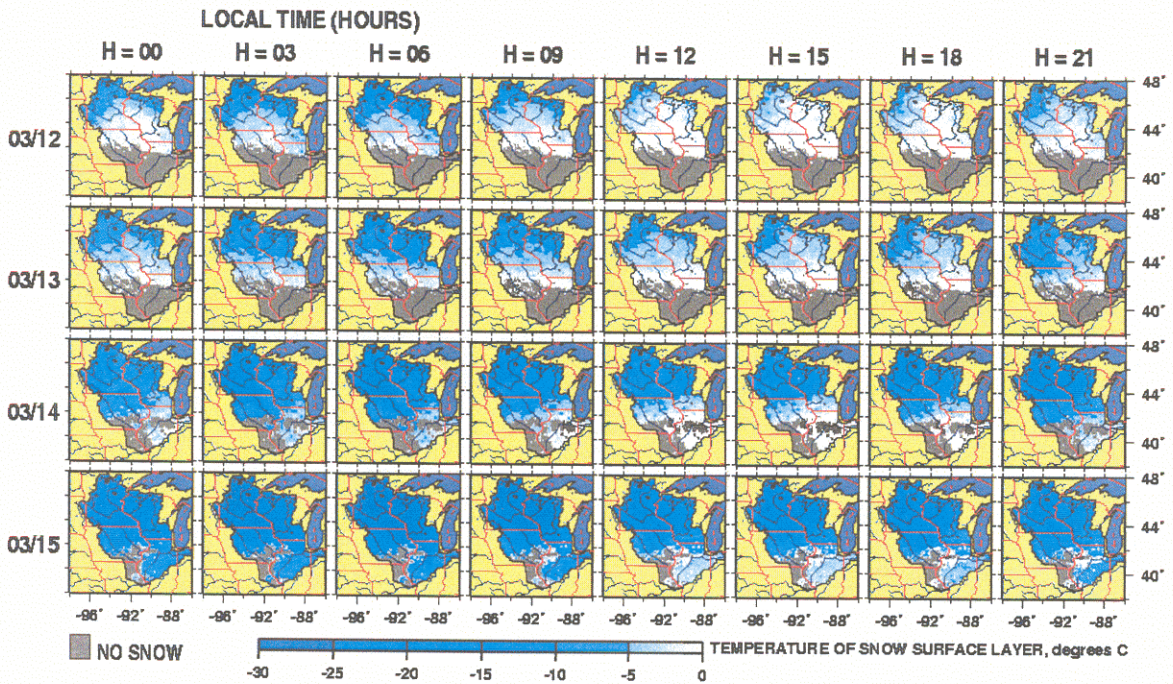


Figure 3-18. Diurnal variation in the snow pack surface layer temperature predicted by the VIC model for March 12 to March 15, 1997

March 14 so that by March 15, the snow pack contained no liquid water the entire day.

During the cold snap, σ^0 was consistently stronger in the northern part of the basin – consistent with the presence of a deep, dry snowpack there (Figures 4-19 and 4-20). A region where the model indicated the presence of liquid water in the snow surface layer coincides with a small region of low σ^0 in northern Illinois in the descending orbit image on March 14. The small area that is visible in the ascending orbit image for March 15 indicates exceptionally high σ^0 but little of the image is visible. The plots do not indicate any snow surface conditions that coincided with the increase in σ^0 on the 15th. Also, an area of high σ^0 in the southeast part of the region in the ascending orbit image for March 14 coincides with the appearance of new snow.

3.4.3 Late season snow storm: April 11 – April 15, 1997

After most of the basin was snow-free, a storm on about April 11th dropped snow in a band reaching from southwest Iowa diagonally to northern Illinois (Figures 4-21 and 4-22).

Temperatures in the region were above freezing through most of the day and some of the night by that time in the season and the snow deposited on the ground began melting as soon as it fell.

The effects of the storm are thus visible in plots of snow surface temperature and liquid water content as a band where melt water appeared and temperatures were at zero degrees C.

Independent of the snowfall that occurred during the storm, in the central and southern parts of the study area, these plots also indicate active melting at the extreme northern part of the basin where the last of the winter

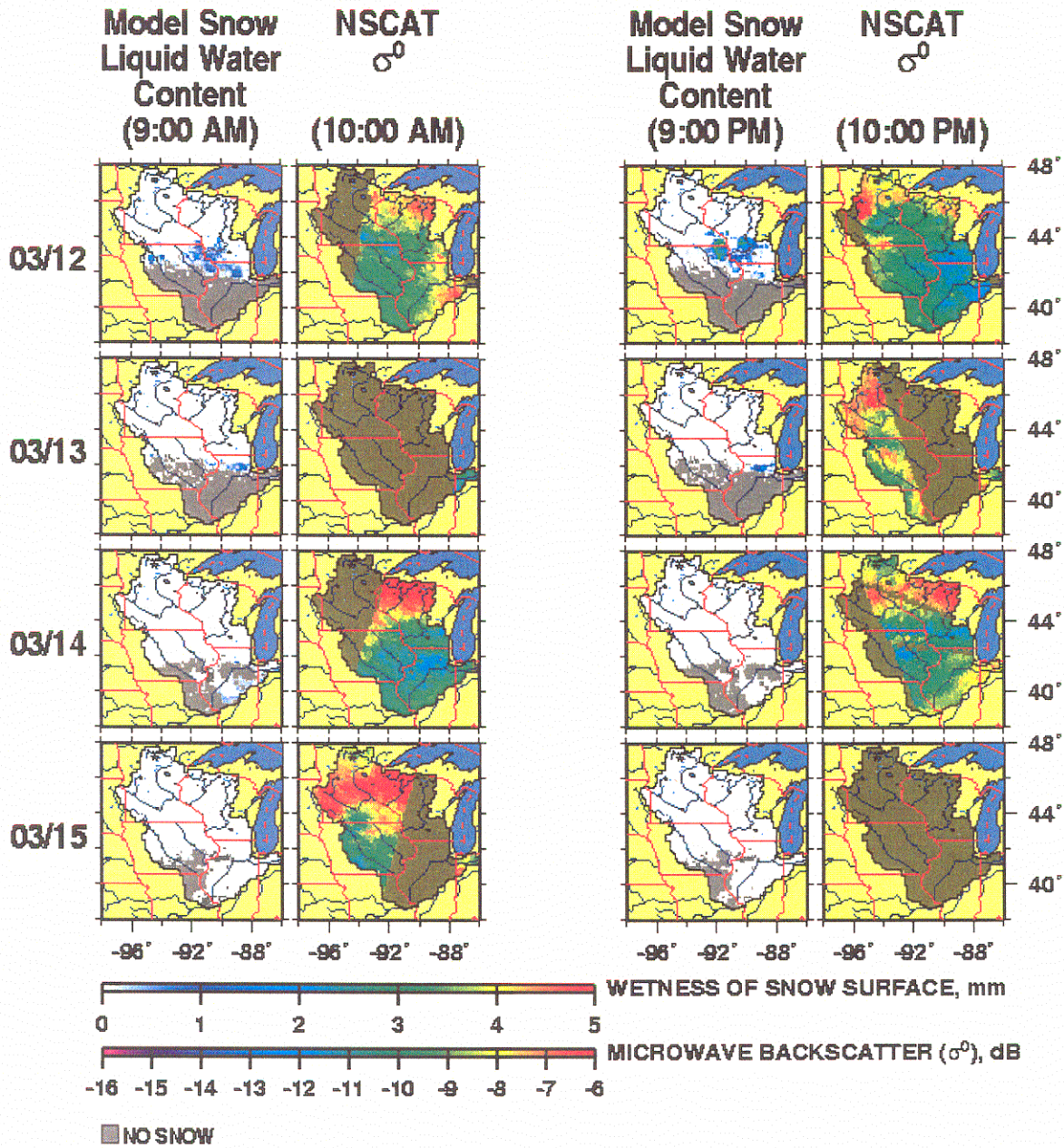


Figure 3-19. Snow pack surface layer liquid water content predicted by VIC and σ^0 for the cold snap from March 12 to March 15, 1997. The σ^0 images in the second column were taken by NSCAT during descending orbital passes which occurred at around 10 AM local time. The σ^0 images in the fourth column were taken by NSCAT during ascending orbital passes which occurred at around 10 PM local time.

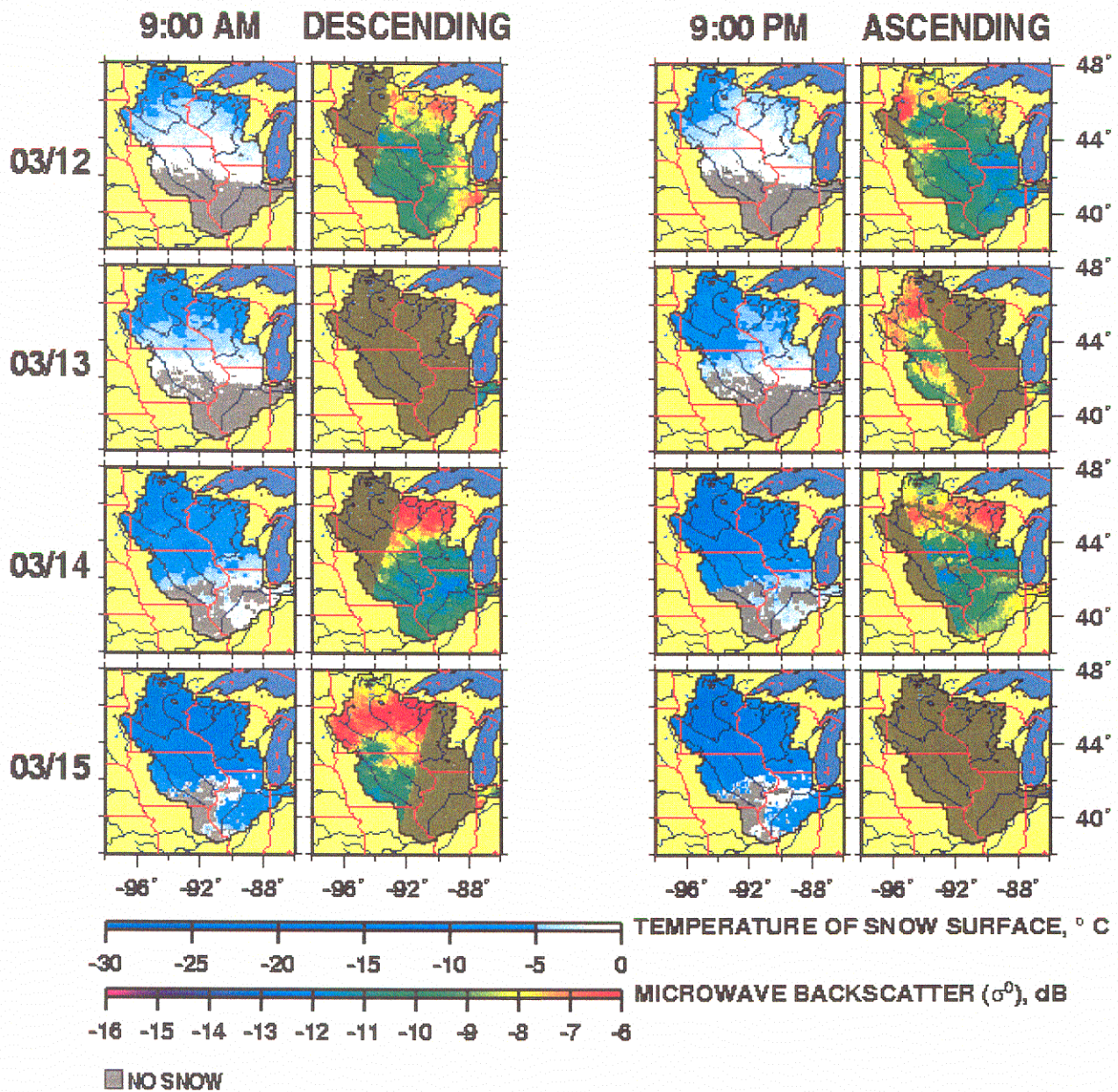


Figure 3-20. Snow pack surface layer temperature predicted by VIC and σ^0 for the cold snap from March 12 to March 15, 1997.

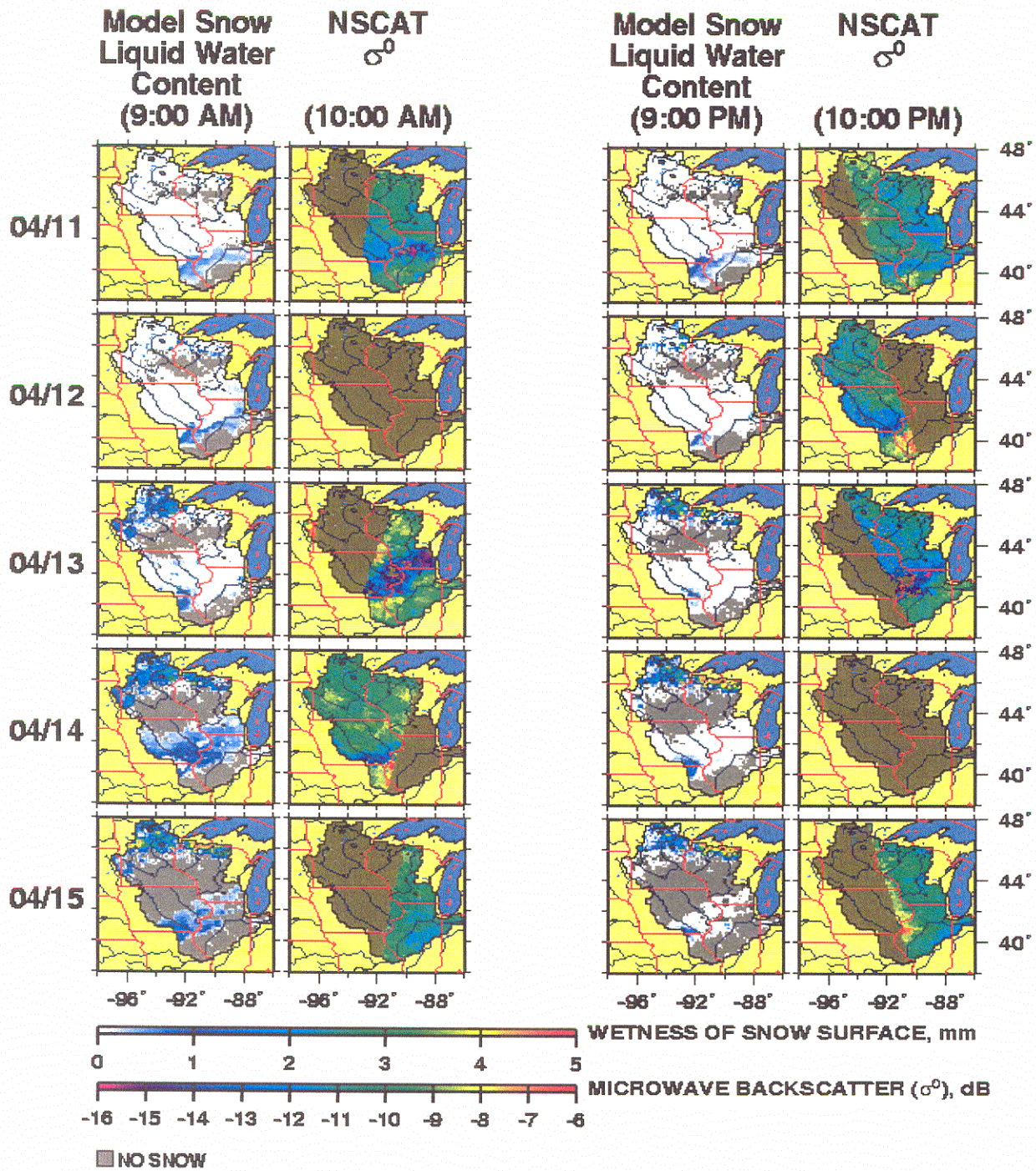


Figure 3-21. Snow pack surface layer liquid water content predicted by the VIC model and σ^0 for the melt period from April 11 to April 14, 1997 which followed a storm.

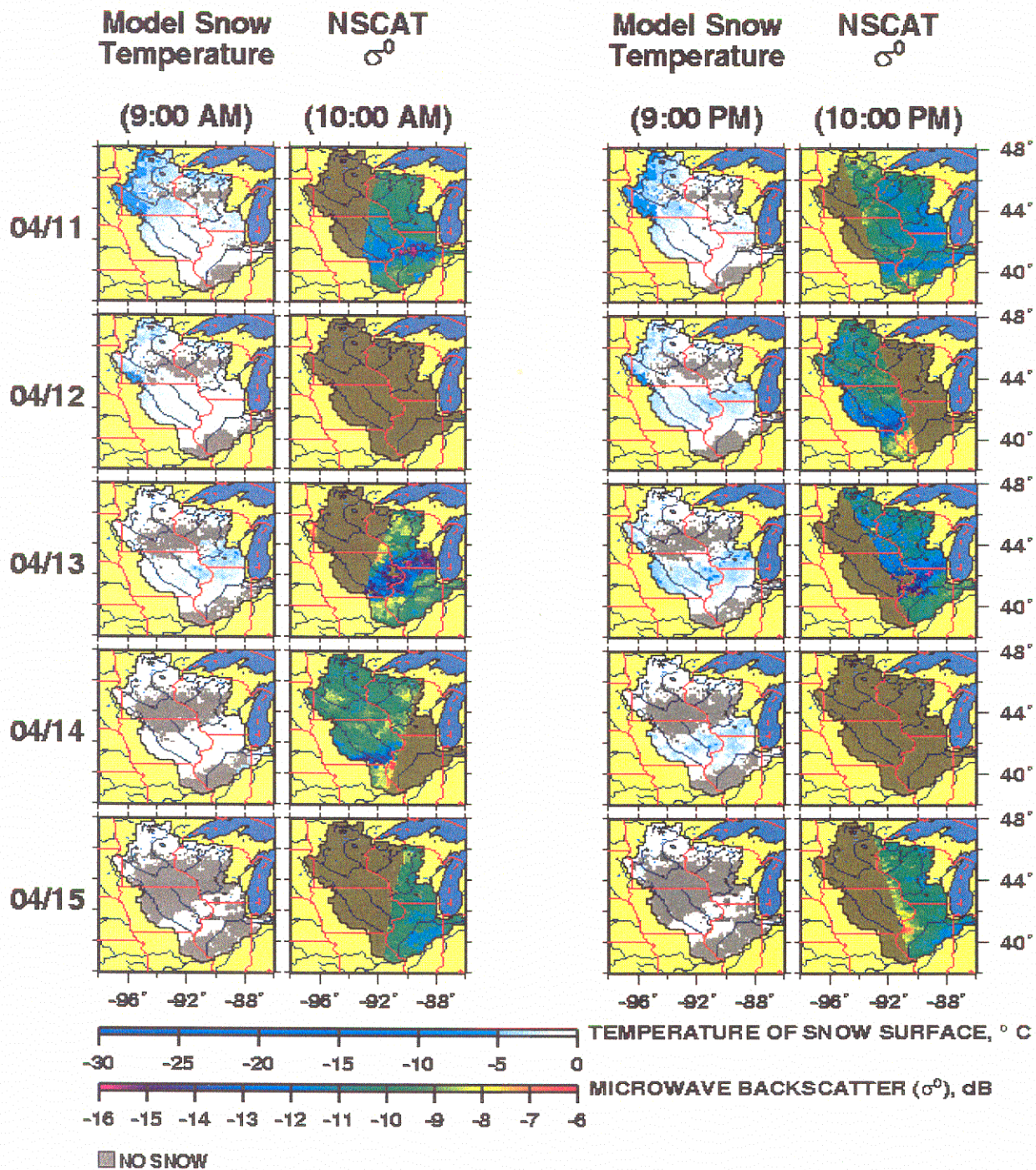


Figure 3-22. Snow pack surface layer temperature predicted by the VIC model and σ^0 for the melt period from April 11 to April 14, 1997 which followed a storm.

snowpack was melting. The liquid water content of the snow surface layer was at the maximum (model) liquid water holding capacity of 5mm in some portion of the north extreme of the basin.

The response of σ^0 to the snow melt following the storm is the most consistent seen among the events examined. A band of low σ^0 values appears in the April 11th descending orbit NSCAT images at a location that coincides closely with the location of the southern extent of the new fallen snow and plots of liquid water in the snow surface layer indicate melt was active in the snow pack at this southernmost extreme. The band is not visible in the ascending orbit data taken later that day and NSCAT did not image the study area in its descending pass on the next day, April 12th. The band is visible again in the ascending orbital pass image for the 12th, though. The band of low σ^0 is wide in both orbital passes on the 13th but liquid water is present in only a single region at the time of the coinciding model time step. The band of low σ^0 matches the shape of the wide band of liquid water that appears a day later on the 14th, though. The band narrows again in the descending orbital pass image of the 14th.

No backscatter response to the melting in the northern extreme of the study area is visible in the images for these days. Even on the 13th when liquid water values reached their allowed maximum, σ^0 across the north of the study area was no different than σ^0 across regions where no melt is indicated by the VIC model plots.

3.5 Freeze/Thaw updating

3.5.1 Snow depth spatial predictions

Summary statistics (see Section 3.6.2) indicate that updating based on microwave backscatter has a barely noticeable effect on snow depth predictions. The error values are all high, which is consistent with model overprediction of snow depth mentioned in Section 4.2.1. Tables 4-1 and 4-2 show that the general result was a slight improvement in predictions, though.

Table 3-1. Summary statistics: observed – predicted snow depth, winter 1996-97

Statistic description	Value
RMSE, model without updating	221 mm
RMSE, model with updating	206 mm
Mean Fractional Error, model without updating	89%
Mean Fractional Error, model with updating	84%
Normalized RMSE, model without updating	56%
Normalized RMSE, model with updating	56%

Table 3-2. Summary statistics: observed – predicted snow depth, winter 1999/2000

Statistic description	Value
RMSE, model without updating	83.1 mm
RMSE, model with updating	84.8 mm
Mean Fractional Error, model without updating	33%
Mean Fractional Error, model with updating	33%
Normalized RMSE, model without updating	15%
Normalized RMSE, model with updating	14%

3.5.2 Discharge

3.5.2.1 NSCAT

Consistent with the summary statistics, the hydrographs demonstrate that the updating scheme has little effect on the model predictions, especially given the integrated effect of a single discharge value for an entire basin. The effect the updating does have is to slightly increase the magnitude of the snowmelt peak in early May slightly and to change the shape of the second predicted flood peak such that the flood peaks sooner, tails off sooner, and is lower (Figure 4-23).

For the station at Anoka, updating freeze/thaw state increases the volume of the spring flood peak significantly (10%) and decreases the volume of the incorrectly predicted second peak. Late fall model error is due to processes other than snowmelt, and although it is not clear whether updating improves or worsens model predictions for the entire season, updating does appear to improve the shape of the spring hydrograph (Figure 4-24).

3.5.2.2 QuikSCAT

USGS Gage discharge was unavailable for water year 2000 at the time of this writing, therefore the two simulation were compared with each other. Nevertheless, cooperative station

observation (see Section 4.3.1.2) indicate that snow on the ground during the winter of 1999/2000 was several centimeters less deep throughout most of the basin and melted away a month earlier than in the winter of 1996/1997. These meteorological conditions suggest substantially diminished discharge for the winter of 1999/2000.

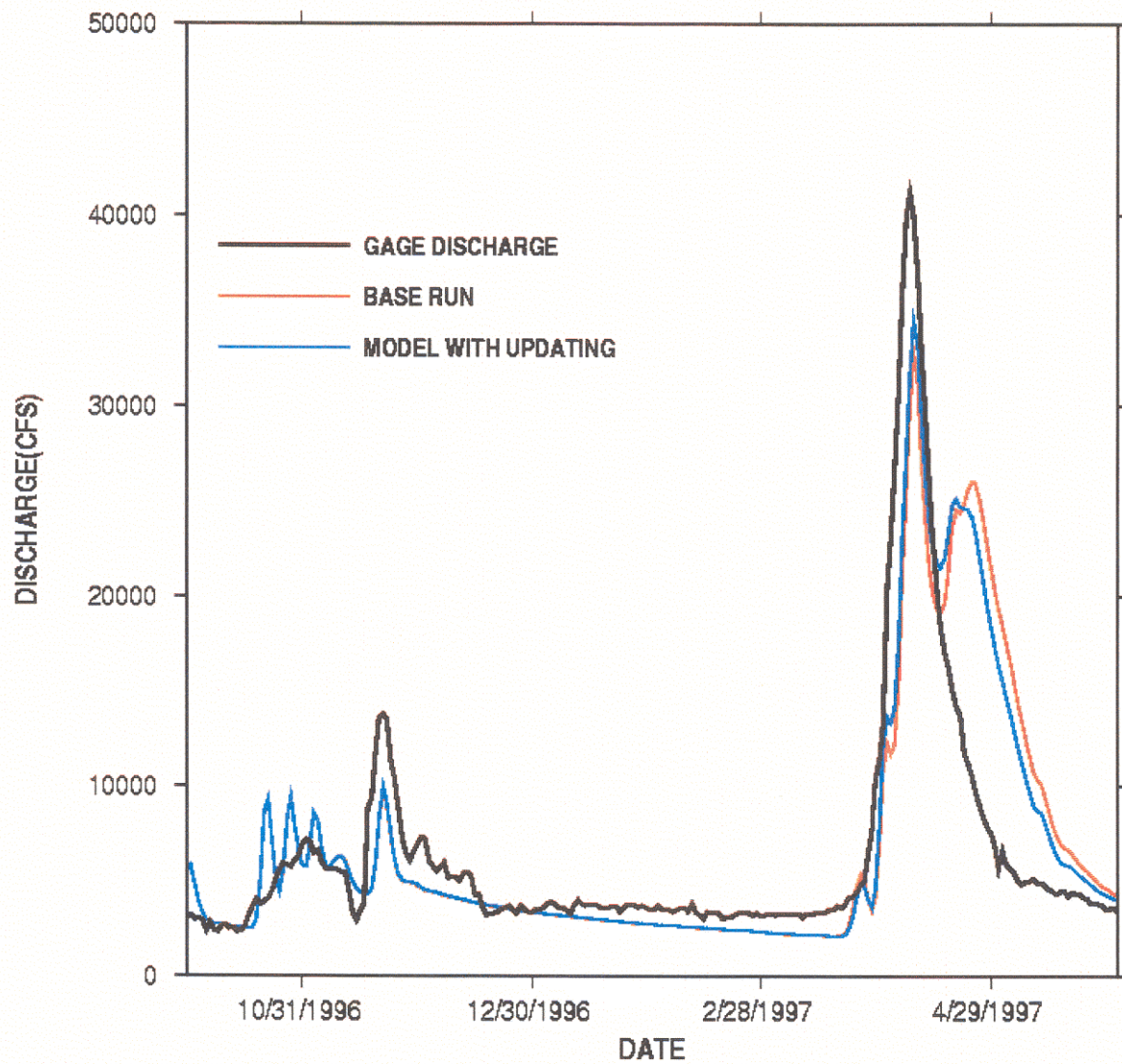


Figure 3-23. Hydrograph of observed and simulated discharge for the St. Croix River for winter 1996/97. Simulated discharge is from the unadjusted model; updated model uses snow surface freeze/thaw state information derived from NSCAT microwave backscatter.

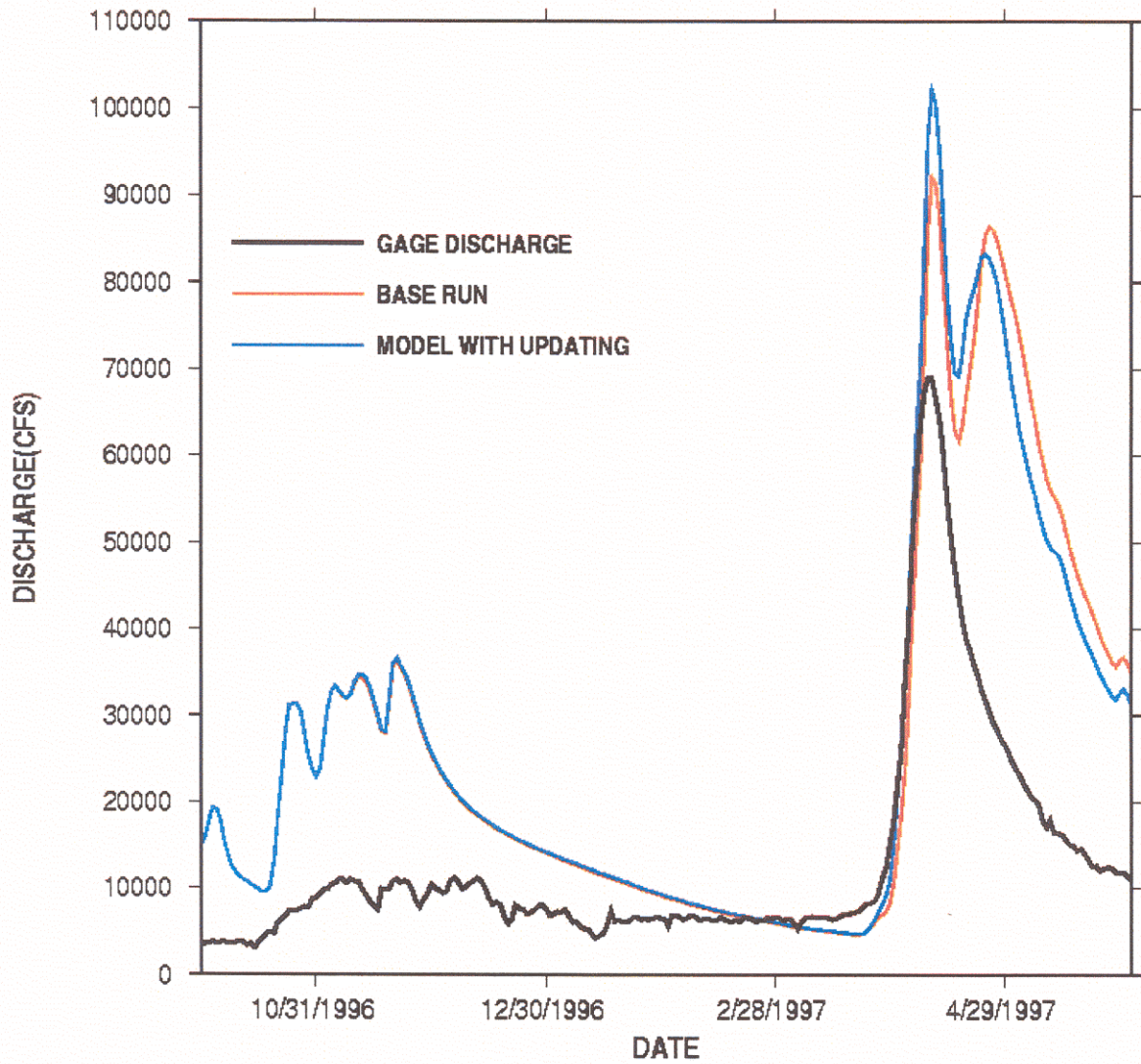


Figure 3-24. Hydrograph of observed and simulated discharge for the gage on the Mississippi River at Anoka, Minnesota for winter 1996/97. Simulated discharge is from the unadjusted model ; updated model uses snow surface freeze/thaw state information derived from NSCAT microwave backscatter.

Updating had such a slight effect on predictions (Figure 4-25) that the two simulation hydrographs overlap almost exactly with the exception of the peak discharge predicted for early March. The difference between the discharge predictions never exceeded 120 cfs which is only slightly more than 2% of the simulated discharge for the peak. For the Mississippi River at Anoka, updating based on backscatter had little effect on discharge (Figure 4-26). The difference between the two simulated hydrographs is somewhat more clear for the peak event in early March than for the St. Croix River (Figure 4-25).

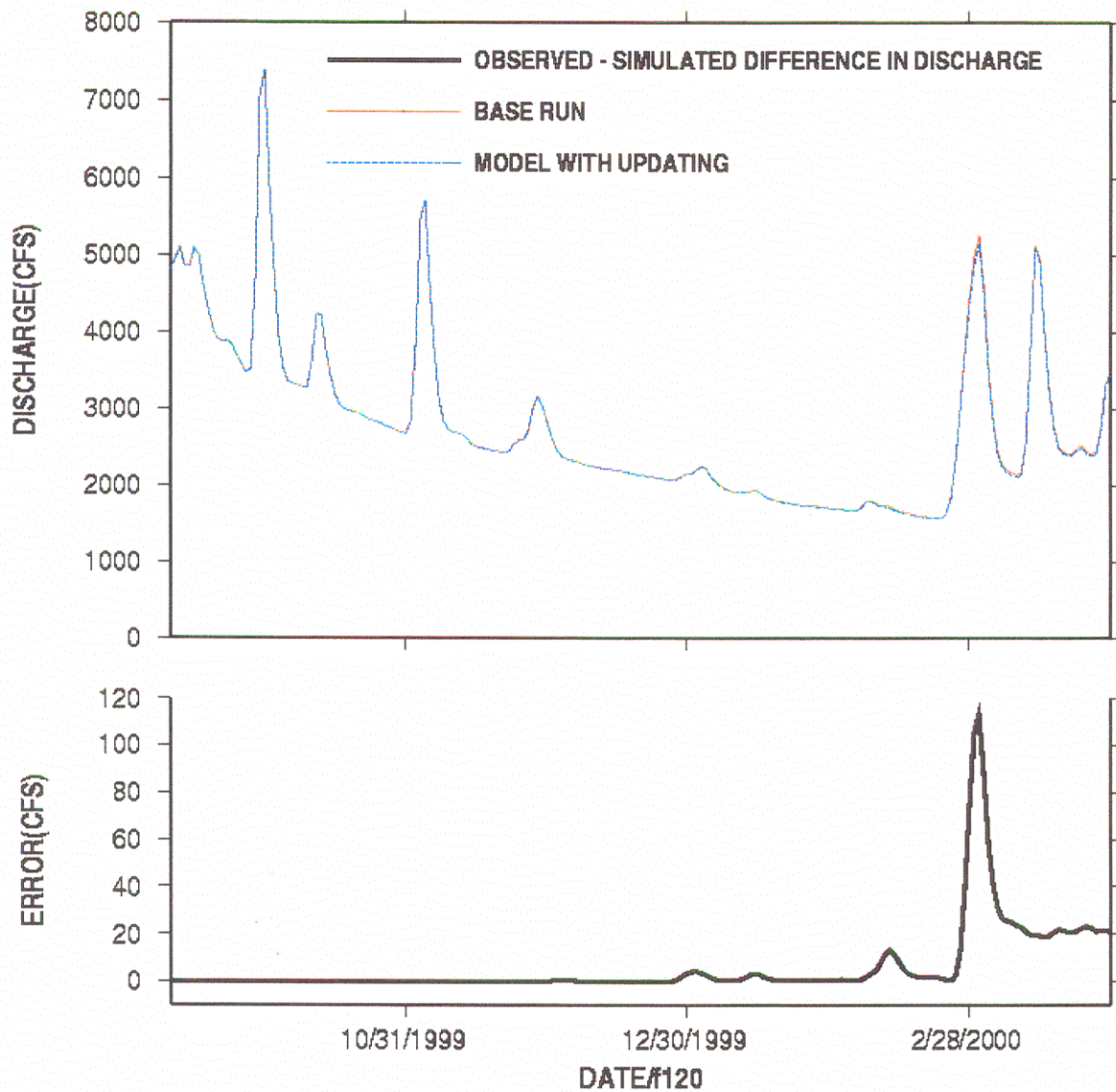


Figure 3-25. Simulated discharge for the St. Croix River at St Croix Falls, Wisconsin for winter 1999/2000, with and without updating with microwave backscatter measurements by QuikSCAT. The top plot presents hydrographs with and without updating while the observed bottom plot gives the difference in simulated discharge with and without updating. Observed discharge was not available.

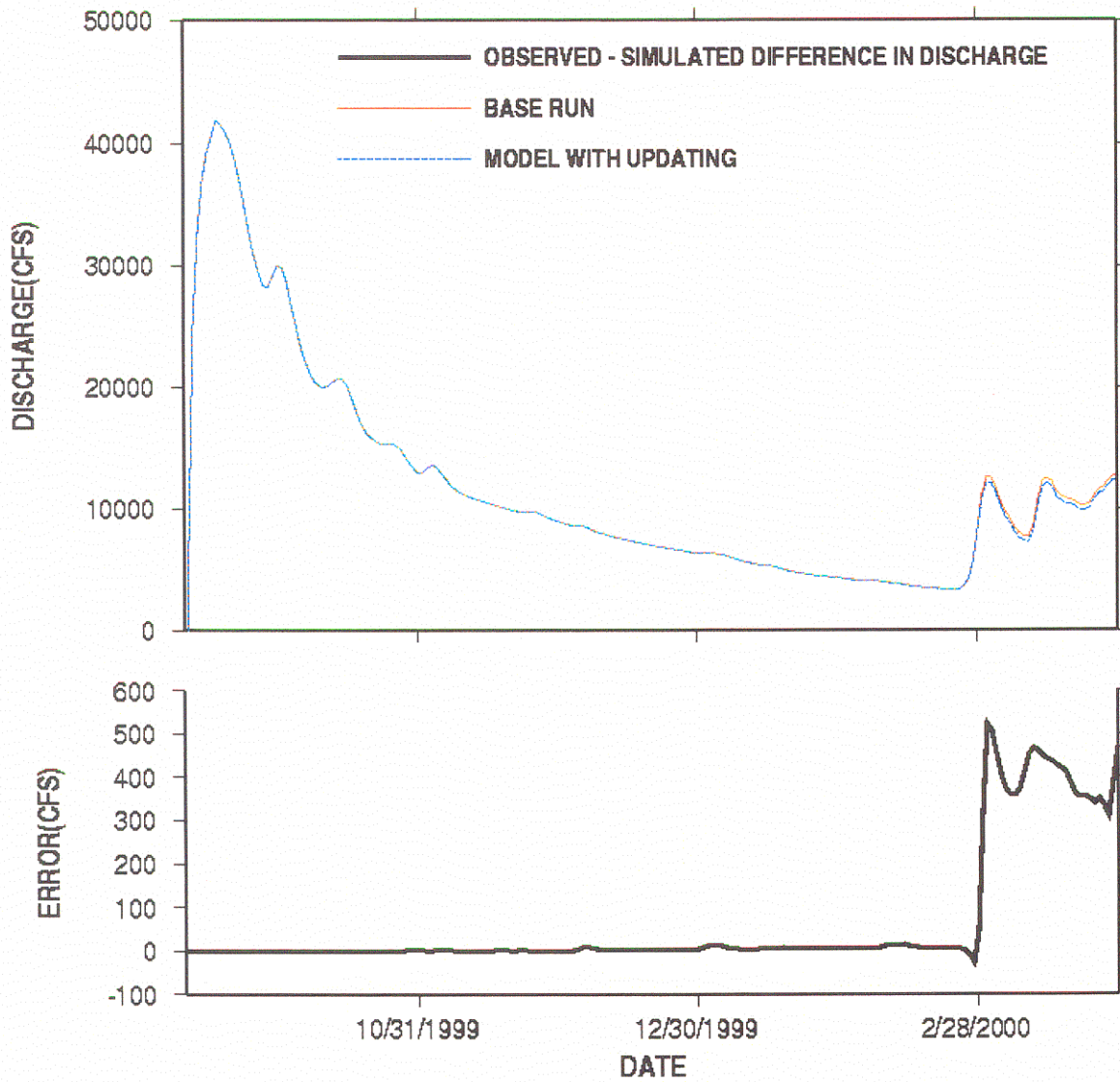


Figure 3-26. Simulated discharge for the Mississippi River near Anoka, Minnesota for winter 1999/2000 with and without updating with microwave backscatter measurements by QuikSCAT. The top plot presents hydrographs with and without updating while the observed bottom plot gives the difference in simulated discharge with and without updating. Observed discharge was not available.

Discussion

3.6 Overview

As noted in previous chapters, the goal of this thesis is to evaluate the hydrologic utility of microwave scatterometers for updating of a macroscale hydrologic model. The two main elements of the approach were to develop a scheme for updating snow state variables within the macroscale hydrologic model (VIC), and to develop a method for converting microwave backscatter observations into estimates of hydrologic state variables or related conditions in a form usable by the model. The analyses performed included a preliminary trial to evaluate the benefits of updating a hydrologic model using snow depth data, a comparative analysis of scatterometer data and meteorological data for the study area, and, finally, a trial use of scatterometer data to update snow state variables. This section discusses the results of these trials.

3.7 Snow depth updating

3.7.1 Snow depth spatial predictions

Model predictions of snow extent before updating were consistently biased with snow cover extending too far south and too late in the season as compared with surface observations and visible band satellite data. The model parameters may explain some of this bias. The model had been calibrated previously for the purpose of studying the long-term water balance of the upper Mississippi River basin by Maurer et al, 1999. Snow aerodynamic roughness length, in

particular, was assigned a relatively low value to compensate for problems in accumulating sufficient snow to match observed runoff peaks in the spring. This choice of model parameters allowed sufficient snow to accumulate but extended the persistence of the snow pack later into the season than was indicated by historical observations. Updating snow depth improved snow extent predictions dramatically with only 18 adjustments over the entire winter season, by removing snow where the snow extended too far south or too late into the season but also adding snow in the north where the moisture balance within the model indicated a deficit of precipitation accumulation. The adjustments had such a large effect because snow accumulation and ablation persist over a timescale of days to weeks, therefore the effect of each individual adjustment was still apparent days afterward.

3.7.2 Runoff

Updating snow depth changed the amount of snow on the ground available for runoff, (Figure 5-1) which, in turn, improved the accuracy of the predicted spring floods when snow melt was responsible for discharge. The comparison of updated versus unadjusted snow water equivalent and runoff indicates that updating eliminated the a secondary runoff peak in Spring 1997 which the model predicted but which was not present in the observed discharge (see Figure 4-1) by eliminating the spurious snow on the ground prior to the onset of melt. This test demonstrated that even a simple updating scheme can improve predictions dramatically when the data available are high quality and provide estimates of a model state variables such as snow which strongly affects model predictions.

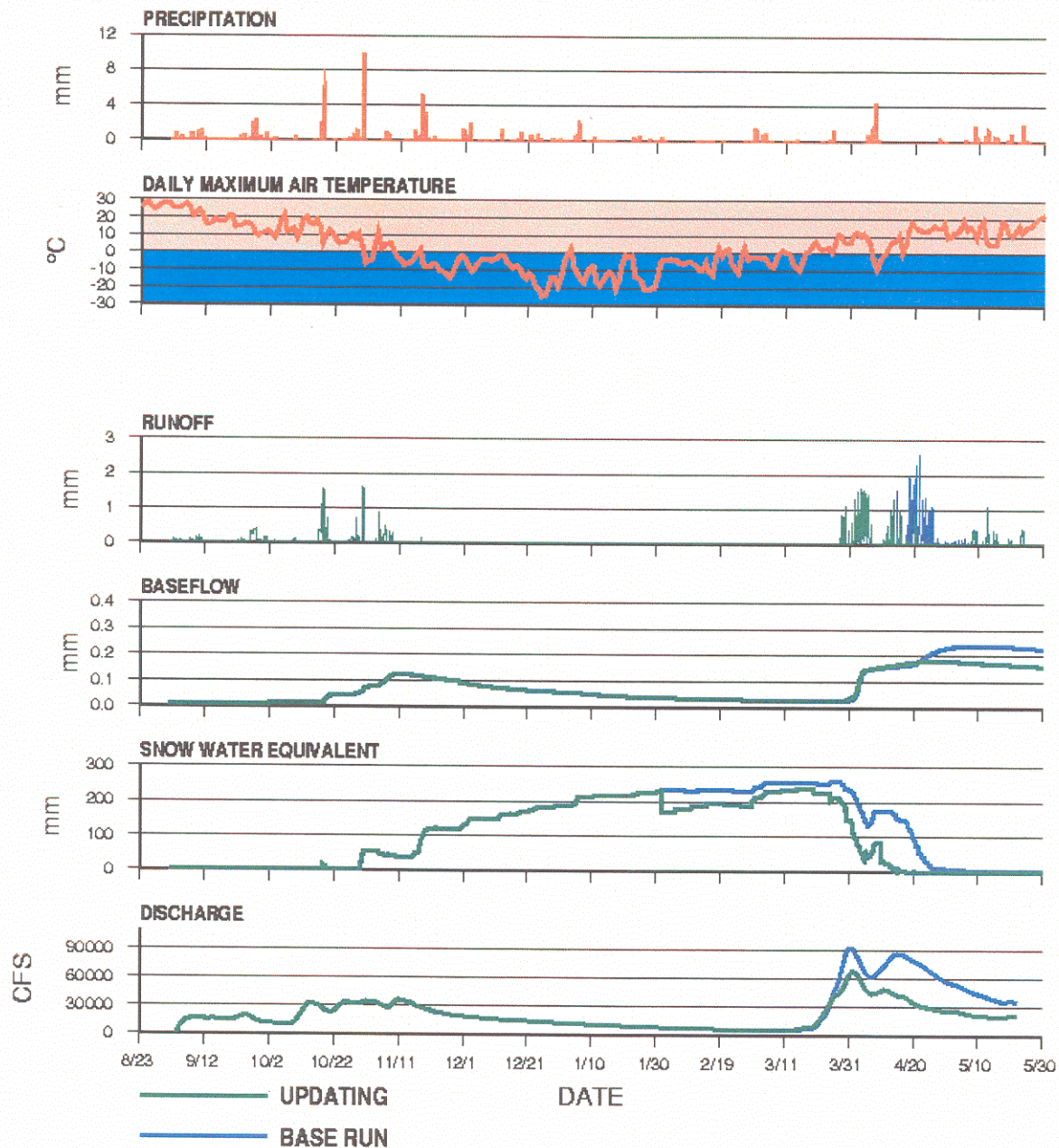


Figure 3-27. Timeseries of model variables in the St. Croix River sub-basin and runoff for the St. Croix River – unadjusted model and model with snow depth updating. The points where snow water equivalent decreases with no apparent response in the other variables are where snow depth was updated.

3.8 Visual comparison of specific events

3.8.1 Overview.

The results of the comparison between microwave backscatter response and model-predicted meteorological variables described in Sections 4.3 and 4.4 indicated that strong relationships were absent. The VIC snow model has been demonstrated to reproduce snow accumulation and ablation (Cherkauer and Lettenmaier, 1994; Bowling et al, 2000; Nijssen et al, 2000; Storck, 2000). Because the data used to force the model are derived from historical observations and the model is physically based, the predictions of temperatures and presence/absence of liquid water in the snow surface layer by the VIC model should be quite accurate. It was hoped that a consistent and close match between the presence of low σ^0 values and evidence of liquid water in the pack would be evident, which would justify model updating based on microwave backscatter. The visual comparison between σ^0 and snow surface variables during specific four and five day events (Section 4.3) failed to indicate such relationships. The discrepancies between patterns of observed σ^0 drops and the appearance of liquid water in the snow are sufficiently large that estimates of snow conditions based on microwave backscatter are unlikely to improve model predictions. It is therefore not surprising that the sensitivities to updating with scatterometer data (Section 5.4) are modest. In the remainder of this section, some reasons why σ^0 patterns do not agree consistently and closely with patterns of snow surface wetness and temperature are explored.

3.8.2 Signal-to-noise ratio

Figures 5-2, 5-3 and 5-4 compare raw and smoothed images for the three events described in Section 4.4. The images demonstrate that smoothing removed or attenuated “hotspots” that appeared day to day. In general, though, the smoothed images appear to follow the surface conditions better than the raw images. Some information is lost in the smoothing process, however. As indicated in Section 3.2.2.1, the number of satellite overpasses in the upper Mississippi River basin compared to previously studied areas at higher latitude (e.g., Frolking et al, 1999) led to a loss of signal in the smoothing process.

σ^0 measurements by the NSCAT and QuikSCAT scatterometers have large spatial variability which makes smoothing necessary (see also Figure 2-8 and Figure 3-2 which compare the smoothed signal to the raw signal). The ability of the smoothing process to filter noise, however, depends on the spatial completeness of the raw data. The mid-latitude spatial density reduction in NSCAT and QuikSCAT signals may have been responsible for the failure of σ^0 to follow surface conditions to some extent.

3.8.3 Time of observation

As in Section 4.4.1, surface variables vary during the day between maximum and minimum values (see Figures 4-12 and 4-13). Typically, the time of day coinciding with the warmest temperatures and the greatest melt activity is around 3 PM and the time of day coinciding with the coolest temperatures and the least melt is around 3 AM. NSCAT flew over the Upper

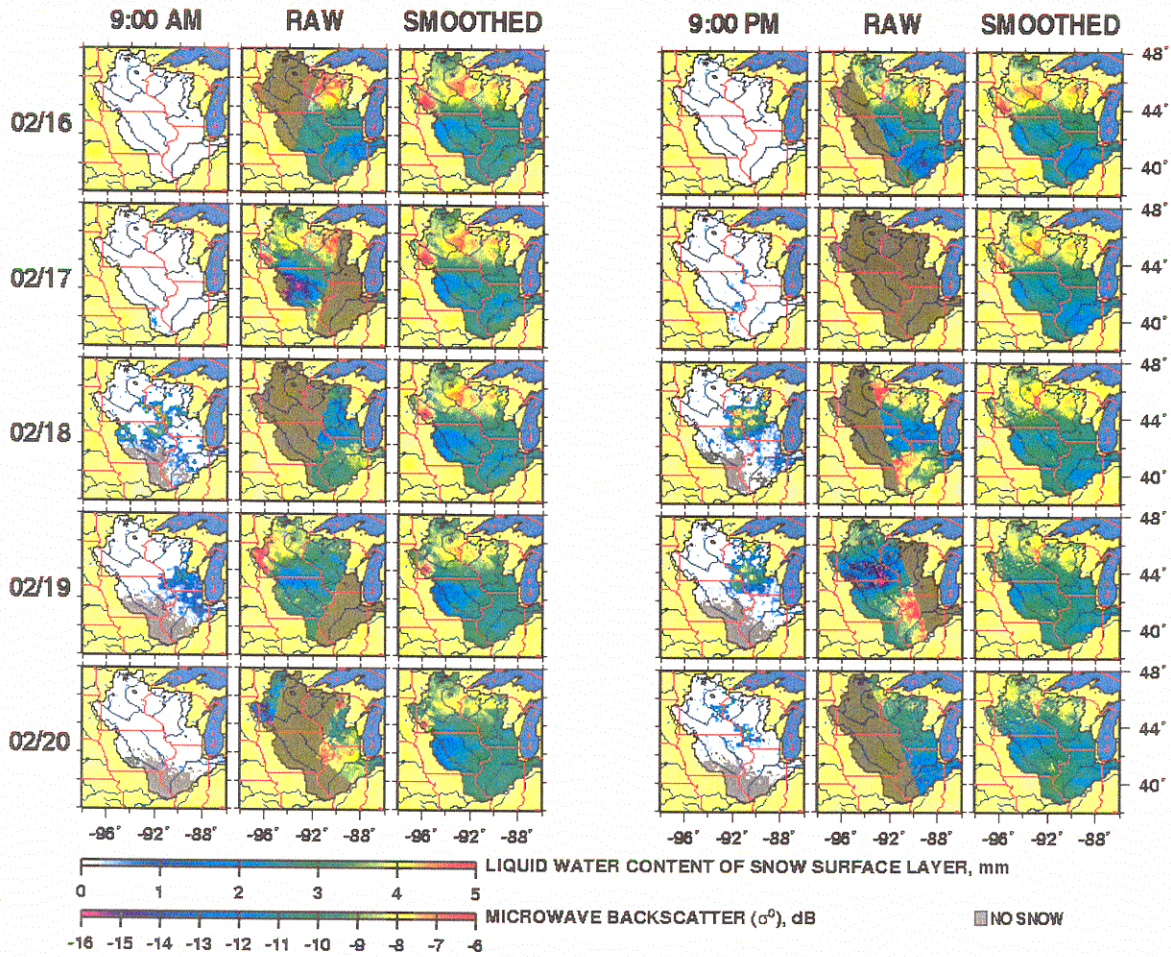


Figure 3-28. Snow surface layer liquid water content predicted by VIC and raw and smoothed σ^0 measured by NSCAT, February 16 to February 20, 1999. Note that many hotspots in the raw data do not appear in the smoothed data.

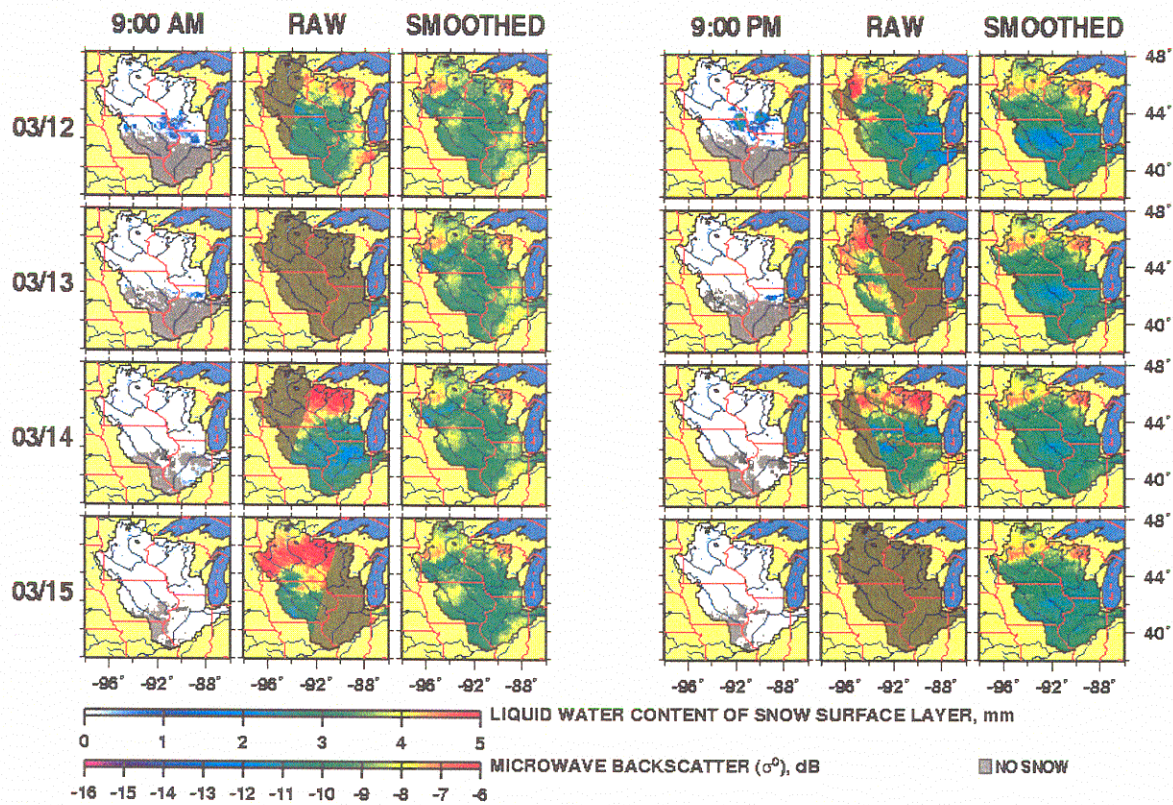


Figure 3-29. Snow surface layer liquid water content predicted by VIC and raw and smoothed σ^0 measured by NSCAT, March 12 to March 15, 1997.

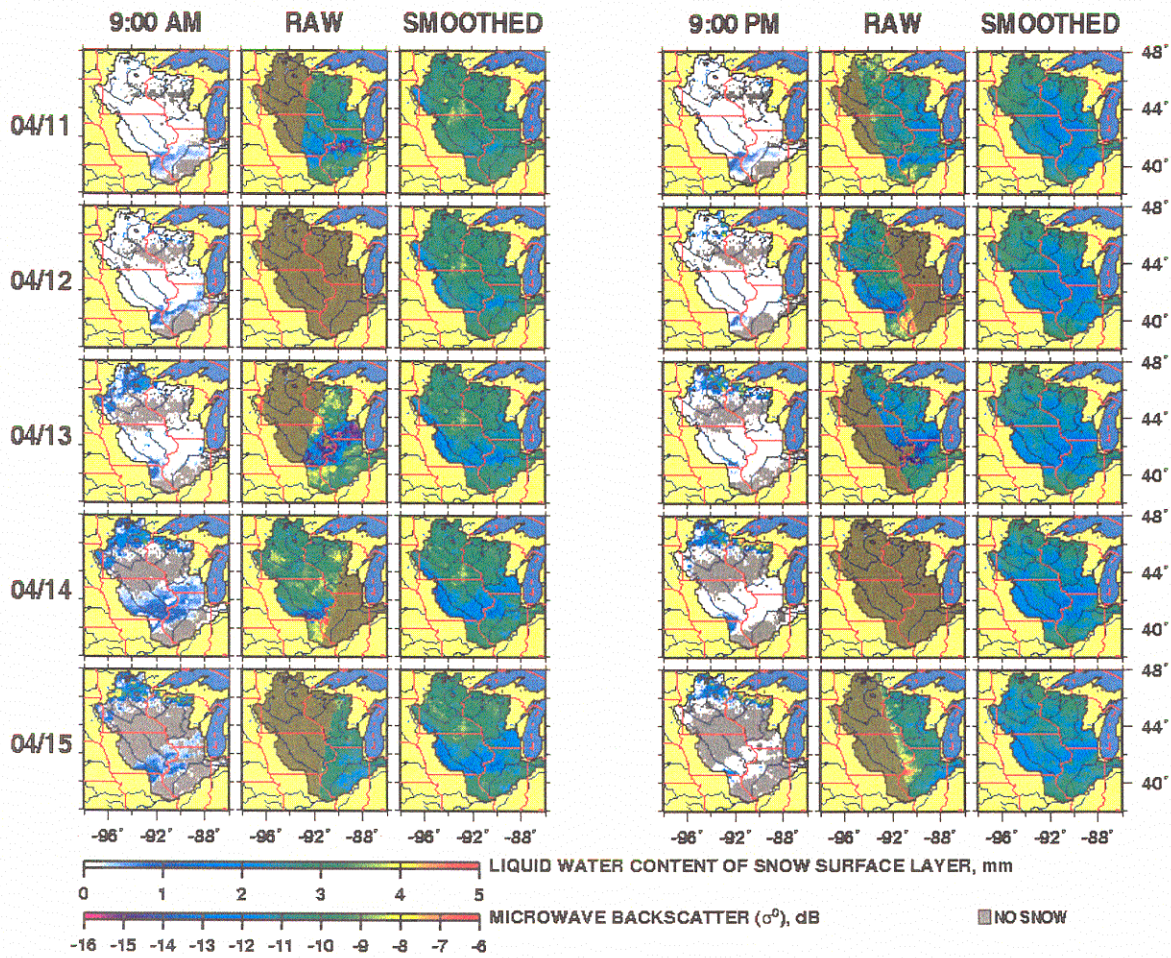


Figure 3-30. Snow surface layer liquid water content predicted by VIC and raw and smoothed σ^0 measured by NSCAT, April 11 to April 15, 1997.

Mississippi each day at about 10AM and 10PM, though, and QuikSCAT flew over the area at 6 AM and 6 PM. This shift between time of peak surface activity and time of observation may reduce the usefulness of NSCAT and QuikSCAT data for predicting surface variables.

One effect of the mismatch between time of peak activity and time of observation is that the surface conditions at the time of satellite overpass may not indicate melting conditions on a day when snow did melt and vice versa. Surface variables might indicate melt before or after a satellite flyover but not at the same time. Another effect is that little contrast was present between morning and evening snow water content and snow surface temperature at the time nearest to when NSCAT flew over the area (see 9 AM and 9 PM images in Figure 4-12) as compared to the contrast between 3 AM vs. 3 PM conditions for the same days. The appearance of such a contrast could otherwise be used as an indicator of the onset of melt conditions.

3.8.4 Mismatch between model predictions and backscatter response

Inevitably, there is some difference between the snow surface variables represented by the model and the snow conditions to which microwave backscatter responds. The snow surface variables in the VIC snow model are averages for the entire depth of the surface layer (12.5 cm of snow water equivalent). K_u -band microwave radiation may not penetrate even as deep as 1 cm when snow is wet (Ulaby et al, 1981). Testing with different snow surface layer depths in the model indicated that the VIC snow model no longer predicted snow processes when thinner surface layers (e.g., 1 cm) were used.

This different thickness of the model surface layer may cause discrepancies in magnitude and timing of snow surface variable predictions. Snow water content and temperature may differ between the model and truth because surface water that might be present at the very top of the snow (and, hence, influence the scatterometer backscatter) might be averaged to a small apparent quantity in the model. Alternately, drainage of surface water might cause moisture content at the top of the pack to be lower than represented by the model. Timing may cause discrepancies in the appearance of snow water and temperature because of thermodynamic inertia. Stiles and Ulaby (1980) observed that measured snow wetness in a 5 cm snow surface layer lagged behind air temperature and backscatter trends and speculated that snow wetness from a thinner layer would likely more closely match air temperature and σ^0 measurements.

3.8.5 Backscatter response to vegetation

Microwave backscatter responds to surface conditions other than the presence of liquid water in snow and this response may be strong enough to obscure the effect of liquid water in the snow. Microwave backscatter responds to the dielectric properties of soil and vegetation to varying degrees depending on wavelength. Rignot et al (1994), among others, discuss the microwave backscatter response to the conditions of soil, and to different types of vegetation in detail, although their work was at C-band. Stiles and Ulaby (1980) observed that microwave response to snow wetness was particularly strong at frequencies near to K_u band.

In the far northern part of the study area, vegetation conditions might have affected backscatter response. During the winter of 1996/97, snow was deep there until late in the season. σ^0 measurements were correspondingly high throughout this area relative to other parts of the basin until about March 20 (although values were low for a few episodes for a day or two at a time). σ^0 was particularly low in the northern part of the basin, -15db to -13db, for the period from March 21 to March 25. After the 25th, though, σ^0 was in the same range in the north as elsewhere in the basin, regardless of snow cover. As indicated by Figure 2-6, the northeast part of the basin is characterized by broadleaf deciduous forest and mixed cover rather than the cropland which dominates the rest of the basin. From March 25 on, backscatter response in the northeast part of the basin did not drop even though that region experienced significant melt, as Figure 4-20 indicates. An explanation for this behavior might be that the response seen up until March 21 in the northeast was due to the state of the canopy. By March 21, daytime air temperatures were above freezing in the northeast (Figure 4-4) thus the canopy had likely thawed and the microwave signal may have been responding to the canopy rather than snowpack freeze/thaw state.

3.9 Freeze/Thaw updating

3.9.1 Snow depth spatial predictions

The central motivation of this thesis was to evaluate the potential for updating snow freeze/thaw state based on microwave backscatter as a means of improving model predictions. Freeze/thaw updating had a relatively small effect on model predictions overall but this finding is not

surprising. Updating any parameter in the surface layer of the snow model affects no more than 12.5 cm of water equivalent. The variables that affect freeze/thaw state in the VIC model also, in general, have less thermodynamic influence than do variables that affect infiltration and moisture storage. Small adjustments to these variables will therefore have little effect on the state of the model. Also, because snow temperature and the amount of liquid water in the surface layer vary from hour to hour rather than over the course of days, adjustments to snow wetness and snow surface temperature have modest persisting effect and must be frequent and precisely timed. The scheme employed in this project therefore updated snow wetness and temperature frequently to maximize the effect of updating because the effect of each adjustment was likely to be slight.

Further, the test for updating of snow depth indicated that the model generally correctly predicted snow melt timing. Updating freeze/thaw state is effectively an adjustment to melt onset timing, therefore, the small differences seen that were produced by updating freeze/thaw state in the model are not likely to have had much effect on model-predicted melt water supply.

However, the summary statistics in Tables 4-1 and 4-2 indicate that updating freeze/thaw did result in modest improvements in model predictions of snow depth, despite the generally poor relationships between backscatter and snow surface variables seen in Sections 4.2 and 4.3.

Freeze/thaw updating may have improved snow pack predictions by causing more melt earlier in the season and also by increasing the amount of melt accompanying conditions when melt would have happened regardless of updating, thereby reducing the amount of snow on the ground

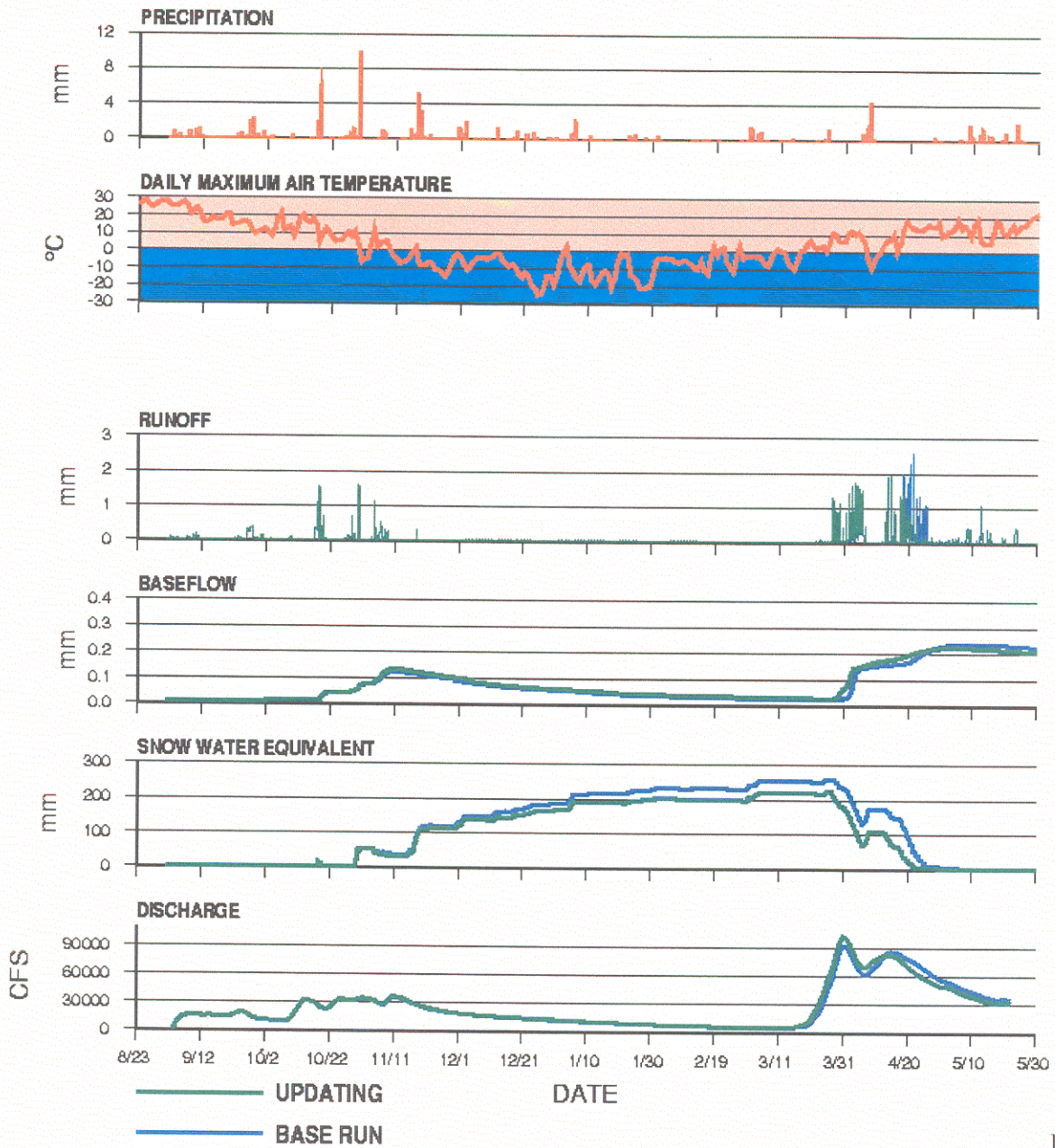
available to melt during the spring thaw. An increase in melt is possible because freeze/thaw was updated in a binary fashion as described in Section 3.4.3. The pack was assumed to be either frozen with no water present or melting with the surface layer at its prescribed capacity for liquid water. During ordinary ripe pack conditions without updating, the pack did not always fill with liquid water, whereas when updating occurred it always did. Thus any given melting event which followed an adjustment due to updating may have produced more melting than would have occurred without updating.

3.9.2 Runoff

Updating freeze/thaw state increased the height of the Spring 1997 flood peak on the Mississippi River at the Anoka gage but decreased the magnitude of the subsequent flood which was predicted by the model but was not observed. An explanation for this is that updating freeze/thaw did not change the amount of snow available for runoff, which was generally too high, but did cause that snow to melt off more quickly and earlier. As a result, the updating caused most of the snow melt to appear in the first runoff peak so that less was available for the second, as compared to the unadjusted model where the snowmelt was distributed almost evenly between the two floods.

Updating had the same affect on the St. Croix River hydrograph. Updating caused the pack to melt more quickly and distributed more of the melted snow to the first flood than to the second.

This effect brought the first Spring 1997 peak closer in magnitude to the observed peak because the amount of snow on the ground was closer to observed conditions in this basin (Figure 5-5).



Figure

Figure 3-31. Timeseries of model variables in the St. Croix River sub-basin and runoff for the St. Croix River – unadjusted model and model with freeze/thaw updating. Note that decreases in snow water equivalent always accompany response by the other model variables plotted here- which all represent mass - because the updating scheme did not alter mass as it did in the case of snow depth updating.

Chapter 4: Conclusions

4.1 Overview

Satellite microwave scatterometers are a recent addition to the suite of among of earth-observing sensors. The first satellite scatterometer, NSCAT, was operational during the winter of 1996/97 and that satellite's replacement, QuikSCAT, became operational in the summer of 1999.

Although originally launched for the purpose of monitoring ocean conditions, several recent studies have suggested a potential exists to extract hydrologically useful data from these satellites. Interest has focused specifically on microwave backscatter response to surface freeze/thaw conditions. The primary goal of this thesis was to evaluate the hydrologic utility of data from satellite microwave scatterometers for updating a macroscale hydrologic model. As an initial test of the hydrologic value of snow updating, the utility of updating model-predicted snow depths was evaluated using surface observations.

Updating was demonstrated to significantly improve hydrologic predictions in a test where snow depth was updated intermittently from gridded observations. Updating snow depth corrected biases in the model spatial prediction of snow and discharge. For a station measuring discharge in the upper reaches of the Mississippi River, updating entirely eliminated a simulated secondary spring peak flow which was not present in the observed discharge. This trial demonstrated that updating has utility when the data source for updating is high quality and the parameter being

updated represents mass within the model and thus has significant and persistent effects on model predictions.

Microwave backscatter measured by NSCAT was demonstrated to have some relationship to snow surface conditions, but the relationship was not consistent enough that updating with backscatter would likely improve model predictions substantially. Comparison of backscatter images of the study area with daily and hourly images of snow surface layer wetness and temperature showed that backscatter reflected snow surface wetness on some days but not on others. There was some indication that a mismatch in timing may be responsible for some lack of relation because NSCAT overpass times were not well matched with the middle of the afternoon and the early morning hours, which are the times of day when the contrast in hydrologic processes should be greatest.

Despite the lack of a close relationship between backscatter and surface conditions, the model was modified so that snow surface and temperature were updated based on microwave backscatter for two periods corresponding to the operational periods of both NSCAT and QuikSCAT. The clearest result of these trials was that updating based on microwave backscatter has little effect on model predictions even though the model was updated over two hundred times during each of the two study periods. Summary statistics demonstrated that, though the effect was slight enough to be of arguable significance, updating based on microwave backscatter did improve model spatial snow predictions. Hydrographs comparing simulated discharge with and

without updating against gage discharge indicate that updating freeze/thaw state did not correct problems in model discharge predictions.

4.2 Recommendations

Microwave backscatter response to surface conditions demonstrate a signal that varies spatially and over time but, as the results of this project indicate, the conditions “seen” by the sensors are still only beginning to be understood. Ground-based studies of microwave response such as those of Stiles and Ulaby (1980) indicated that snow conditions dominate microwave backscatter signal in the K_u band. However, from earth orbit, factors other than snow freeze/thaw state can also strongly influence backscatter response. These include the type of vegetation present, the liquid moisture content and freeze/thaw state of that vegetation and likely other factors, as well. The influence of other factors make accurate and precise estimation of snow conditions such as freeze/thaw state from microwave data difficult.

Further research is necessary to determine precisely which surface conditions determine microwave backscatter response as seen by scatterometers flown on satellite platforms.

Discrepancies between the results of studies with ground-based and aircraft-mounted microwave sensor studies and satellite-sensor results indicate that studies in the future should focus on satellite data rather than on explaining microwave satellite response based on ground sensor and aircraft sensor studies. In particular, the analysis of data from a microwave satellite whose orbit allows the satellite to frequently view well-instrumented snow-covered areas in the contiguous

United States during the local mid-afternoon and early morning hours would eliminate some uncertainty about response to snow conditions. More generally, research with the intent of developing useful hydrologic products from microwave satellite data may need to depart further from theoretical explorations in favor of empirical studies. With better understanding of the relationship between surface conditions and microwave backscatter, satellite microwave remote sensing data may yet prove to be useful for hydrologic prediction.

LIST OF REFERENCES

- Anderson, E. A., (1976) A point energy and mass balance model of a snow cover, *NWS Technical Report 19*, National Oceanic and Atmospheric Administration, Washington, D. C., 150 p.
- Baghdadi, N., Y. Gauthier, M. Bernier, and J-P. Fortin (2000), Potential and Limitation of RADARSAT SAR Data for Wet Snow Monitoring, *IEEE Trans. On Geoscience and Remote Sensing*, 38(1), pp. 316-320.
- Boehnke, K. and V. R. Wismann (1996), Thawing of Soils in Siberia Observed by the ERS-1 Scatterometer Between 1992 and 1995, *IEEE Geophysics and Remote Sensing Symposium 1996(IGARSS '96), Proceedings*, pp. 2264-2265.
- Bowling, L., D. P. Lettenmaier, and B. V. Matheussen (2000), Hydroclimatology of the Arctic Drainage Basin, *The Freshwater Budget of the Arctic Ocean*, E. L. Lewis et al, eds., Netherlands: Kluwer Academic Publishers, pp. 57-90.
- Bras, R. (1990) *Hydrology: An Introduction to Hydrologic Science*, Menlo Park, California: Addison-Wesley, 643 p.
- Carroll, S. S., T. R. Carroll, and R.W. Poston (1999), Spatial Modeling And Prediction Of Snow-Water Equivalent Using Ground-Based, Airborne, And Satellite Snow Data, *J. Geophys. Res.*, 104 (D16) pp. 19623-19629.
- Cherkauer, K. A. and D. P. Lettenmaier (1999), Hydrologic Effects Of Frozen Soils In The Upper Mississippi River Basin, *J. Geophys. Res.*, 104 (D16), pp. 19599-19610.
- Cleveland, W.S. (1979) Robust Locally Weighted Regression and Smoothing Scatterplots, *Journal of the American Statistical Association*, 74, pp. 829-836.
- Cleveland, W.S. and Devlin, S.J. (1988) Locally Weighted Regression: An Approach to Regression Analysis by Local Fitting, *Journal of the American Statistical Association*, 83, pp. 596-610
- Dubin, A. M. and D. P. Lettenmaier (1999), Assessing The Influence Of Digital Elevation Model Resolution On Hydrologic Modeling, *Water Resources Series, Technical Report No. 159*, University of Washington, Department of Civil Engineering Environmental Engineering and Science, 143 p.

- Dougenik, J. A. and D. E. Sheehan (1979), SYMAP User's Reference Manual, Cambridge. Massachusetts: Laboratory for Computer Graphics and Spatial Analysis.
- Francini, M., and M. Pacciani (1991), Comparative Analysis of Several Conceptual Rainfall-Runoff Models, *J. Hydrology*, 122, pp. 161-219.
- Hallikainen, M. T., F. T. Ulaby, M. Abdelrazik (1986), Dielectric Properties Of Snow in the 3 to 37 Ghz Range, *IEEE Transaction on Antennas and Propagation*, AP-34(11), pp. 1329-40.
- Hansen, M.C., R.S. DeFries, J.R.G. Townshend, and R. Sohlberg, Global Land Cover Classification at 1km Spatial Resolution Using a Classification Tree Approach, *International Journal of Remote Sensing* (in press).
- Houser, P. R., W. J. Shuttleworth, J. S. Famiglietti, H. V. Gupta, K. H. Syed, and D. C. Goodrich (1998), Integration of Soil Moisture Remote Sensing and Hydrologic Modeling Using Data Assimilation, *Water Resour. Res.*, 34(12), pp. 3405-3420.
- International Red River Basin Task Force, IRRBTF (1999), The Next Flood: Getting Prepared, *Final Report to the International Joint Commision*, 162 p.
- Jordan, R. (1991), *A One-Dimensional Temperature Model for a Snow Cover*, Technical Documentation for SNTHERM89, U.S. Army Corps of Engineers, CRREL, Special Report 91-16, 49 p.
- Josberger, E. G., N. M. Mognard, B. Lind, R. Matthews, and T. Carroll (1998), Snowpack Water-Equivalent Estimates from Satellite and Aircraft Remote-Sensing Measurements of the Red River Basin, North-Central U.S.A., *Annals of Glaciology*, 26, pp. 119-124.
- Kimball, J. S., K. C. McDonald, A. R. Keyser, S. Froking, and S. W. Running (2000), Application of the NASA Scatterometer (NSCAT) for Determining the Daily Frozen and Non-Frozen Landscape of Alaska, *Rem. Sens. Environ.*, (in review).
- Koivusalo H. J. and S. J. Burges (1996), *Use of a One-Dimensional Snow Cover Model to Analyze Measured Snow Depth and Snow Temperature Data from Southern Finland*, University of Washington Department of Civil Engineering, Water Resources Series, Technical Report No. 150, 91 p.
- Koskinen, J. T., J. T. Pulliainen, and M. T. Hallikainen (1997), The Use of ERS-1 SAR Data in Snow Melt Monitoring, *IEEE Trans. On Geoscience and Remote Sensing*, 35(3), pp. 601-610.

Kurvonen, L. and M. Hallikainen, Influence of Land-Cover Category on Brightness Temperature of Snow (1997), *IEEE Trans. on Geoscience and Remote Sensing*, 35(2), pp. 367-377.

Leung, R.L., A.F. Hamlet, D.P. Lettenmaier, and A. Kumar (1999), Simulations of the ENSO Hydroclimate Signals in the Pacific Northwest Columbia River Basin., *Bulletin of the American Meteorological Society*, 80(11) pp. 2313-2329.

Liang, X. D. P. Lettenmaier, E. F. Wood, and S. J. Burges (1994), A Simple Hydrologically Based Model of Land Surface Water and Energy Fluxes for General Circulation Models, *J. Geophys. Res.* 99(D7) pp. 14415-14428.

Lillesand, T. M. and R. W. Kiefer (1994), *Remote Sensing And Image Interpretation*, 2nd ed., John Wiley and Sons, 750 p.

Linlor, W. I., F. D. Clapp, D. J. Angelakos, J. L. Smith, N. Berg, and J. Bergman (1981) Snow Wetness Measurements and Runoff Forecasting, *Proceeding of the Western Snow Conference, 49th Annual Meeting*, pp. 1 –12.

Linlor, W. I. (1980) Permittivity and Attenuation of Wet Snow between 4 and 12 GHz, *J. Applied. Physics*, 51(5), pp. 2811-2816.

Lohman, D. E. Raschke, B. Nijssen, and D.P. Lettenmaier (1998) Regional Scale Hydrology: II. Application of the VIC-2L Model to the Weser River, Germany, *Hydrological Sciences* 43(1), pp. 143-158.

Maurer, E.P., G.M. O'Donnell, D.P. Lettenmaier, J.O. Roads, and E.F. Wood (2000), LDAS Long-Term Retrospective Analyses, *EOS Trans*, 81(19) pp. S201-202. (presented at AGU Spring Meeting, 5/31/2000)

McDonald, K. personal communication via email, 7/20/2000.

McDonald, K., J. Kimball, R. Zimmerman, J. Way, S. Frolking, and S. Running (1999) Application of Spaceborne Scatterometer for Mapping Freeze-Thaw State in Northern Landscapes as a Measure of Ecological and Hydrological Processes, *IEEE Geophysics and Remote Sensing Symposium 1999 (IGARSS '99), Proceedings*, pp. 2121-2123.

McLaughlin, D. (1995) Recent Developments in Hydrologic Data Assimilation, *Reviews of Geophysics*, Supplement: U.S. National Report to International Union of Geodesy and Geophysics 1991-1994, July 1995, pp.. 977-984.

Moore, R. J., V. A. Bell, R. M. Austin, and R. J. Harding (1999) Methods for Snowmelt Forecasting in Upland Britain, *Hydrology and Earth System Sciences*, 3(2), pp. 233-249.

- New York Times*, "No Ordinary Disaster", Opinions & Editorials Section, April 24, 1997.
- Nghiem, S. personal communication via email, 7/10/2000.
- Newkirk, M. H. and G. S. Brown (1996) A Waveform Model for Surface and Volume Scattering from Ice and Snow, *IEEE Trans. on Geoscience and Remote Sensing*, 34(2), pp. 444-456.
- Nijssen, B., D. P. Lettenmaier, X. Liang, S. W. Wetzel, and E. F. Wood (1997) Streamflow Simulation for Continental-Scale River Basins, *Water Resour. Res.* 33(2), pp. 711-724.
- Nijssen, B., R. Schnur, and D. P. Lettenmaier (Accepted 2000), Global Retrospective Estimation of Soil Moisture Using the VIC Land Surface Model, 1980-1993. *Journal of Climate*.
- Peck, E. L., T. R. Carroll., and S. C. Vandemark (1980), Operational Aerial Snow Surveying in the United States, *Hydrological Sciences Bulletin*, 25(1), pp. 51-62.
- Pullianen, J.T., T. Manninen and M. T. Hallikainen (1998) Application of ERS-1 Wind Scatterometer Data to Soil Frost and Soil Moisture Monitoring in Boreal Forest Zone, *IEEE Trans. On Geoscience and Remote Sensing*, 36(3), pp. 849-863.
- Rignot, E. and J. B Way (1994), Monitoring Freeze-Thaw Cycles along North-South Alaskan Transects Using ERS-1 SAR, *Remote Sens. Environ.*, 49(2) pp. 131-137.
- Rignot, E., J. B. Way, K. C. McDonald, L. Viereck, C. Williams, P. Adams, C. Payne, W. Wood, and J. Shi (1994) Monitoring of Environmental Conditions in Taiga Forests Using ERS-1 SAR, *Remote Sens. Environ.*, 49(2), pp. 145-153.
- Running, S. W., J. B. Way, K. C. McDonald, J. S. Kimball, S. Frolking, A. R. Keyser, and R. Zimmerman (1999) Radar Remote Sensing Proposed for Monitoring Freeze/Thaw Transitions in Boreal Regions, *EOS Trans.*, 80(19), pp. 220-221.
- Schowengerdt, R. A. (1997) *Remote Sensing, Model and Methods for Image Processing*, 2nd ed., San Diego, CA: Academic Press, 522 p.
- Storck. P. (2000) Trees, Snow and Flooding: An Investigation Of Forest Canopy Effects on Snow Accumulation and Melt at the Plot and Watershed Scales in the Pacific Northwest, *Water Resources Series, Technical Report No. 161*, University of Washington, Department of Civil Engineering, Environmental Engineering and Science, 176 p.
- Stiles W. H. and Ulaby, F. T. (1980) The Active and Passive Microwave Response to Snow Parameters, I. Wetness. *J. Geophysical Research*, 85(C2), pp. 1037-1049.

Ulaby, F. T., R. K. Moore and A. K. Fung (1981) *Microwave Remote Sensing: Active and Passive, Vol. I Microwave Remote Sensing Fundamentals and Radiometry*, Menlo Park, California: Addison-Wesley, 456 p.

Ulaby, F. T., R. K. Moore and A. K. Fung (1982), *Microwave Remote Sensing: Active and Passive, Vol. II Radar Remote Sensing and Surface Scattering and Emission Theory*, Menlo Park, California: Addison-Wesley, pp. 457-1064.

Ulaby, F. T., R. K. Moore and A. K. Fung (1986), *Microwave Remote Sensing: Active and Passive, Vol. III*, Menlo Park, California: Artech House Incorporated, pp. 1065-2162.

U. S. Department of Agriculture, (1972) Snow Survery and Water Supply Forecasting, *Agriculture Information Bulletin 536*.

Way, J. B., E. J. M. Rignot, K. C., McDonald, R. Oren, R. Kwok, G. Bonan, M. C. Dobson, L. A. Viereck, and J. E. Roth 1994) Evaluating the Type and State of Alaska Taiga Forests with Imaging Radar for Use in Ecosystem Models, *IEEE Trans. On Geoscience and Remote Sensing*, 32(2), pp. 353-369.

Way, J. B., R. Zimmerman, E. Rignot, K. McDonald, and R. Oren (1997), Winter and Spring Thaw as Observed with Imaging Radar at BOREAS, *J. Geophys. Res.*, 102(D24), pp. 29673-29684.

Wisman V. R. and K. Boehnke (1996), Dramatic Decrease in Radar Cross Section over Greenland Observed by the ERS-1 Scatterometer Between 1991 and 1995, *IEEE Geophysics and Remote Sensing Symposium 1996(IGARSS '96), Proceedings*, pp. 2014-2016.

Wood, E. F., D. P. Lettenmaier, X. Liang, B. Nijssen, S. W. Wetzel (1997) Hydrological Modeling of Continental Scale Basins, *Annu. Rev. Earth Planet. Sci.* 25, pp. 279-300.

